

# Regression analysis of properties of [Au(IPr)(CHR<sub>2</sub>)] complexes

Richard M. P. Veenboer,<sup>a</sup> Luis M. Azofra,<sup>b,c</sup> Danila Gasperini,<sup>d</sup> Alba Collado,<sup>e</sup> David B. Cordes,<sup>a</sup> Alexandra M. Z. Slawin,<sup>a</sup> Luigi Cavallo<sup>f</sup> and Steven P. Nolan<sup>g,h</sup>

<sup>a</sup> EaStCHEM, School of Chemistry  
University of St. Andrews, Purdie Building, North Haugh  
St. Andrews, KT16 9ST, United Kingdom

<sup>b</sup> CIDIA-FEAM (Unidad Asociada al Consejo Superior de Investigaciones Científicas, CSIC, avalada por el Instituto de Ciencia de Materiales de Sevilla, Universidad de Sevilla)  
Instituto de Estudios Ambientales y Recursos Naturales (i-UNAT)  
Universidad de Las Palmas de Gran Canaria (ULPGC)  
Campus de Tafira, 35017, Las Palmas de Gran Canaria, Spain.

<sup>c</sup> Departamento de Química  
Universidad de Las Palmas de Gran Canaria (ULPGC)  
Campus de Tafira, 35017  
Las Palmas de Gran Canaria, Spain.

<sup>d</sup> Department of Chemistry  
University of Bath, Claverton Down  
Bath, BA2 7AY, United Kingdom

<sup>e</sup> Department of Inorganic and Biochemistry  
Complutense University of Madrid  
Plaza de Ramón y Cajal, 28040 Madrid, Spain

<sup>f</sup> KAUST Catalysis Center (KCC)  
King Abdullah University of Science and Technology (KAUST)  
Thuwal 23955-6900, Saudi Arabia.

<sup>g</sup> Department of Inorganic and Physical Chemistry  
Ghent University, Building S3, Krijgslaan 281  
9000 Gent, Belgium

<sup>h</sup> Department of Chemistry  
College of Science, King Saud University, P. O. Box 2455  
Riyadh 11451, Saudi Arabia

# 1. Contents

<b>1. Contents</b> .....	<b>2</b>
<b>2. General information</b> .....	<b>4</b>
<b>3. Complex synthesis and characterization data</b> .....	<b>5</b>
3.1. Synthesis of [Au(CH <sub>3</sub> )(IPr)] ( <b>3</b> ) <sup>7</sup> .....	5
3.2. General procedure for the synthesis of [Au(CR <sub>2</sub> H)(IPr)] complexes.....	5
3.3. Synthesis of [Au(CH <sub>2</sub> COPh)(IPr)] ( <b>7</b> ) .....	5
3.4. Synthesis of [Au(CH <sub>2</sub> CN)(IPr)] ( <b>8</b> ).....	5
3.5. Synthesis of [Au(CH(CN) <sub>2</sub> )(IPr)] ( <b>9</b> ) .....	5
3.6. Synthesis of [Au(CH(Ph)CN)(IPr)] ( <b>10</b> ) .....	6
3.7. Synthesis of [Au(CH <sub>2</sub> NO <sub>2</sub> )(IPr)] ( <b>11</b> ).....	6
3.8. Synthesis of [Au(CH(CH <sub>3</sub> )NO <sub>2</sub> )(IPr)] ( <b>12</b> ).....	6
<b>4. NMR Spectra</b> .....	<b>7</b>
<b>5. Solid-state ATR-IR Spectra</b> .....	<b>14</b>
<b>6. Solid-state structures</b> .....	<b>18</b>
6.1. Crystallographic information.....	18
<b>7. Thermal ellipsoid representation and assignments</b> .....	<b>19</b>
7.1. Inspection and comparison with literature data.....	20
7.1.1. Bond lengths in functional groups .....	20
7.1.2. Flattening of carbanion ligand .....	21
7.1.3. Coordination mode of carbanion ligand .....	22
7.1.4. Adjustment of NHC geometry.....	22
<b>8. Competition experiments</b> .....	<b>23</b>
8.1. Experimental procedure for competition experiments.....	23
8.2. Conversion of ratios .....	24
8.3. Correction for non-constant concentration .....	24
<b>9. Computational modelling</b> .....	<b>26</b>
<b>10. Sets of parameters</b> .....	<b>27</b>
10.1. Component.....	28
10.2. EDA.....	28
10.3. Hammett .....	30
10.4. IR.....	32
10.5. NMR.....	33
10.6. Order .....	35
10.7. Population .....	36
10.8. Structure.....	37
<b>11. Regression analysis</b> .....	<b>42</b>
11.1. Data preparation .....	42
11.2. Model generation.....	43
11.3. Model validation .....	43
11.4. Parameter selection .....	43
11.5. Model selection.....	44
11.6. Parameter and model grouping .....	44
<b>12. Correlation analysis</b> .....	<b>45</b>

<b>13.</b>	<b>Correlation plots</b> .....	<b>47</b>
<b>14.</b>	<b>Linear models</b> .....	<b>49</b>
14.1.	Main linear models.....	49
14.2.	Additional linear models .....	57
<b>15.</b>	<b>Surface plots</b> .....	<b>61</b>
<b>16.</b>	<b>References</b> .....	<b>62</b>

## 2. General information

All reactions and manipulations were carried out in air. Chlorinated solvents ( $\text{CD}_2\text{Cl}_2$ ,  $\text{CDCl}_3$ ) were filtered through basic alumina to remove traces of HCl. Nuclear Magnetic Resonance (NMR) spectra were recorded on Bruker Avance 300 MHz, 400 MHz and 500 MHz spectrometers. Chemical shifts are expressed in  $\delta$  values (ppm) referenced internally to residual solvent resonances ( $^1\text{H}$ , 7.26 ppm ( $\text{CDCl}_3$ ) and 7.16 ppm ( $\text{C}_6\text{D}_6$ );  $^{13}\text{C}$ , 77.16 ppm ( $\text{CDCl}_3$ )). Assignment was accomplished using 2D NMR techniques:  $^1\text{H}$ - $^1\text{H}$  COSY,  $^1\text{H}$ - $^{13}\text{C}$  HSQC and  $^1\text{H}$ - $^{13}\text{C}$  HMBC. Peaks are assigned as s (singlet), d (doublet), t (triplet), q (quartet), m (multiplet) or br (broad). Peaks of aromatic nuclei are assigned *i* (*ipso*), *o* (*ortho*), *m* (*meta*) or *p* (*para*). FTIR (ATR) spectra were recorded on a Shimadzu spectrophotometer. Elemental analyses were performed at London Metropolitan University 166-220 Holloway Road, London, N7 8DB, UK. Statistical analyses were performed using the R software package.<sup>6</sup>

### 3. Complex synthesis and characterization data

#### Synthesis of [Au(CH<sub>3</sub>)(IPr)] (3)<sup>7</sup>

Dry THF (4.5 mL, 5.5 mmol, 1.1 equivalents) was added to methyl magnesium bromide (1.7 mL, 5.0 mmol) at 0 °C under argon.<sup>8</sup> After stirring for 16 hours, cooling to -20 °C for 2 hours resulted in the formation of a white precipitate that was then separated from the clear liquid. To [AuCl(IPr)] (1) (100 mg, 0.16 mmol) under argon was added 2 mL of the dimethylmagnesium solution (excess).<sup>9</sup> After stirring for 24 hours, the turbid reaction mixture was exposed to air, water was added and it was filtered over Celite®. The water was removed under reduced pressure, the crude product was suspended in toluene and filtered over Celite®. The solvent was removed from the clear solution under reduced pressure to give **3** as a fine white solid (70.6 mg, 73%).

<sup>1</sup>H-NMR (400 MHz, CDCl<sub>3</sub>): δ = 7.47 (t, <sup>3</sup>J<sub>H,H</sub> = 7.8 Hz, 2H; *p*-PhH), 7.28 (d, <sup>3</sup>J<sub>H,H</sub> = 7.8 Hz, 4H; *m*-PhH), 7.06 (s, 2H; CH), 2.65 (h, <sup>3</sup>J<sub>H,H</sub> = 6.9 Hz, 4H; CH<sub>3</sub>), 1.36 (d, <sup>3</sup>J<sub>H,H</sub> = 6.9 Hz, 12H; CH<sub>3</sub>), 1.21 (d, <sup>3</sup>J<sub>H,H</sub> = 6.9 Hz, 12H; CH<sub>3</sub>), -0.21 (s, 2H; CH<sub>3</sub>). <sup>13</sup>C{<sup>1</sup>H}-NMR (101 MHz, CDCl<sub>3</sub>): δ = 202.0 (1C; C<sub>carb</sub>), 145.9 (4C; *o*-PhC), 135.0 (2C; *i*-PhC), 130.1 (2C; *p*-PhC), 124.0 (4C; *m*-PhC), 122.5 (2C; CH), 28.8 (4C; CH), 24.5 (4C; CH<sub>3</sub>), 24.1 (4C; CH<sub>3</sub>), -2.3 (2C; CH<sub>2</sub>). Anal. calcd for C<sub>28</sub>H<sub>39</sub>AuN<sub>2</sub>: C, 55.90; H, 6.70; N, 4.66. Found: C, 54.32 H, 6.14; N, 4.60.

#### General procedure for the synthesis of [Au(CR<sub>2</sub>H)(IPr)] complexes

A vial equipped with a stirrer bar was charged, under air, with [Au(OH)(IPr)] (2) and the organic substrate (R-H). Solvent was added and the mixture was stirred at reflux temperature until full conversion to the final product was observed by <sup>1</sup>H-NMR analysis of an aliquot of the reaction mixture. After this time, the mixture was concentrated, pentane was added to precipitate the product and it was dried under vacuum.

#### Synthesis of [Au(CH<sub>2</sub>COPh)(IPr)] (7)

According to the general procedure, **2** (60 mg, 10 μmol), acetophenone (12.8 μL, 11 μmol, 1.1 equiv.) and THF (1 mL) were used. After 20 hours at 60 °C and work-up, **7** was obtained as a white solid (36.2 mg, 52% yield).

<sup>1</sup>H-NMR (500 MHz, CDCl<sub>3</sub>): δ = 7.57–7.55 (m, 4H; *o*-PhH), 7.47 (t, <sup>3</sup>J<sub>H,H</sub> = 7.8 Hz, 2H; *p*-PhH), 7.25–7.22 (m, 1H; *p*-PhH), 7.22 (d, <sup>3</sup>J<sub>H,H</sub> = 7.8 Hz, 4H; *m*-PhH), 7.09 (s, 2H, CH), 7.08 (t, <sup>3</sup>J<sub>H,H</sub> = 7.7 Hz, 2H; *m*-PhH), 2.50 (h, <sup>3</sup>J<sub>H,H</sub> = 6.9 Hz, 4H; CH), 2.46 (s, 2H; CH<sub>2</sub>), 1.19 (d, <sup>3</sup>J<sub>H,H</sub> = 6.9 Hz, 12H; CH<sub>3</sub>), 1.17 (d, <sup>3</sup>J<sub>H,H</sub> = 6.9 Hz, 12H; CH<sub>3</sub>). <sup>13</sup>C{<sup>1</sup>H}-NMR (126 MHz, CDCl<sub>3</sub>): δ = 204.6 (1C; C), 192.6 (1C; C<sub>carb</sub>), 145.7 (4C; *o*-PhC), 140.5 (1C; *i*-PhC), 134.4 (2C; *i*-PhC), 130.4 (2C; *p*-PhC), 129.7 (1C; *p*-PhC), 127.6 (2C; *o*-PhC), 127.4 (2C; *m*-PhC), 124.1 (2C; *m*-PhC), 122.8 (2C; CH), 36.2 (2C; CH<sub>2</sub>), 28.8 (4C; CH), 24.4 (4C; CH<sub>3</sub>), 24.1 (4C; CH<sub>3</sub>). Anal. calcd for C<sub>35</sub>H<sub>43</sub>AuN<sub>2</sub>O: C, 59.65; H, 6.15; N, 3.98. Found: C, 59.49; H, 5.98; N, 4.14. FTIR (ATR):  $\tilde{\nu}$  = 1620 cm<sup>-1</sup> (C=O).

#### Synthesis of [Au(CH<sub>2</sub>CN)(IPr)] (8)

According to the general procedure, **2** (500 mg, 0.83 mmol) and acetonitrile (1 mL) were used. After 20 hours at 80 °C and work-up, **8** was obtained as a white solid (480.1 mg, 92 % yield). <sup>1</sup>H-NMR (400 MHz, CDCl<sub>3</sub>): δ = 7.51 (t, <sup>3</sup>J<sub>H,H</sub> = 7.8 Hz, 2H; *p*-PhH), 7.30 (d, <sup>3</sup>J<sub>H,H</sub> = 7.8 Hz, 4H; *m*-PhH), 7.13 (s, 2H; CH), 2.58 (h, <sup>3</sup>J<sub>H,H</sub> = 6.9 Hz, 4H; CH<sub>3</sub>), 1.34 (d, <sup>3</sup>J<sub>H,H</sub> = 6.9 Hz, 12H; CH<sub>3</sub>), 1.22 (d, <sup>3</sup>J<sub>H,H</sub> = 6.9 Hz, 12H; CH<sub>3</sub>), 1.00 (s, 2H; CH). <sup>13</sup>C{<sup>1</sup>H}-NMR (101 MHz, CDCl<sub>3</sub>): δ = 192.7 (1C; C<sub>carb</sub>), 145.8 (4C; *o*-PhC), 134.3 (2C; *i*-PhC), 130.6 (2C; *p*-PhC), 129.6 (1C; CN), 124.2 (4C; *m*-PhC), 123.0 (2C; CH), 28.9 (4C; CH), 24.5 (4C; CH<sub>3</sub>), 24.1 (4C; CH<sub>3</sub>), -2.9 (2C; CH<sub>2</sub>). Anal. calcd for C<sub>29</sub>H<sub>38</sub>AuN<sub>3</sub>: C, 55.68; H, 6.12; N, 6.72. Found: C, 55.49 H, 6.02; N, 6.50. FTIR (ATR):  $\tilde{\nu}$  = 2197 cm<sup>-1</sup> (C≡N).

#### Synthesis of [Au(CH(CN)<sub>2</sub>)(IPr)] (9)

According to the general procedure, **2** (50 mg, 0.08 mmol), malononitrile (52.8 mg, 0.8 mmol, 10 equiv.) and toluene (0.5 mL) were used. After 1 hour at 60 °C, solvent was removed under reduced pressure and diethyl ether was added. The mixture was filtered over Celite® with additional diethyl ether and the filtrate was discarded. The filter plug was then washed with dichloromethane and the filtrate was dried under reduced pressure to give **9** as a white solid (yield not determined)

<sup>1</sup>H-NMR (500 MHz, CDCl<sub>3</sub>): δ = 7.54 (t, <sup>3</sup>J<sub>H,H</sub> = 7.8 Hz, 2H; *p*-PhH), 7.33 (d, <sup>3</sup>J<sub>H,H</sub> = 7.8 Hz, 4H; *m*-PhH), 7.21 (s, 2H; CH), 2.53 (h, <sup>3</sup>J<sub>H,H</sub> = 6.9 Hz, 4H; CH), 2.37 (s, 1H; CH), 1.34 (d, <sup>3</sup>J<sub>H,H</sub> = 6.9 Hz, 12H; CH<sub>3</sub>), 1.24 (d, <sup>3</sup>J<sub>H,H</sub> = 6.9 Hz, 12H; CH<sub>3</sub>). <sup>13</sup>C{<sup>1</sup>H}-NMR (126 MHz, CDCl<sub>3</sub>): δ = 184.7 (1C; C<sub>carb</sub>), 145.7 (4C; *o*-PhC), 133.7 (2C; *i*-PhC), 131.1 (2C; *p*-PhC), 124.5 (4C; *m*-PhC), 123.5 (2C; CH), 118.8 (1C; CN), 29.0 (4C; CH), 24.6 (4C; CH<sub>3</sub>), 24.2 (4C; CH<sub>3</sub>), -0.5 (4 C; CH). Anal. calcd for C<sub>30</sub>H<sub>37</sub>AuN<sub>4</sub>: C, 55.38; H, 5.73; N, 8.61. Found: C, 53.18; H, 4.62; N, 9.54. FTIR (ATR):  $\tilde{\nu}$  = 2214 cm<sup>-1</sup> (C≡N).

### Synthesis of [Au(CH(Ph)CN)(IPr)] (10)

According to the general procedure, **2** (100 mg, 0.17 mmol), phenylacetonitrile (19.4 mg, 1 equiv.) and toluene (2 mL) were used. After 1 hour at 80 °C and work-up, **10** was obtained as a white solid (102.4 mg, 86% yield).

$^1\text{H-NMR}$  (500 MHz,  $\text{CDCl}_3$ ):  $\delta$  = 7.48 (t,  $^3J_{\text{H,H}} = 7.8$  Hz, 2H; *p*-PhC), 7.26–7.22 (m, 4H; *m*-PhH), 7.12 (s, 2 H; CH), 6.93–6.89 (m, 2H; *m*-PhH), 6.76 (t,  $^3J_{\text{H,H}} = 7.3$  Hz, 1H; *p*-PhH), 6.64–6.62 (m, 2H; *o*-PhH), 2.95 (s, 1H;  $\text{CH}_2$ ), 2.47 (h,  $^3J_{\text{H,H}} = 6.9$  Hz, 2H; CH), 2.47 (h,  $^3J_{\text{H,H}} = 6.9$  Hz, 2H; CH), 1.22 (d,  $^3J_{\text{H,H}} = 6.9$  Hz, 6 H;  $\text{CH}_3$ ), 1.19 (d,  $^3J_{\text{H,H}} = 6.9$  Hz, 6H;  $\text{CH}_3$ ), 1.18 (d,  $^3J_{\text{H,H}} = 6.9$  Hz, 12H;  $\text{CH}_3$ ),  $^{13}\text{C}\{^1\text{H}\}$ -NMR (126 MHz,  $\text{CDCl}_3$ ):  $\delta$  = 189.3 (1C;  $\text{C}_{\text{carb}}$ ), 145.7 (4C; *o*-PhC), 142.7 (1C; *i*-PhC), 134.2 (2C; *i*-PhC), 130.5 (2C; *p*-PhC), 127.8 (2C; *o*-PhC), 127.5 (1C; C), 125.9 (2C; *m*-PhC), 124.2 (4C; *m*-PhC), 122.9 (2C; CH), 122.3 (1C; *p*-PhC), 28.9 (2C; CH), 28.8 (2C; CH), 24.4 (2C;  $\text{CH}_3$ ), 24.3 (2C;  $\text{CH}_3$ ), 24.1 (4C;  $\text{CH}_3$ ), 23.2 (1C; CH), Anal. calcd for  $\text{C}_{35}\text{H}_{42}\text{AuN}_3$ : C, 59.91; H, 6.03; N, 5.99. Found: C, 59.76; H, 5.94; N, 6.05. FTIR (ATR):  $\tilde{\nu} = 2193\text{ cm}^{-1}$  (C $\equiv$ N).

### Synthesis of [Au(CH<sub>2</sub>NO<sub>2</sub>)(IPr)] (11)

According to the general procedure, **2** (100 mg, 0.17 mmol) and nitromethane (0.2 mL) were used. After 1 hour at 60 °C and work-up, **11** was obtained as a white solid (65.0 mg, 65 % yield).

$^1\text{H-NMR}$  (500 MHz,  $\text{CDCl}_3$ ):  $\delta$  = 7.51 (t,  $^3J_{\text{H,H}} = 7.8$  Hz, 2H; *p*-PhH), 7.29 (d,  $^3J_{\text{H,H}} = 7.8$  Hz, 4H; *m*-PhH), 7.15 (s, 2H; CH), 4.32 (s, 2H;  $\text{CH}_2$ ), 2.54 (h,  $^3J_{\text{H,H}} = 6.9$  Hz, 4H; CH), 1.30 (d,  $^3J_{\text{H,H}} = 6.9$  Hz, 12H;  $\text{CH}_3$ ), 1.22 (d,  $^3J_{\text{H,H}} = 6.9$  Hz, 12H;  $\text{CH}_3$ ).  $^{13}\text{C}\{^1\text{H}\}$ -NMR (126 MHz,  $\text{CDCl}_3$ ):  $\delta$  = 189.8 (1C;  $\text{C}_{\text{carb}}$ ), 145.8 (4C; *o*-PhC), 134.1 (2C; *i*-PhC), 130.7 (2C; *p*-PhC), 124.3 (4C; *m*-PhC), 123.2 (2C; CH), 74.9 (1C;  $\text{CH}_2$ ), 28.9 (4C; CH), 24.5 (4C;  $\text{CH}_3$ ), 24.1 (4C;  $\text{CH}_3$ ), Anal. calcd for  $\text{C}_{28}\text{H}_{38}\text{AuN}_3\text{O}_2$ : C, 52.09; H, 5.93; N, 6.51. Found: C, 52.08; H, 6.01; N, 6.47. FTIR (ATR):  $\tilde{\nu} = 1358\text{ cm}^{-1}$  (N=O).

### Synthesis of [Au(CH(CH<sub>3</sub>)NO<sub>2</sub>)(IPr)] (12)

According to the general procedure, **2** (100 mg, 0.08 mmol) and nitroethane (0.5 mL) were used. After 2 hours at 60 °C and work-up, **12** was obtained as a white solid (52.6 mg, 96 % yield).

$^1\text{H-NMR}$  (500 MHz,  $\text{CDCl}_3$ ):  $\delta$  = 7.50 (t,  $^3J_{\text{H,H}} = 8.0$  Hz, 2H; *p*-PhH), 7.29 (d,  $^3J_{\text{H,H}} = 7.8$  Hz, 4H; *m*-PhH), 7.14 (s, 2H; CH), 2.58 (h,  $^3J_{\text{H,H}} = 6.9$  Hz, 4H; CH), 4.40 (q,  $^3J_{\text{H,H}} = 6.5$  Hz, 1H; CH), 1.31 (d,  $^3J_{\text{H,H}} = 6.8$  Hz, 6H;  $\text{CH}_3$ ), 1.30 (d,  $^3J_{\text{H,H}} = 6.9$  Hz, 6H;  $\text{CH}_3$ ), 1.29 (d,  $^3J_{\text{H,H}} = 6.5$  Hz, 3H; CH), 1.21 (d,  $^3J_{\text{H,H}} = 6.9$  Hz, 12H;  $\text{CH}_3$ ).  $^{13}\text{C}\{^1\text{H}\}$ -NMR (126 MHz,  $\text{CDCl}_3$ ):  $\delta$  = 189.1 (1C;  $\text{C}_{\text{carb}}$ ), 145.8 (4C; *o*-PhC), 134.1 (2C; *i*-PhC), 130.7 (2C; *p*-PhC), 124.2 (4C; *m*-PhC), 123.1 (2C; CH), 83.6 (1C; C), 28.9 (4C; CH), 24.5 (4C;  $\text{CH}_3$ ), 24.1 (4C;  $\text{CH}_3$ ), 19.8 (4C; CH). Anal. calcd for  $\text{C}_{29}\text{H}_{40}\text{AuN}_3\text{O}_2$ : C, 52.81; H, 6.11; N, 6.37. Found: C, 52.78; H, 6.15; N, 6.32. FTIR (ATR):  $\tilde{\nu} = 1334\text{ cm}^{-1}$  (N=O).

## 4. NMR Spectra

Figure S1.  $^1\text{H-NMR}$  spectrum of  $[\text{Au}(\text{CH}_3)(\text{IPr})]$  (**3**) in  $\text{CDCl}_3$  at ambient temperature.

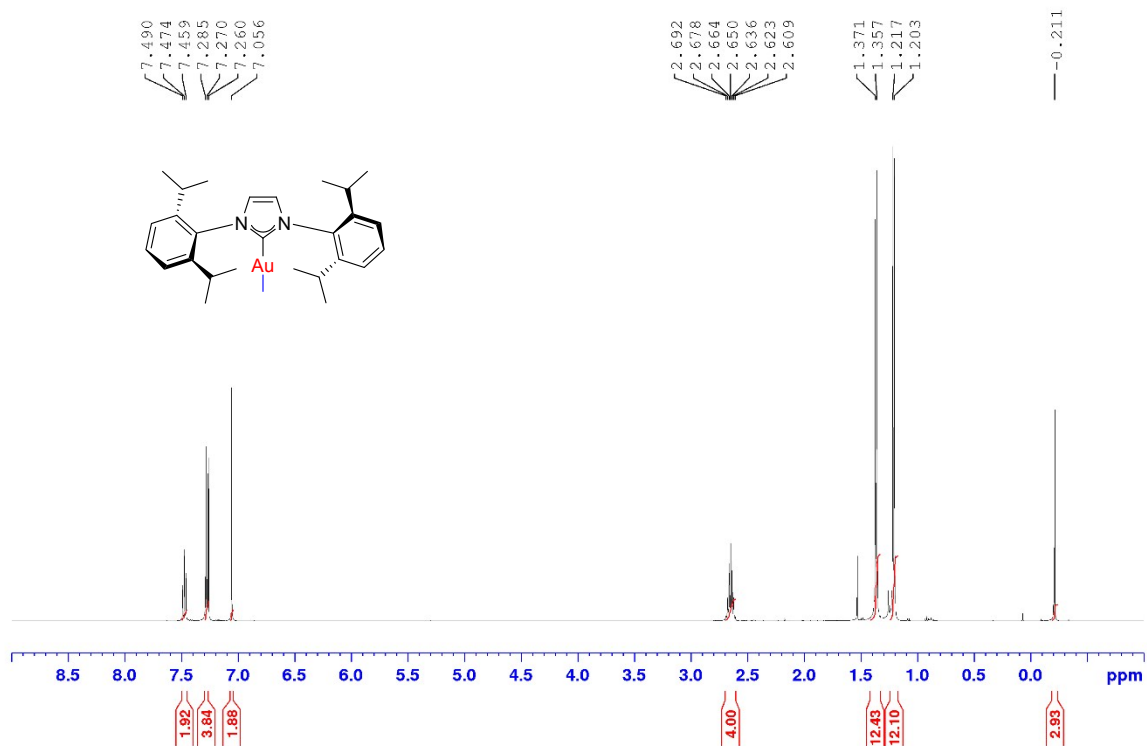
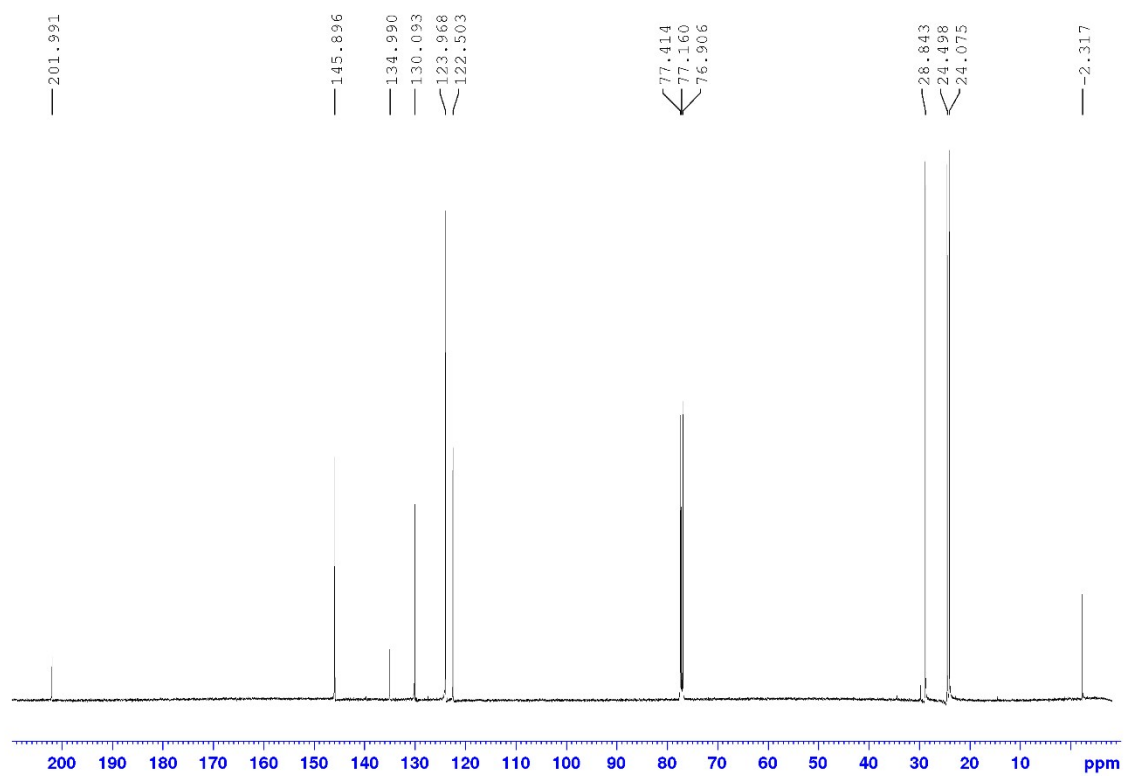
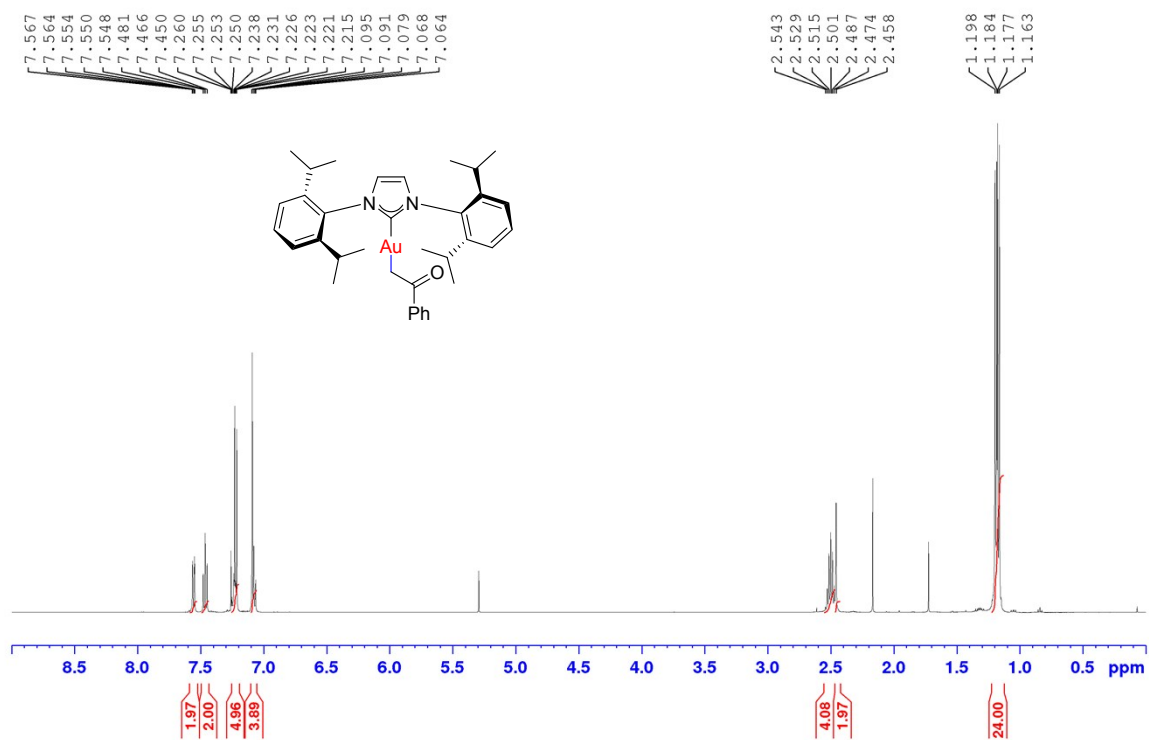


Figure S2.  $^{13}\text{C}\{^1\text{H}\}$ -NMR spectrum of  $[\text{Au}(\text{CH}_3)(\text{IPr})]$  (**3**) in  $\text{CDCl}_3$  at ambient temperature.



**Figure S3.**  $^1\text{H-NMR}$  spectrum of  $[\text{Au}(\text{CH}_2\text{C}(\text{O})\text{Ph})(\text{IPr})]$  (**7**) in  $\text{CDCl}_3$  at ambient temperature.



**Figure S4.**  $^{13}\text{C}\{^1\text{H}\}$ -NMR spectrum of  $[\text{Au}(\text{CH}_2\text{C}(\text{O})\text{Ph})(\text{IPr})]$  (**7**) in  $\text{CDCl}_3$  at ambient temperature.

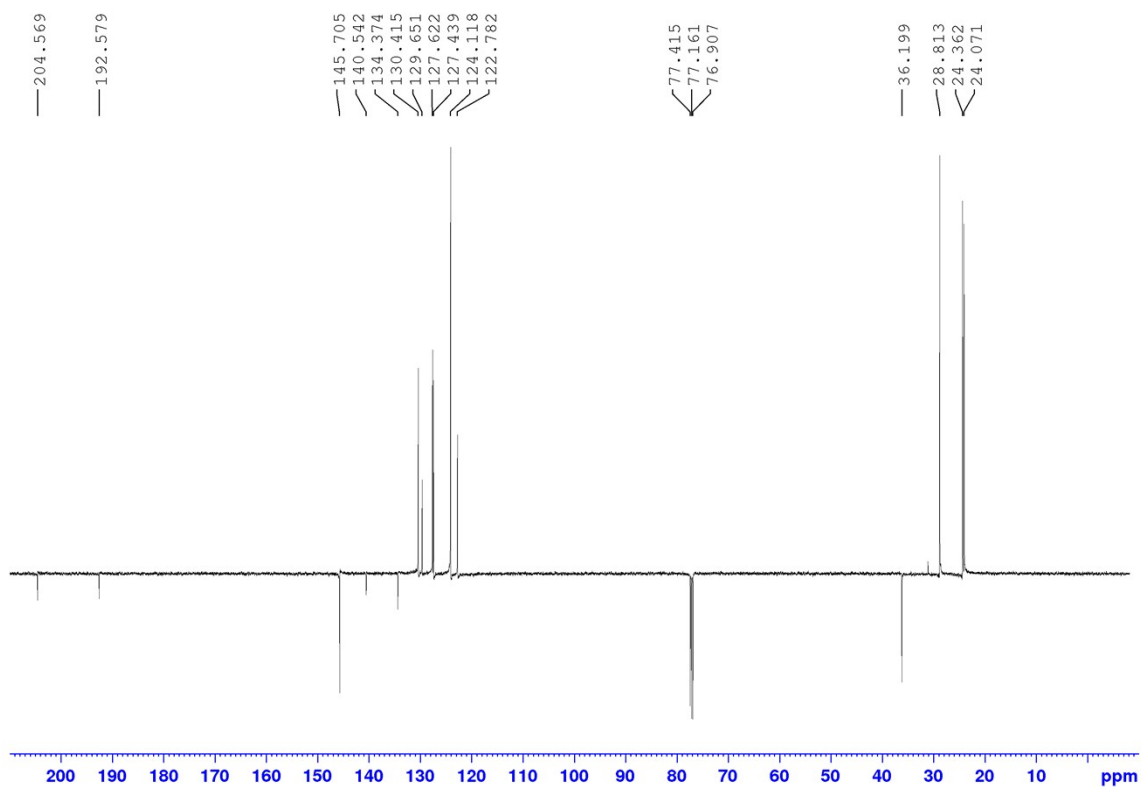


Figure S5.  $^1\text{H}$ -NMR spectrum  $[\text{Au}(\text{CH}_2\text{CN})(\text{IPr})]$  (**8**) in  $\text{CDCl}_3$  at ambient temperature.

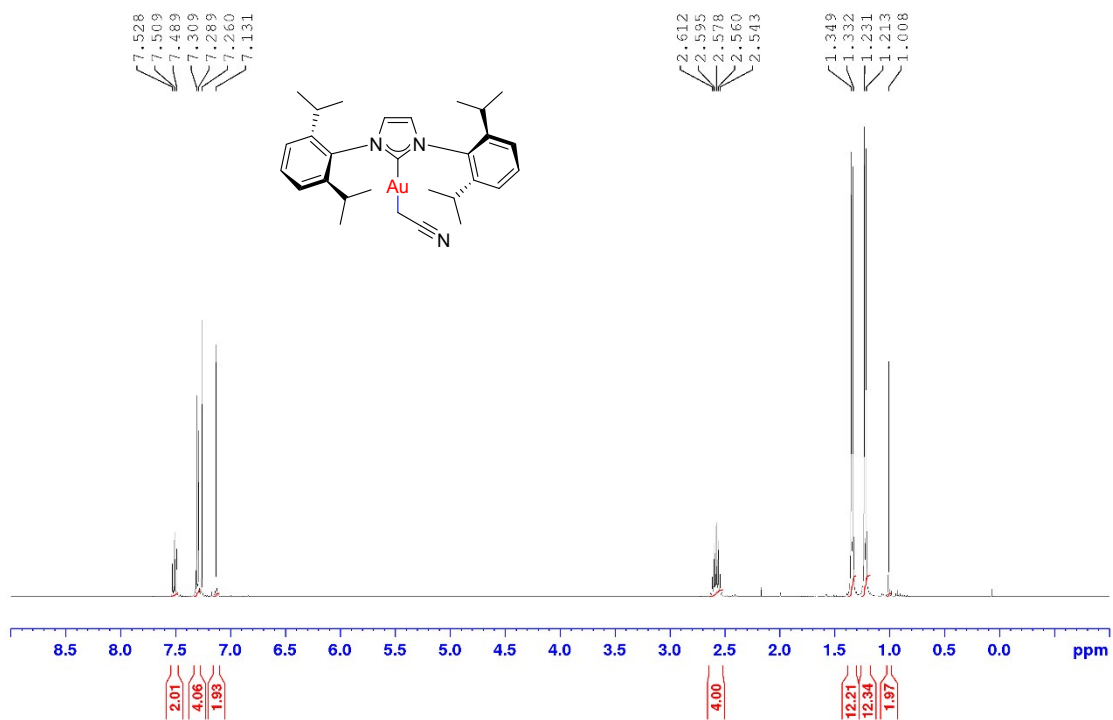


Figure S6.  $^{13}\text{C}\{^1\text{H}\}$ -NMR spectrum of  $[\text{Au}(\text{CH}_2\text{CN})(\text{IPr})]$  (**8**) in  $\text{CDCl}_3$  at ambient temperature.

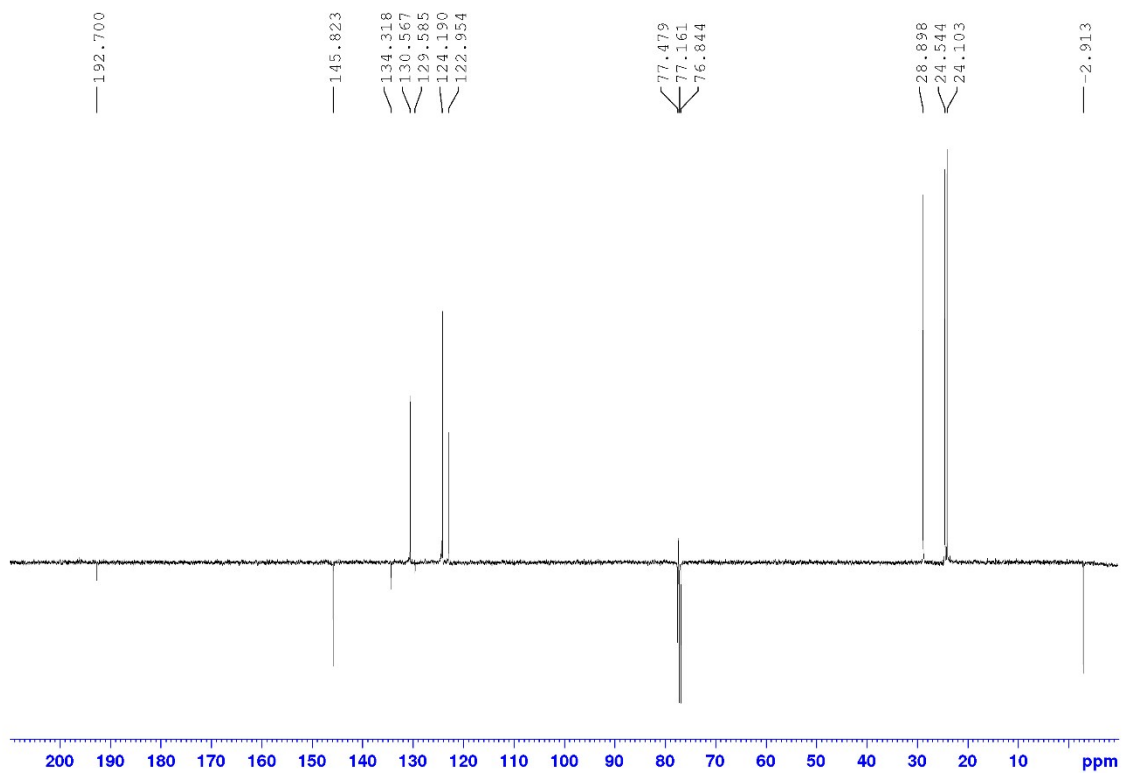


Figure S7.  $^1\text{H}$ -NMR spectrum of  $[\text{Au}(\text{CH}(\text{CN})_2)(\text{IPr})]$  (**9**) in  $\text{CDCl}_3$  at ambient temperature.

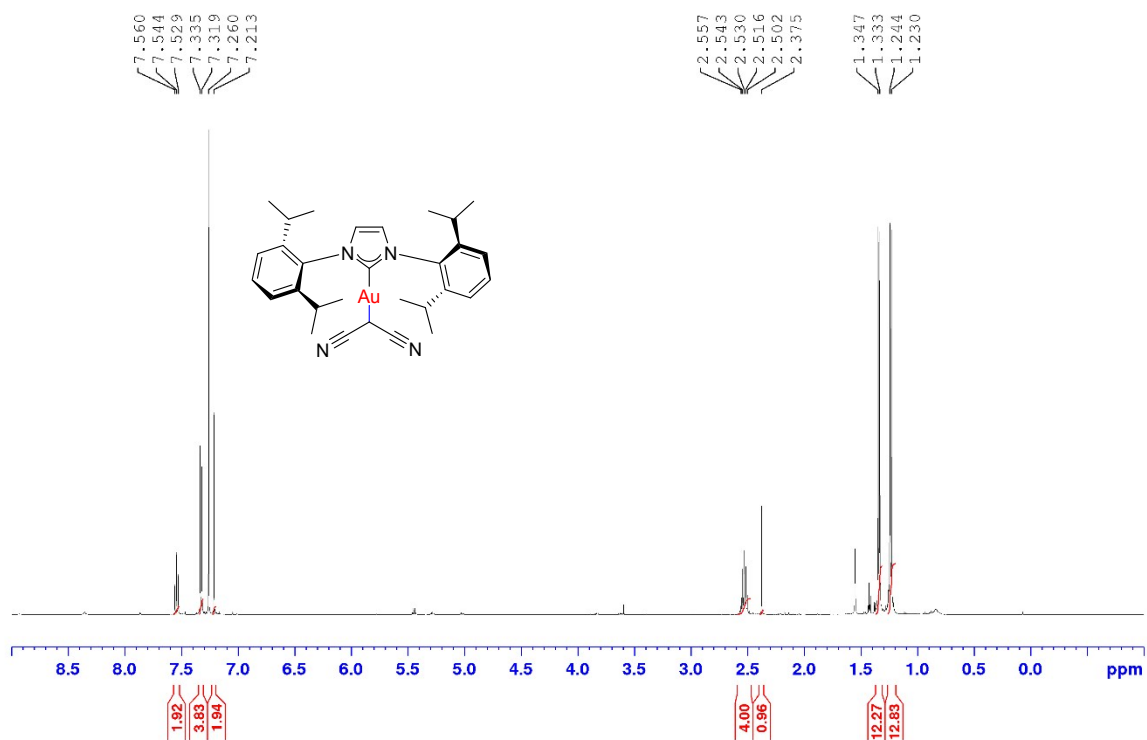


Figure S8.  $^{13}\text{C}\{^1\text{H}\}$ -NMR spectrum of  $[\text{Au}(\text{CH}(\text{CN})_2)(\text{IPr})]$  (**9**) in  $\text{CDCl}_3$  at ambient temperature.

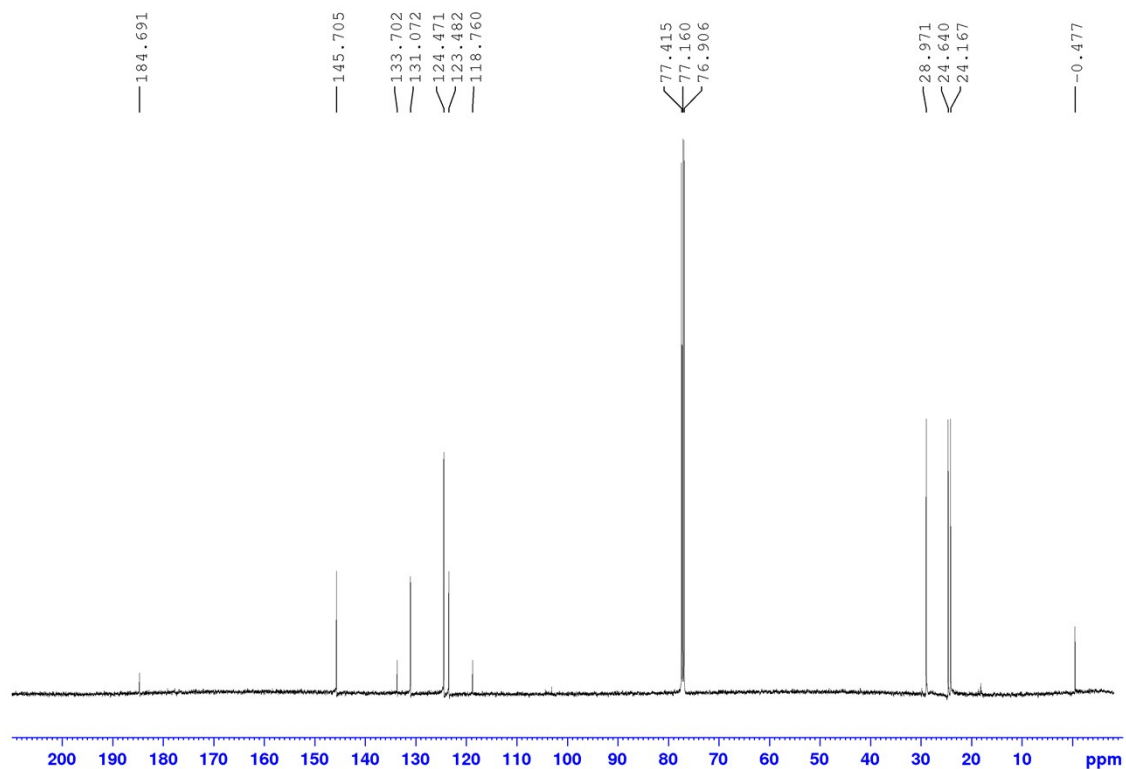


Figure S9.  $^1\text{H}$ -NMR spectrum of  $[\text{Au}(\text{CH}(\text{Ph})\text{CN})(\text{IPr})]$  (**10**) in  $\text{CDCl}_3$  at ambient temperature.

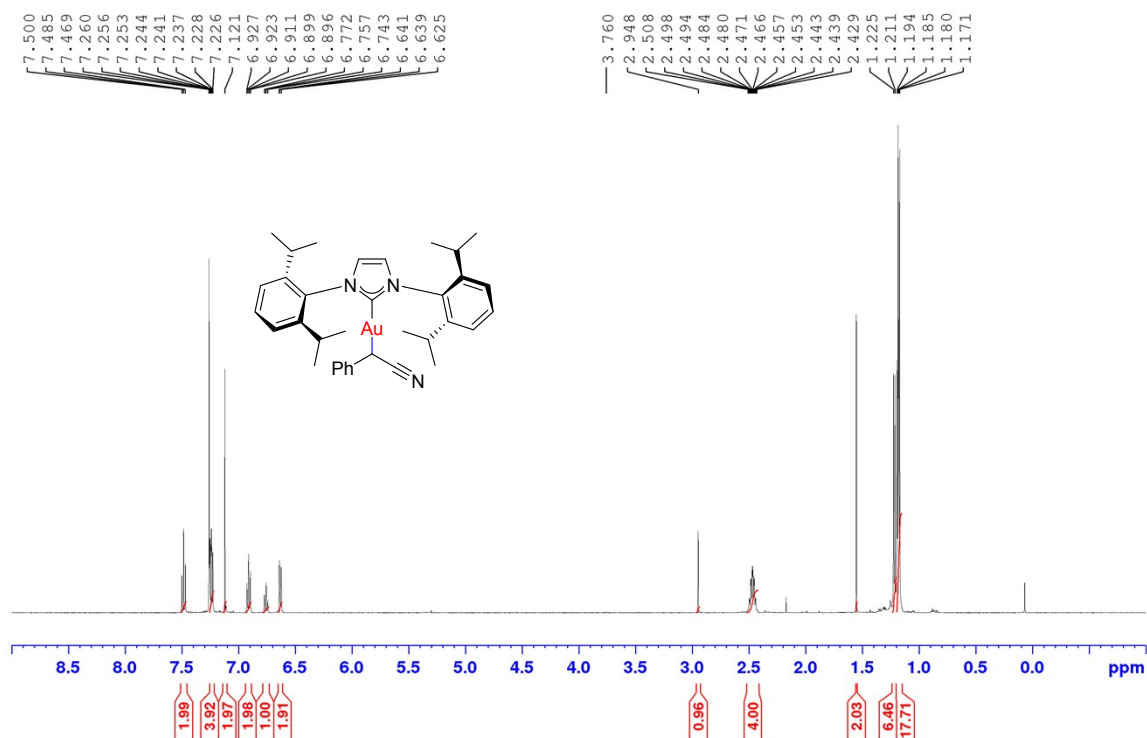


Figure S10.  $^{13}\text{C}\{^1\text{H}\}$ -NMR spectrum of  $[\text{Au}(\text{CH}(\text{Ph})\text{CN})(\text{IPr})]$  (**10**) in  $\text{CDCl}_3$  at ambient temperature.

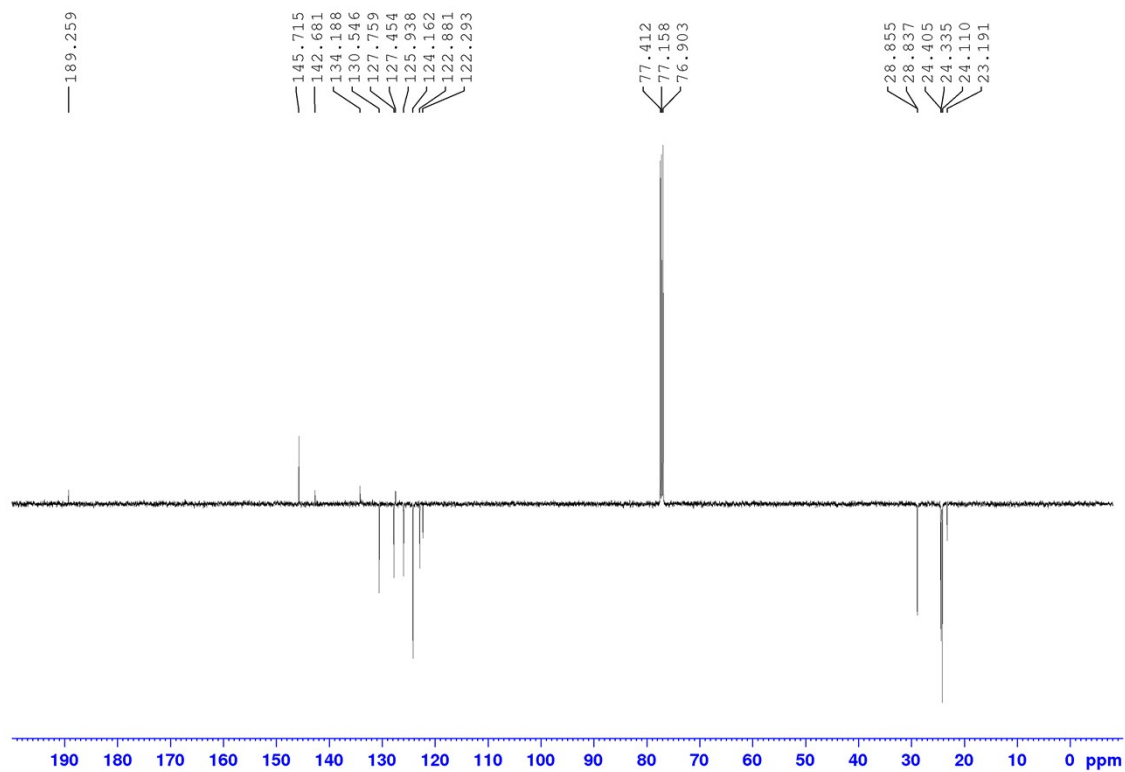
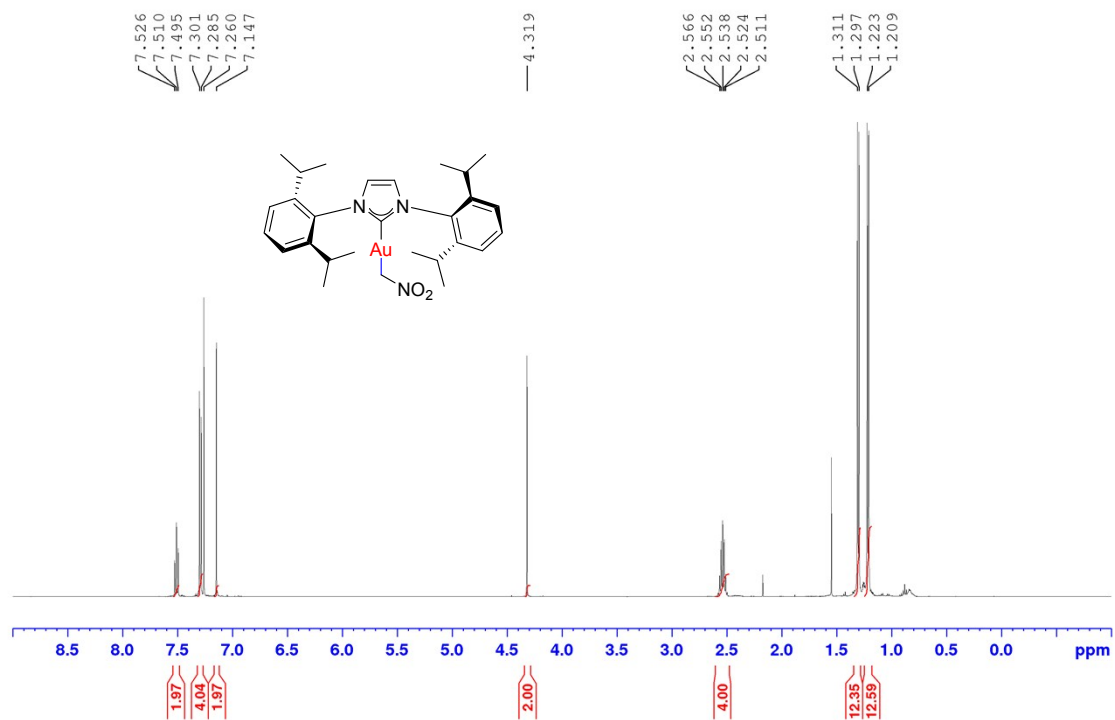


Figure S11.  $^1\text{H}$ -NMR spectrum of  $[\text{Au}(\text{CH}_2\text{NO}_2)(\text{IPr})]$  (**11**) in  $\text{CDCl}_3$  at ambient temperature.



$^{13}\text{C}\{^1\text{H}\}$ -NMR spectrum of  $[\text{Au}(\text{CH}_2\text{NO}_2)(\text{IPr})]$  (**11**) in  $\text{CDCl}_3$  at ambient temperature.

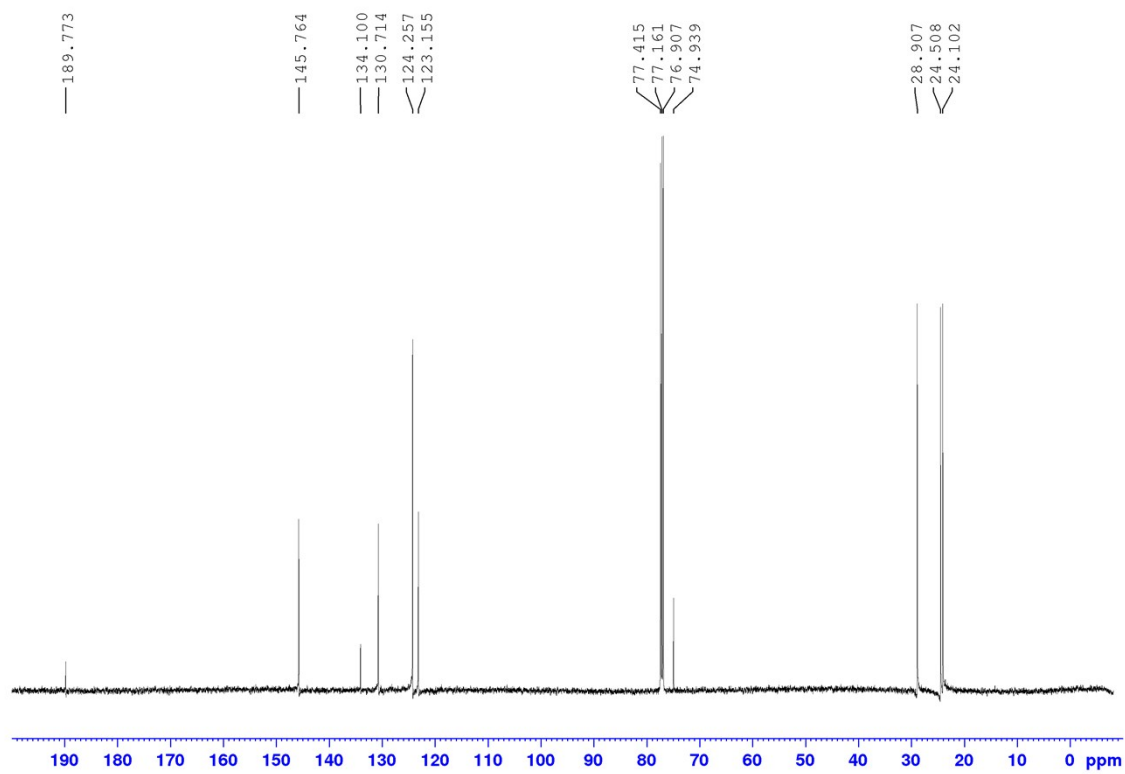
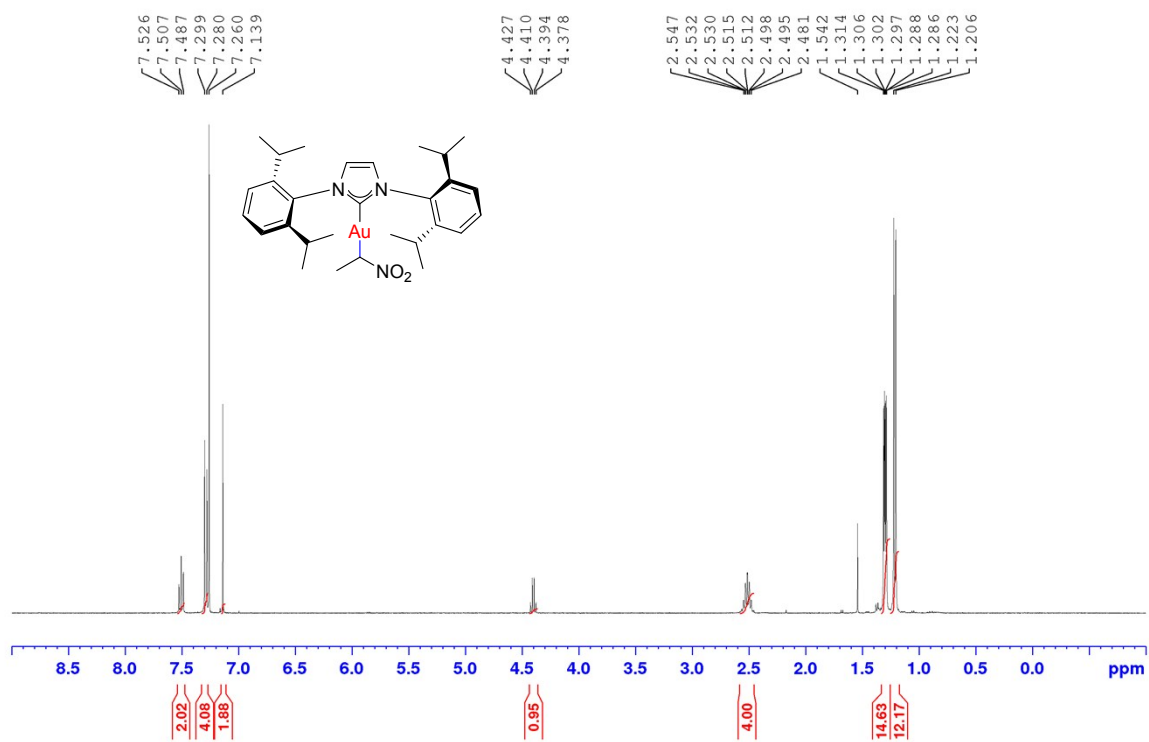
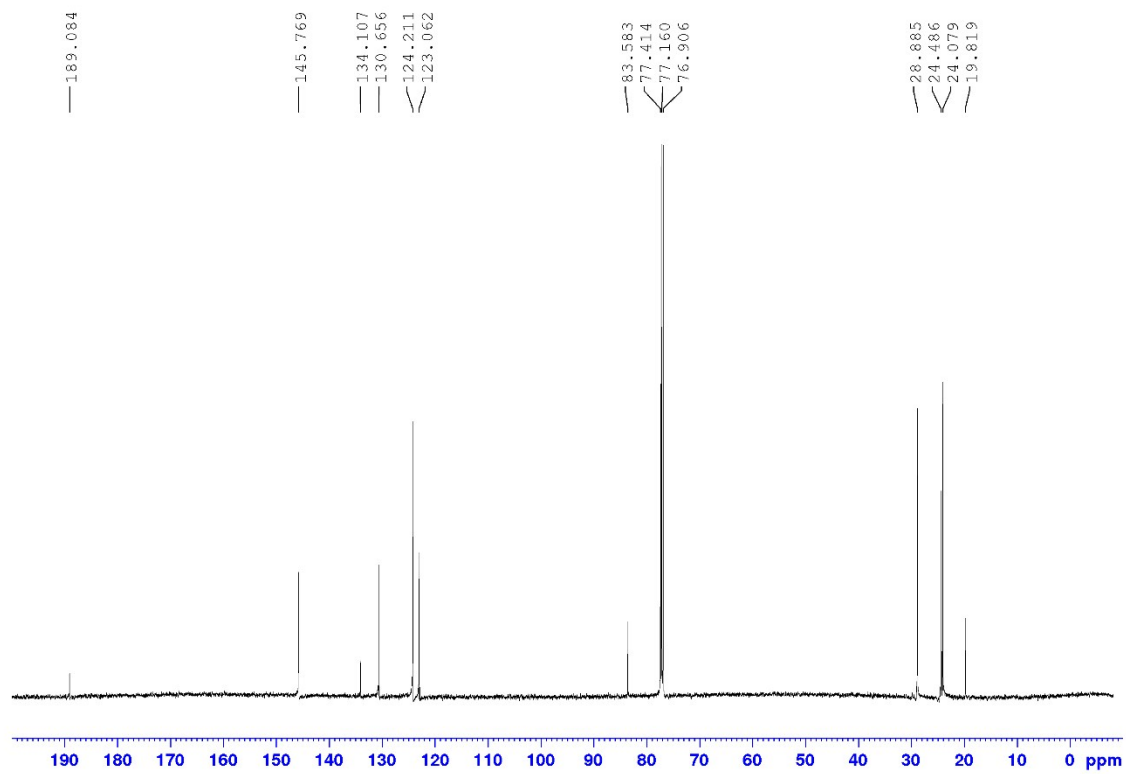


Figure S12.  $^1\text{H}$ -NMR spectrum of  $[\text{Au}(\text{CH}(\text{CH}_3)\text{NO}_2)]$  (**12**) in  $\text{CDCl}_3$  at ambient temperature.



$^{13}\text{C}\{^1\text{H}\}$ -NMR spectrum of  $[\text{Au}(\text{CH}(\text{CH}_3)\text{NO}_2)]$  (**12**) in  $\text{CDCl}_3$  at ambient temperature.



## 5. Solid-state ATR-IR Spectra

Figure S13. Spectrum of  $[\text{Au}(\text{CH}(\text{COCH}_3)_2(\text{IPr}))]$  (**5**). FTIR (ATR):  $\tilde{\nu} = 1635 \text{ cm}^{-1}$  (C=O).

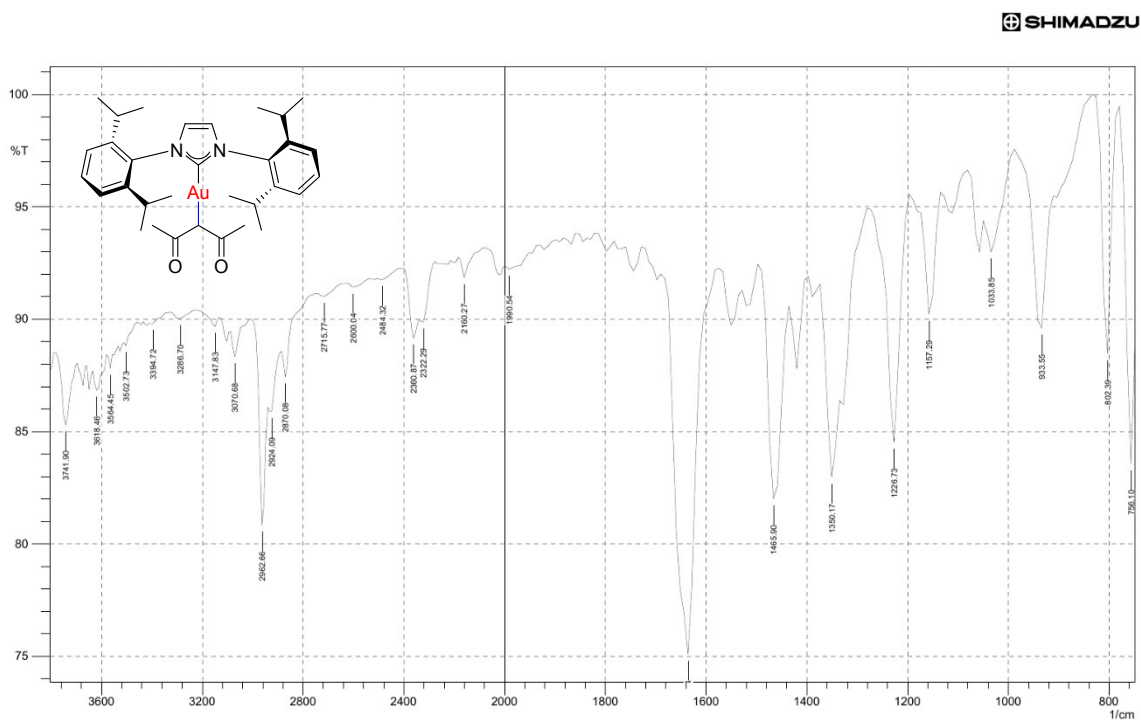


Figure S14. Spectrum of  $[\text{Au}(\text{CH}_2\text{COPh})(\text{IPr})]$  (**7**). FTIR (ATR):  $\tilde{\nu} = 1620 \text{ cm}^{-1}$  (C=O).

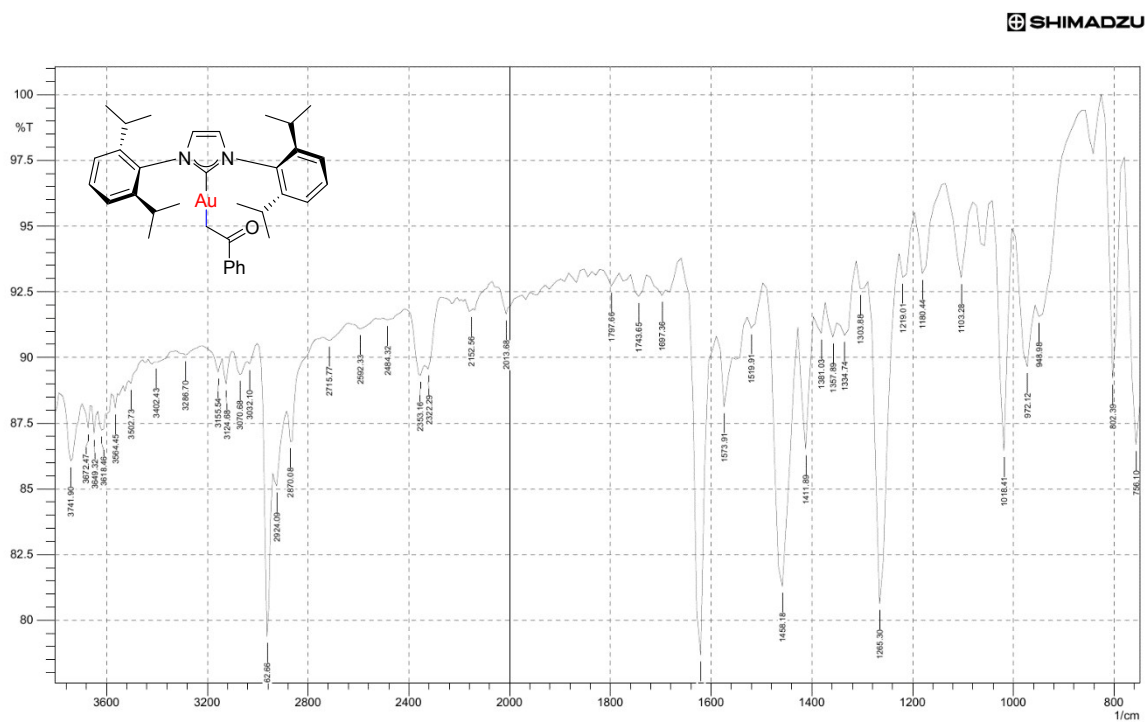


Figure S15. Spectrum of [Au(CH<sub>2</sub>CN)(IPr)] (8). FTIR (ATR):  $\tilde{\nu} = 2197 \text{ cm}^{-1}$  (C≡N).

SHIMADZU

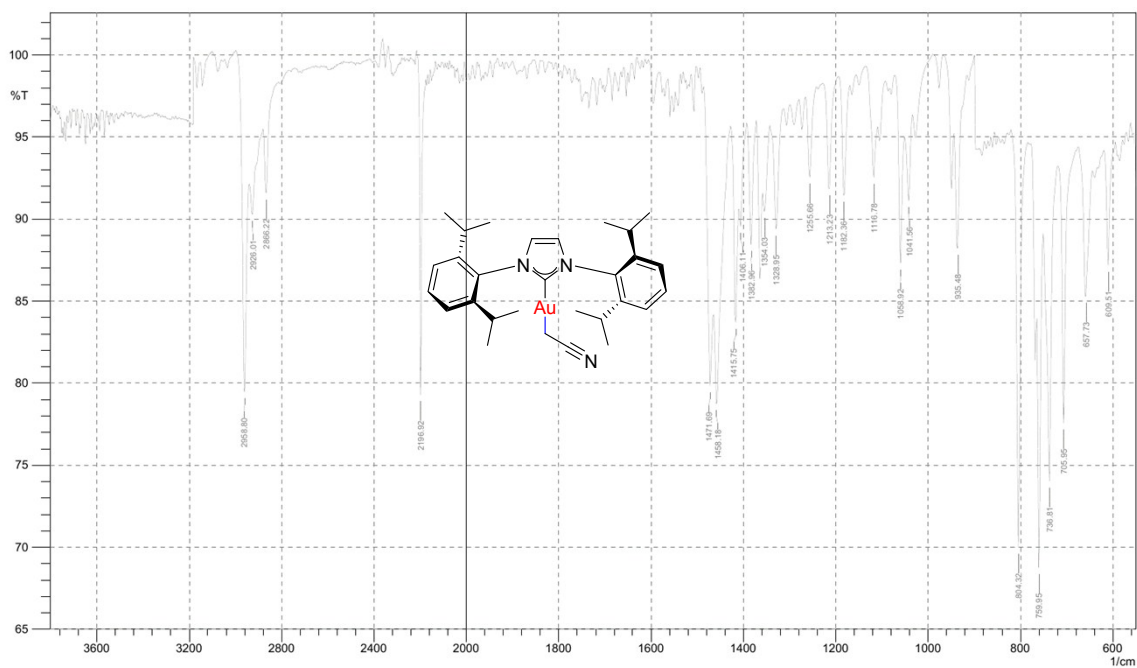


Figure S16. Spectrum of [Au(CH(CN)<sub>2</sub>)(IPr)] (9). FTIR (ATR):  $\tilde{\nu} = 2214 \text{ cm}^{-1}$  (C≡N).

SHIMADZU

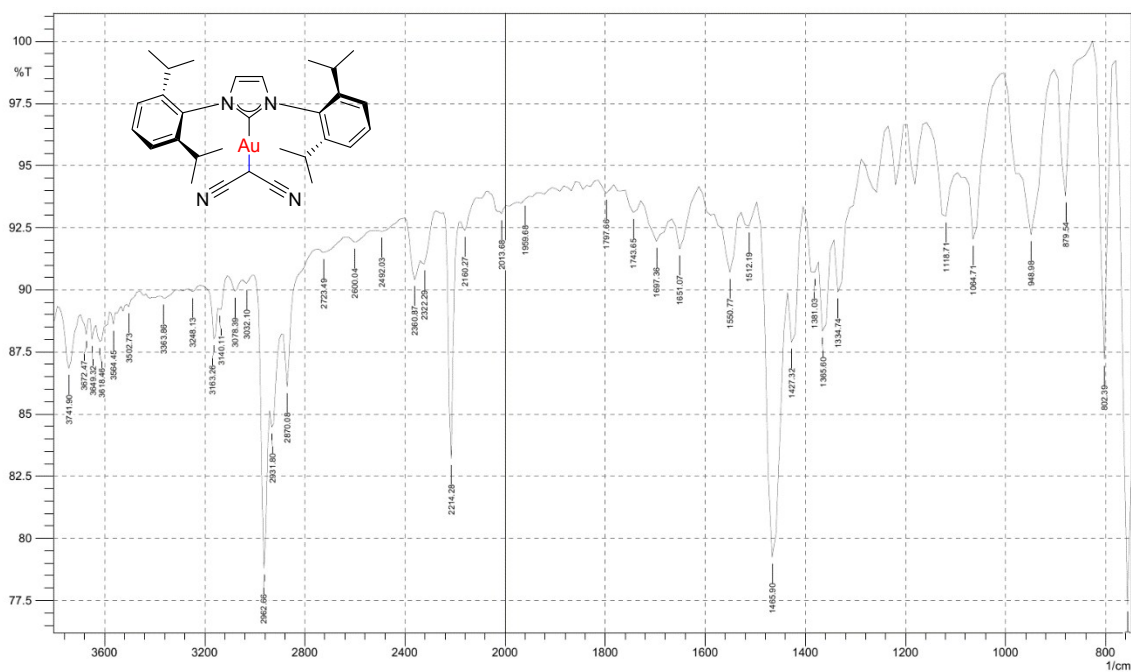


Figure S17. Spectrum of  $[\text{Au}(\text{CH}(\text{Ph})\text{CN})(\text{IPr})]$  (**10**). FTIR (ATR):  $\tilde{\nu} = 2193 \text{ cm}^{-1}$  ( $\text{C}\equiv\text{N}$ ).

SHIMADZU

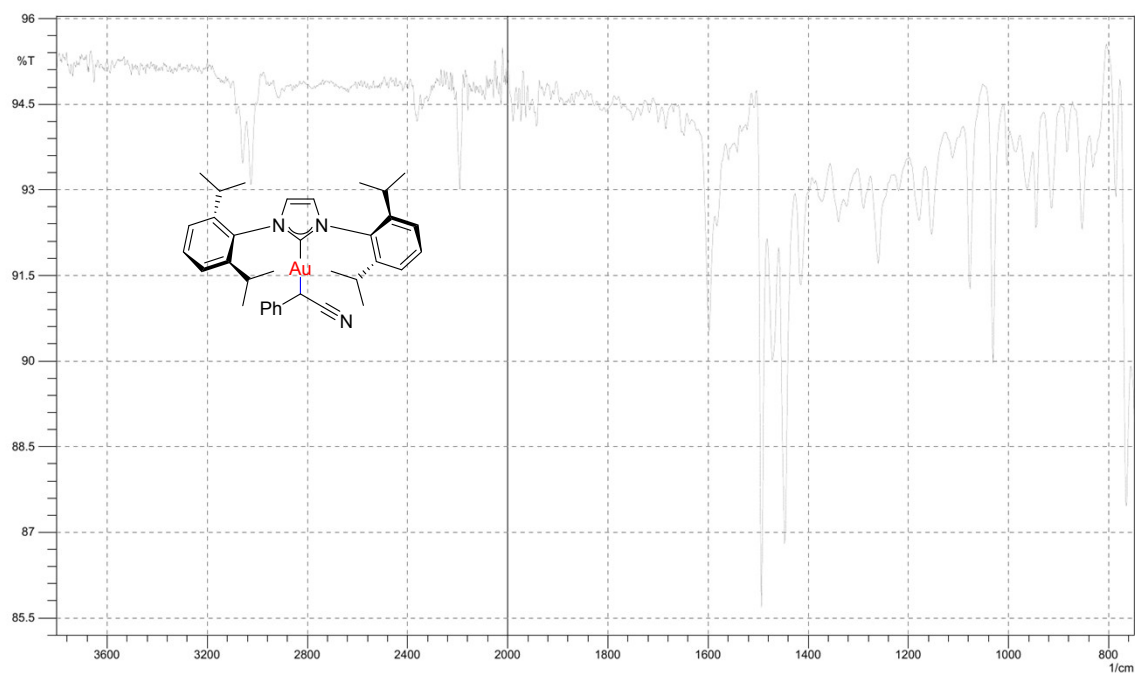


Figure S18.

Figure S19. Spectrum of  $[\text{Au}(\text{CH}_2\text{NO}_2)(\text{IPr})]$  (**11**). FTIR (ATR):  $\tilde{\nu} = 1358 \text{ cm}^{-1}$  ( $\text{N}=\text{O}$ ).

SHIMADZU

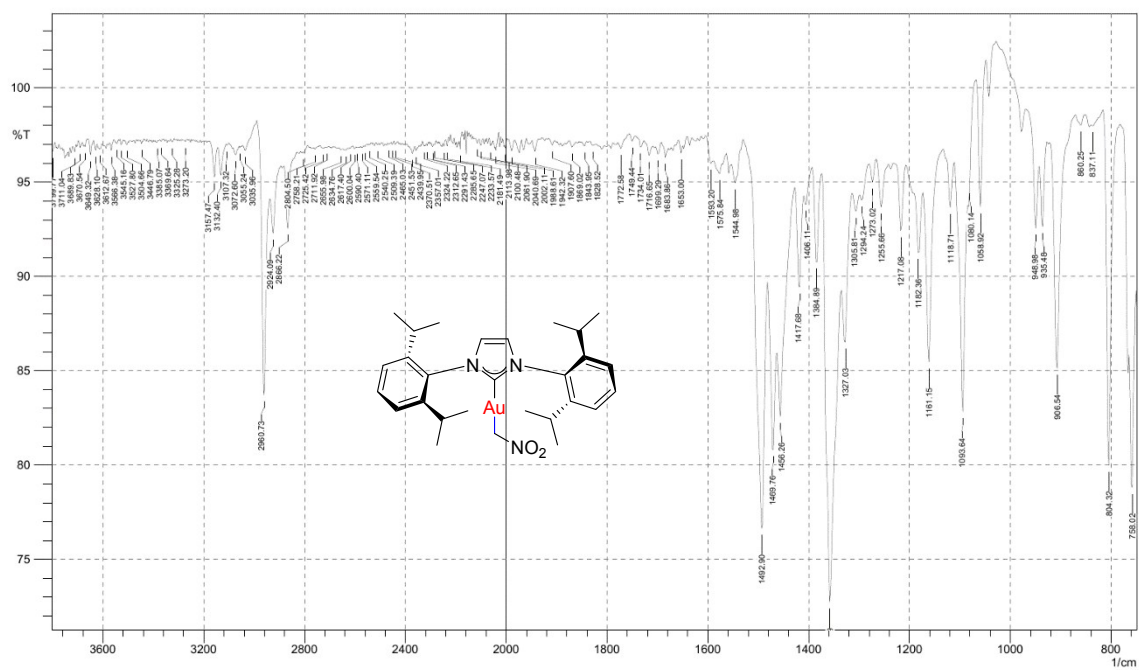
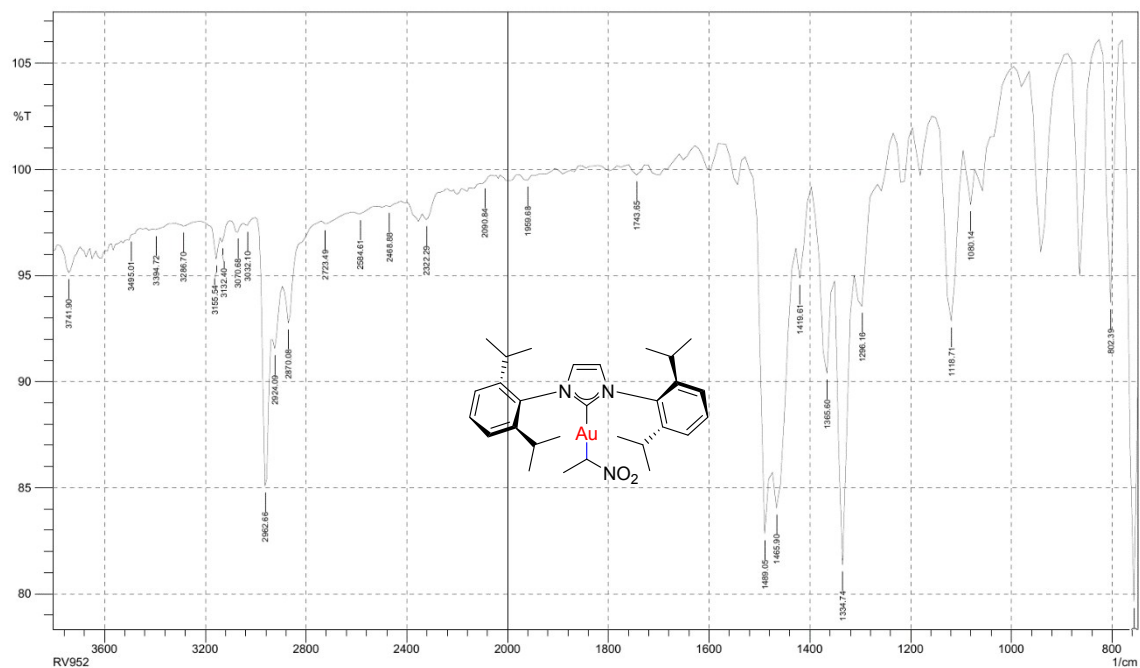


Figure S20. Spectrum of  $[\text{Au}(\text{CH}(\text{CH}_3)\text{NO}_2)(\text{IPr})]$  (**12**). FTIR (ATR):  $\tilde{\nu} = 1334 \text{ cm}^{-1}$  (N=O).

SHIMADZU



## 6. Solid-state structures

### Crystallographic information

Crystals suitable for X-ray diffraction studies were grown from slow diffusion of pentane into solutions of [Au(CH<sub>2</sub>C(O)Ph)(IPr)] (**7**), [Au(CH<sub>2</sub>CN)(IPr)] (**8**) and [Au(CH(CH<sub>3</sub>)NO<sub>2</sub>)(IPr)] (**12**) in dichloromethane, of hexanes into solutions of [Au(CH<sub>2</sub>(CN)<sub>2</sub>)(IPr)] (**9**) and [Au(CH<sub>2</sub>NO<sub>2</sub>)(IPr)] (**11**) in dichloromethane, and of pentane into a solution of [Au(CH(Ph)CN)(IPr)] (**10**) in acetone. X-ray diffraction data for compound **7** were collected at 173 K using a Rigaku SCXmini CCD system with a SHINE monochromator (Mo K $\alpha$  radiation,  $\lambda = 0.71075$  Å). Diffraction data for compounds **8–12** were collected at either 173 K (**8, 10–12**) or 93 K (**9**) by using a Rigaku FR-X Ultrahigh Brilliance Microfocus RA generator/confocal optics and XtaLAB P200 system (Mo K $\alpha$  radiation,  $\lambda = 0.71075$  Å). Intensity data were collected using  $\omega$  steps accumulating area detector images spanning at least a hemisphere of reciprocal space. All data were corrected for Lorentz polarization effects. A multiscan absorption correction was applied by using CrystalClear.<sup>10</sup> Structures were solved by Patterson (PATTY),<sup>11</sup> intrinsic phasing (SHELXT),<sup>12</sup> or direct (SIR2011)<sup>13</sup> methods and refined by full-matrix least-squares against F<sup>2</sup> (SHELXL-2014).<sup>14</sup> Non-hydrogen atoms were refined anisotropically, and hydrogen atoms were refined using a riding model. All calculations were performed using the CrystalStructure.<sup>15</sup>

**Table S1.** Crystallographic data for **7, 8** and **10-12**.

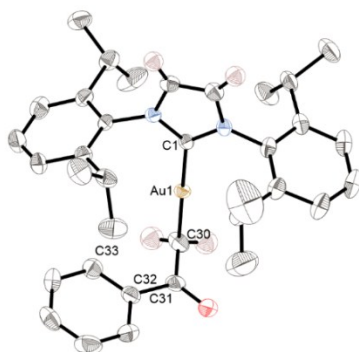
	<b>7</b>	<b>8</b> ·(CH <sub>2</sub> Cl <sub>2</sub> ) <sub>1/2</sub>	<b>9</b> ·(C <sub>6</sub> H <sub>12</sub> ) <sub>1/4</sub>	<b>10</b>	<b>11</b>	<b>12</b> ·EtOAc
Formula	C <sub>35</sub> H <sub>43</sub> AuN <sub>2</sub> O	C <sub>29.5</sub> H <sub>39</sub> AuCl <sub>2</sub> N <sub>3</sub>	C <sub>30</sub> H <sub>37</sub> AuN <sub>4</sub>	C <sub>35</sub> H <sub>42</sub> AuN <sub>3</sub>	C <sub>29.5</sub> H <sub>41</sub> AuN <sub>3</sub> O <sub>2</sub>	C <sub>29</sub> H <sub>40</sub> AuN <sub>3</sub> O <sub>2</sub>
M / g × mol <sup>-1</sup>	704.70	668.07	650.62	701.70	666.63	659.62
Dimensions	0.36x0.21x0.18	0.15x0.15x0.04	0.10x0.10x0.02	0.21x0.03x0.02	0.20x0.10x0.02	0.12x0.05x0.03
Appearance	colourless prism	colourless prism	colourless platelet	colourless prism	colourless platelet	colourless chip
Crystal system	monoclinic	monoclinic	triclinic	monoclinic	orthorhombic	triclinic
Space group	P2 <sub>1</sub> /c	P2 <sub>1</sub> /c	p $\bar{1}$	P2 <sub>1</sub>	Cmce	p $\bar{1}$
$\rho_{\text{calc}} / \text{g} \times \text{cm}^3$	1.501	1.516	1.475	1.434	1.481	1.495
a / Å	13.5755(11)	18.3600(11)	9.124(2)	9.4018(10)	17.633(3)	9.0077(6)
b / Å	15.6401(14)	19.2696(14)	10.042(2)	17.0518(16)	19.164(3)	9.9502(8)
c / Å	14.707(2)	16.5604(12)	18.195(4)	10.6058(12)	17.699(3)	17.9844(18)
$\alpha / ^\circ$	90	90	95.388(2)	90	90	82.893(7)
$\beta / ^\circ$	93.344(7)	91.999(2)	95.668(3)	107.126(3)	90	86.365(8)
$\gamma / ^\circ$	90	90	116.658(5)	90	90	66.360(5)
V / Å <sup>3</sup>	3117.3(6)	5855.3(7)	1464.6(5)	1624.9(3)	5980.8(17)	1465.1(2)
Z	4	8	2	2	8	2
# reflections	32313	70349	35281	20048	20364	18146
# unique reflections	7122	10675	5322	5874	2842	5308
# variables	360	638	316	360	175	325
R <sub>1</sub> [I > 2 $\sigma$ (I)]	0.0228	0.0209	0.0603	0.0194	0.0207	0.0389
wR <sub>2</sub> (all data)	0.0516	0.0510	0.1609	0.0374	0.0639	0.0930
GOF	1.011	1.079	1.017	0.918	1.077	1.084

## 7. Thermal ellipsoid representation and assignments

Thermal ellipsoid representations of  $[\text{Au}(\text{CR}_2\text{H})(\text{IPr})]$  (**7-8** and **10-12**) are drawn at 50% probability and most hydrogen atoms and molecules of solvent are omitted for clarity. Atoms on the carbene and the carbanion are labelled as  $\text{C}^2$ ,  $\text{C}^\alpha$  and  $\text{C}^\beta$  (Figure 1). Labels  $\text{C}^{\text{ipso}}$  and  $\text{C}^{\text{ortho}}$  are defined for aromatic moieties in the  $\text{CR}_2\text{H}^-$  ligands.

**Pane S1.** Structure and assignment of  $[\text{Au}(\text{CH}_2\text{C}(\text{O})\text{Ph})]$  (**7**).

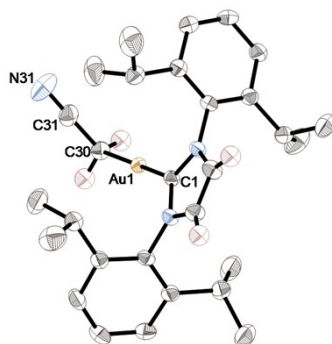
**Figure S21.** Thermal ellipsoid representation. **Table S2.** Assignments.



Atom label	Assignment
C1	$\text{C}^2$
C30	$\text{C}^\alpha$
C31	$\text{C}^\beta$
C32	$\text{C}^{\text{ipso}}$
C33	$\text{C}^{\text{ortho}}$

**Pane S2.** Structure and assignment of  $[\text{Au}(\text{CH}_2\text{CN})(\text{IPr})]$  (**8**).

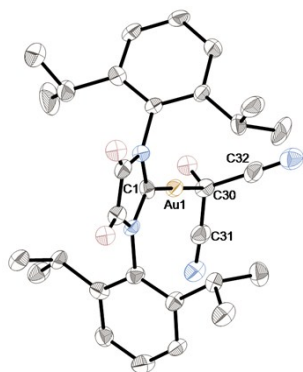
**Figure S22.** Thermal ellipsoid representation. **Table S3.** Assignments.



Atom label	Assignment
C1	$\text{C}^2$
C30	$\text{C}^\alpha$
C31	$\text{C}^\beta$

**Pane S3.** Structure and assignment  $[\text{Au}(\text{CH}(\text{CN})_2)(\text{IPr})]$  (**9**).

**Figure S23.** Thermal ellipsoid representation. **Table S4.** Assignments.



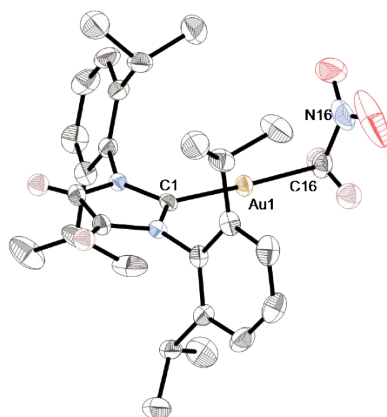
Atom label	Assignment
C1	$\text{C}^2$
C30	$\text{C}^\alpha$
C31	$\text{C}^\beta$
C32	$\text{C}^{\beta'}$

**Pane S4.** Structure and assignment of  $[\text{Au}(\text{CH}(\text{Ph})\text{CN})(\text{IPr})]$  (**10**).  
**Figure S24.** Thermal ellipsoid representation. **Table S5.** Assignments.



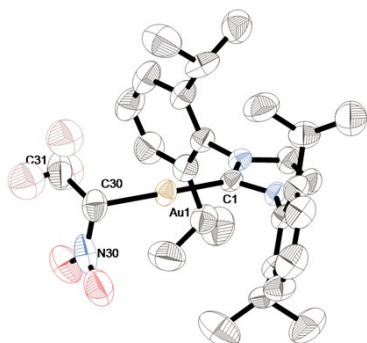
Atom label	Assignment
C1	C <sup>2</sup>
C30	C <sup>α</sup>
C31	C <sup>β</sup>
C32	C <sup>β'</sup> / C <sup>ipso</sup>
C33	C <sup>ortho</sup>

**Pane S5.** Structure and assignment of  $[\text{Au}(\text{CH}_2\text{NO}_2)(\text{IPr})]$  (**11**).  
**Figure S25.** Thermal ellipsoid representation. **Table S6.** Assignments.



Atom label	Assignment
C1	C <sup>2</sup>
C16	C <sup>α</sup>

**Pane S6.** Structure and assignment of  $[\text{Au}(\text{CH}(\text{CH}_3)\text{NO}_2)(\text{IPr})]$  (**12**).  
**Figure S26.** Thermal ellipsoid representation. **Table S7.** Assignments.



Atom label	Assignment
C1	C <sup>2</sup>
C30	C <sup>α</sup>
C31	C <sup>β</sup>

### Inspection and comparison with literature data

All experimentally measured bond lengths, angles as well as those from computationally modelled (DFT) structures and derived parameters are given in the tables in Section 10.8.

### Bond lengths in functional groups

Slight elongation of the C=O bond in  $[\text{Au}(\text{CH}_2\text{C}(\text{O})\text{Ph})(\text{IPr})]$  (**7**), C≡N bonds in  $[\text{Au}(\text{CH}_2\text{CN})(\text{IPr})]$  (**8**) and  $[\text{Au}(\text{CH}(\text{CN})_2)(\text{IPr})]$  (**9**) and N-O bonds in  $[\text{Au}(\text{CH}_2\text{NO}_2)(\text{IPr})]$  (**11**) and  $[\text{Au}(\text{CH}(\text{CH}_3)\text{NO}_2)(\text{IPr})]$  (**12**) compared to

those of the corresponding unbound starting materials (Table S8) was consistent with the measured redshifted stretching vibrations associated with these bonds (Section 10.4, Table S21) and agreed with the apparent transfer of electron density measured by chemical shifts  $C^{\alpha}H-\delta(^1H)$  (Section 10.5, Table S23 and Table S24). As an exception, a slightly contracted  $C\equiv N$  bond was present in  $[Au(CH(Ph)CN)(IPr)]$  (**10**) (Table S8), entry 4).

**Table S8.** Bond lengths substrates and their IPr-gold complexes  $[Au(CR_2H)(IPr)]$  (**7-12**).<sup>a</sup>

Entry	Bond (C-X)	Compound	d(C-X) [Å]	Complex	d(C-X) [Å]
1	C=O	acetophenone	1.22 <sup>16</sup>	$[Au(CH_2C(O)Ph)(IPr)]$ ( <b>7</b> )	1.23
2	$C\equiv N$	acetonitrile	1.13 <sup>17</sup>	$[Au(CH_2CN)(IPr)]$ ( <b>8</b> )	1.14
3	$C\equiv N$	malononitrile	1.13 <sup>18</sup>	$[Au(CH(CN)_2)(IPr)]$ ( <b>9</b> )	1.15
4	$C\equiv N$	phenylacetonitrile	1.14 <sup>19</sup>	$[Au(CH(Ph)CN)(IPr)]$ ( <b>10</b> )	1.13
5	N=O	nitromethane	1.22 <sup>20</sup>	$[Au(CH_2NO_2)(IPr)]$ ( <b>11</b> )	1.23
6	N=O	nitroethane	1.22 <sup>21</sup>	$[Au(CH(CH_3)NO_2)(IPr)]$ ( <b>12</b> )	1.26

<sup>a</sup>Average values of multiple molecules found in the crystal lattice and multiple bonds within substrates and complexes are given, rounded to two decimal places.

### Flattening of carbanion ligand

Motivated by ongoing efforts to relate properties of complexes of group 11 metals bearing tertiary phosphine ligands to those bearing NHC ligands,<sup>22</sup> selected angles of  $[Au(CR_2H)(IPr)]$  (**4-12**) were inspected closely (Table S9).

**Table S9.** Selected angles in  $[Au(CR_2H)(PR_3)]$  and  $[Au(CR_2H)(IPr)]$  (**4-12**).

Entry	$CR_2H$	$R^1$	$R^2$	L (complex)	$\angle Au-C^{\alpha}-R^1$ [°]	$\angle Au-C^{\alpha}-R^2$ [°]	$\angle R^1-C^{\alpha}-R^2$ [°]
1 <sup>23</sup>	$CH_2COCH_3$	H	$COCH_3$	PMes <sub>3</sub>		114.5(2)	
2	$CH_2COCH_3$	H	$COCH_3$	IPr ( <b>4</b> )		103.1(5)	
3 <sup>24</sup>	$CH_2C(O)Ph$	H	$C(O)Ph$	PPh <sub>3</sub>		107.3(4)	
4	$CH_2C(O)Ph$	H	$C(O)Ph$	IPr ( <b>7</b> )		104.0(2)	
5 <sup>25</sup>	$CH(C(O)CH_3)_2$	$COCH_3$	$COCH_3$	PPh <sub>3</sub>	106.2	107.1	122.8(2)
6	$CH(C(O)CH_3)_2$	$COCH_3$	$COCH_3$	IPr ( <b>5</b> )	102.3(2)	103.2(2)	115.1(8)
7	$CH(C(O)OCH_3)_2$	$CO_2CH_3$	$CO_2CH_3$	IPr ( <b>6</b> )	99.5(5)	111.5(5)	117.0(7)
8 <sup>26</sup>	$CH_2CN$	H	CN	PPh <sub>3</sub>		111.9(2)	
9 <sup>o</sup>	$CH_2CN$	H	CN	IPr ( <b>8</b> )		110.5(2)-111.2(3)	
10 <sup>27</sup>	$C(CN)CH_2N(iPr)_2$	$CH_2N(iPr)_2$	CN	IPr	108.4(8)	109.9(9)	113(1)
11	$CH(CN)_2$	CN	CN	IPr ( <b>9</b> )	107.6(7)	108.9(7)	114(1)
12	$CH(Ph)CN$	Ph	CN	IPr ( <b>10</b> )	107.6(4)	111.1(4)	113.5(5)
13	$CH_2NO_2$	H	$NO_2$	IPr ( <b>11</b> )		111.4(0)	
14	$CH(CH_3)NO_2$	$CH_3$	$NO_2$	IPr ( <b>12</b> )	111.3(6)	105.3(6)	112.2(8)

<sup>o</sup>Two molecules were found in the crystal lattice of this complex; the range angles of obtained is given.

The angles  $\angle Au-C^{\alpha}-R^2$  in  $[Au(CH_2C(O)CH_3)(IPr)]$  (**4**) and  $[Au(CH_2C(O)CH_3)(PMes_3)]$  showed opposite deviations from 109.5° (Table S9, entries 1-2). This trend continued in  $[Au(CH_2C(O)Ph)(IPr)]$  (**7**) and in  $[Au(CH_2C(O)Ph)(PPh_3)]$  (Table S9, entries 3-4). An even bigger difference was measured between  $[Au(CH(C(O)OCH_3)_2)(IPr)]$  (**5**) and  $[Au(CH(C(O)OCH_3)_2)(PPh_3)]$  (Table S9, entries 5-6). Moreover, while the carbonyl groups in the former complex (**5**) were oriented parallel (dihedral angle of 1.2(3)°), those in the phosphine-bearing complex were strongly twisted (dihedral angle of 125(1)°). A similar analysis of angles  $\angle C^2-Au-C^{\alpha}$  and  $\angle Au-C^{\alpha}-R^{1/2}$  (Table S9, entry 7) and a dihedral angle of about 14° in  $[Au(CH(C(O)OCH_3)_2)(IPr)]$  (**6**) indicated smaller flattening of the dimethyl malonate moiety, presumably because of a mesomeric effect by the ester groups. This flattening could be observed in complexes containing nitrile functional groups as well, as apparent from the smaller angle  $\angle Au-C^{\alpha}-R^2$  in  $[Au(CH_2CN)(IPr)]$  (**8**) than in  $[Au(CH_2CN)(PPh_3)]$  (Table S9, entries 8-9). The nitrile moiety was oriented unsymmetrically relative to the plane of the NHC as measured by the corresponding dihedral angle,  $\angle NHC-C^{\alpha}-CN$ , of the two different molecules observed in the crystal lattice of **8** (60-74°). Similar angles  $\angle Au-C^{\alpha}-R^{1/2}$  and a dihedral angle  $\angle NHC-C^{\alpha}-CN$  of 70(1)° have previously been

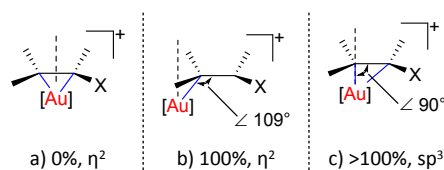
measured in related complex  $[\text{Au}(\text{C}(\text{CN})\text{CH}_2\text{N}(\text{Pr})_2)(\text{IPr})]$  (Table S9, entry 10). In **9**, angle  $\angle \text{R}^1\text{-C}^\alpha\text{-R}^2$  (Table S9, entry 11) versus  $110.8^\circ$  in unbound malononitrile<sup>18</sup> represented a slight deviation of the near-planar malononitril fragment from tetrahedral geometry and angles  $\angle \text{Au-C}^\alpha\text{-R}^{1/2}$  indicated a tilt towards the gold center. One of the cyano groups occupied a near-parallel orientation relative to the plane of the NHC ( $\angle \text{NHC-C}^\alpha\text{-R}^1 = 7(1)^\circ$ ), while the other ( $\angle \text{NHC-C}^\alpha\text{-R}^2 = 61(1)^\circ$ ) pointed towards a methyl of the IPr ligand. While less pronounced in  $[\text{Au}(\text{CH}(\text{Ph})\text{CN})(\text{IPr})]$  (**10**), the angle  $\angle \text{R}^1\text{-C}^\alpha\text{-R}^2$  was slightly larger than that in unbound phenylacetonitrile ( $112.6(1)^\circ$ ).<sup>19</sup> Angles  $\angle \text{Au-C}^\alpha\text{-R}^{1/2}$  were also found indicative of distortion of the  $\text{CR}_2\text{H}^-$  ligand (Table S9, entry 12). This was also apparent from the mutual alignments of the phenyl and nitrile groups, with dihedral angles  $\angle \text{C}^o\text{-C}^i\text{-C}^\alpha\text{-CN}$  of  $160.0(6)^\circ$  in **10** and  $79.0^\circ$  in unbound phenylacetonitrile, with the phenyl ring placed nearly perpendicular to the Au-C  $\alpha$  bond (dihedral angle of  $101.5(6)^\circ$ ) in **10**. The distance between the aryl rings of the  $\text{CR}_2\text{H}^-$  and IPr ligands was too large ( $5.072(9)^\circ \text{ \AA}$ ) to be considered a  $\pi$ - $\pi$  interaction,<sup>28</sup> neither could it be considered a crystal packing effect since these rings occupied orthogonal orientations in the unit cell. Different tilts of the  $\text{NO}_2$  functional groups,  $\angle \text{Au-C}^\alpha\text{-R}^2$ , were measured in **11** and **12**, respectively (Table S9, entries 13-14). This was found to lead to increased angles  $\angle \text{Au-C}^\alpha\text{-R}^{1/2}$  and  $\angle \text{R}^1\text{-C}^\alpha\text{-R}^2$  in the latter complex (Table S9, entry 10).

Deviation of bond angles  $\angle \text{Au-C}^\alpha\text{-R}^{1/2}$  and  $\angle \text{R}^1\text{-C}^\alpha\text{-R}^2$  from  $109.5^\circ$  expected for a purely  $\text{sp}^3$ -hybridised  $\text{C}^\alpha$  atom thus suggested partial rehybridisation of the carbanion ligand ( $\text{CR}_2\text{H}^-$ ) in  $[\text{Au}(\text{CR}_2\text{H})(\text{IPr})]$  (**4-12**).<sup>29</sup>

### Coordination mode of carbanion ligand

The  $\pi$ -coordination mode of gold(I)-alkene complexes has been found to be prone to “slippage” (Figure S27) where the gold center moves away from the position equidistant between the two carbon atoms (Figure S27a). In the most extreme case of 100% slippage, the gold center would be found directly above one of the carbon atoms (Figure S27b). Gold alkene complexes where the angle  $\text{Au-C}^\alpha\text{-C}^\beta$  exceeds  $90^\circ$  are considered  $\text{C}(\text{sp}^3)$ -bound ones (Figure S27c). This phenomenon was first observed in a gold(I) butadiene complex<sup>30</sup> and has since been investigated in vinyl ether<sup>31</sup> and iminium<sup>32</sup> complexes as well. The extent of slippage has been related to the properties of the substituents on the alkene.<sup>33</sup>

**Figure S27.** Slippage (%) and coordination modes ( $\pi$  versus  $\sigma$ ) in gold(I) complexes.



In  $[\text{Au}(\text{CR}_2\text{H})(\text{IPr})]$  (**4-12**), angles  $\angle \text{Au-C}^\alpha\text{-R}^2$  greater than  $90^\circ$  (Table S9) indicated that this deformation had not resulted in slippage from a  $\sigma$ -coordination mode to a  $\pi$ -coordination mode ( $\eta^2$ ). This observation strengthened the notion that carbanion ligands with enolizable groups did not exist as their alkene-like tautomers.

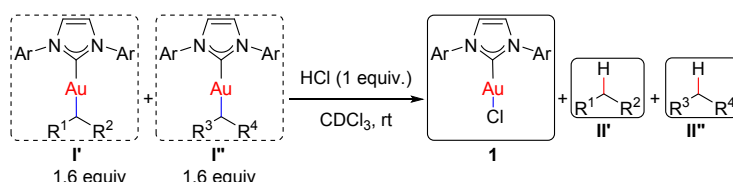
### Adjustment of NHC geometry

Various structural parameters associated with NHC ligands have previously been related to electronic effects:  $\angle \text{N}^1\text{-C}^5\text{-C}^4\text{-N}^3$  in NHC-gold(III) complexes,<sup>34</sup>  $\angle \text{N}^1\text{-C}^2\text{-N}^3$  in NHC-gold(I) complexes,<sup>35</sup> and  $d(\text{C}^2\text{-N}^{1/3})$  and  $\angle \text{N}^1\text{-C}^2\text{-N}^3$  in NHC-gold(I) complexes.<sup>36</sup> Variations in all parameters were investigated in the regression analysis and dihedral angle  $\angle \text{N}^1\text{-C}^5\text{-C}^4\text{-N}^3$  was chosen as a particularly illustrative one.

## 8. Competition experiments

Competitive protodeauration reactions were performed by subjecting equimolar mixtures of two different complexes  $[\text{Au}(\text{CR}_2\text{H})(\text{IPr})]$  (**I'** and **I''**) to a substoichiometric amount of hydrogen chloride (Section 8.1). Hydrochloric acid was used in these experiments to assure the formation of  $[\text{AuCl}(\text{IPr})]$  (**1**) instead of cationic gold complexes that would have formed in reactions with acids such as  $\text{HBF}_4 \cdot \text{OEt}_2$ .<sup>37</sup> The conversion ratios obtained were converted to relative rate values (Sections 8.2). These values were then corrected for non-constant concentration during the reactions (Section 8.3).

**Figure S28.** Competition experiments between two organogold complexes.



Relative rate values *versus*  $[\text{Au}(\text{CH}_2\text{CN})(\text{IPr})]$  (**8**),  $k_{\text{rel}}$ , were then computed.<sup>38</sup> Logarithms of these values relative rate data,  $\log k_{\text{rel}}$ , were subsequently used because of the multiplicative relationship of the relative values.<sup>39</sup> The even higher relative rate of protodeauration estimated for  $[\text{Au}(\text{OH})(\text{IPr})]$  (**2**) than that for  $[\text{Au}(\text{CH}(\text{CH}_3)\text{NO}_2)(\text{IPr})]$  (**12**) (1400) placed the data in context but was not used in further analysis.

### Experimental procedure for competition experiments

Stock solutions (of about 9 mM) of complexes  $[\text{Au}(\text{CR}_2\text{H})(\text{IPr})]$  (**3-12**) and  $[\text{Au}(\text{OH})(\text{IPr})]$  (**1**) were prepared by dissolving about 5 mg (9  $\mu\text{mol}$ ) of the complexes in 1 mL  $\text{CDCl}_3$ . Stock solutions of mesitylene (1.0 mM) and HCl (from 4 M in 1,4-dioxane, to 5.7 mM) in  $\text{CDCl}_3$  were prepared. To 400  $\mu\text{L}$  of  $\text{CDCl}_3$  in a NMR tube were added 25  $\mu\text{L}$  each of the stock solutions of two different complexes and mesitylene was added. After recording a  $^1\text{H}$ -NMR spectrum and confirming the absence of reaction between **I'** and **I''**, 25  $\mu\text{L}$  of the stock solution of HCl was added (32 mol%) and another  $^1\text{H}$ -NMR spectrum was recorded. These reactions completed in the time required to run NMR spectra (minutes) and formed mixtures of the organic molecules **II'** and **II''**,  $[\text{AuCl}(\text{IPr})]$  (**1**).

Absolute and relative conversions of complexes **I'** and **I''** were determined by integration of peak areas of the  $\text{C}^\alpha\text{H}$  protons. Integrals were scaled by the  $\text{CH}_3$  resonance of mesitylene to account for the slight dilution that resulted from the addition of the HCl solution. A series of experiments between different combinations of the different complexes  $[\text{Au}(\text{OH})(\text{IPr})]$  (**1**) and  $[\text{Au}(\text{CR}_2\text{H})(\text{IPr})]$  (**3-12**) gave the relative susceptibility to protodeauration: **1** > **12** > **4** > **7** > **5** > **10** > **3** > **11** > **9** > **8** (Table S10). The intensity of the O-H resonance of **2** is known to be unsuitable for quantification and care must be taken to use the value of this integral.<sup>40</sup> Because of partial overlap of  $\text{C}^\alpha\text{H}$  proton integrals in NMR spectra, conversions were calculated based on the integrals of **12** and **4** instead (Table S10, entry 2). Considering these difficulties, a tentative value for the pair **4/1** was measured instead of **12/1** (Table S10, entry 1). The conversion ratios **10/3**, **3/11**, **11/9** and **9/8** are all significantly greater than 1.05:1, assuring that any impurities in **3** or **9** (potentially up to 5%, see Sections 3.1 and 3.5) do not alter the determined order of relative susceptibility to protodeauration.

**Table S10.** Conversion ratios of pairs I' and I''.

Entry	Pair	Conversion ratio
	[I']/[I'']	$\Delta[I']/\Delta[I'']$
1	2 / 4	3.8:1
2	12 / 4	2.3:1
3	4 / 7	1.8:1
4	7 / 5	1.2:1
5	5 / 10	2.6:1
6	10 / 3	3.8:1
7	3 / 11	1.3:1
8	11 / 9	3.4:1
9	9 / 8	1.5:1

### Conversion of ratios

The competitive protodeauration reaction of two different [Au(CR<sub>2</sub>H)(IPr)] (**3-12**) complexes, I' and I'', with a substoichiometric amount of hydrochloric acid is defined by two rate laws (Eqs. S1 and S2).

$$\frac{d[I']}{dt} = k' \times [I'] \times [H^+] \quad (S1)$$

$$\frac{d[I'']}{dt} = k'' \times [I''] \times [H^+] \quad (S2)$$

Division and rearrangement of those equations relates the formation of organic products II' and II'' to the relative rates *k'* and *k''* of the protodeauration reactions of complexes I' and I'' (Eqs. S3 and S4). Eq. S4, however, dictated that the relative protodeauration rate (*k<sub>rel</sub>*) depended on the relative concentrations of I' and I'' in the reaction mixture.

$$\frac{d[II']}{d[II'']} = \frac{k'}{k''} \times \frac{[I']}{[I'']} \quad (S3)$$

$$k_{rel} = \frac{k'}{k''} = \frac{d[II']}{d[II'']} \times \frac{[I'']}{[I']} \quad (S4)$$

### Correction for non-constant concentration

The modest excess of gold complex to acid used prohibited the simplification that the concentration of I' and I'' would remain constant throughout the competitive reaction. As a result, the experimentally obtained values for  $d[II']/d[II'']$  could not be directly related to *k<sub>rel</sub>*. Instead, the measured “apparent” relative rate values *k<sub>app</sub>* (Eq. S5) reflected the ratios of conversion of complexes I' and I'' or the ratio of products II' and II'' formed after the protodeauration reactions had reached completion (Table S10). These final products ratios resulted from conversion of complexes I' and I'' subject to the “actual” relative rate values *k<sub>rel</sub>*. To generate a list of values for *k<sub>rel</sub>* and the corresponding *k<sub>app</sub>*, reaction profiles for competitive protodeauration reactions were simulated using COPASI.<sup>41</sup> Fitting of resulting values *k<sub>rel</sub>* to modelled reactions with  $1.0 < k_{app} < 4.0$  (0.01 increments) afforded an exponential conversion function (Eq. S6,  $R^2 > 0.99$ ).

$$k_{app} = \frac{\Delta[I']}{\Delta[I'']} = \frac{\Delta[II']}{\Delta[II'']} \quad (S5)$$

$$k_{pair} = 1.0034 \times k_{app}^{1.1898} \quad (S6)$$

Conversion of values *k<sub>app</sub>* from Table S10 using Eq. S6 gave values *k<sub>rel</sub>* (Table S11).

**Table S11.** Relative rates of protodeauration in [Au(CR<sub>2</sub>H)(IPr)] (**3-12**).

Entry	Complex	$k_{\text{pair}}$	$k_{\text{rel}}$	$\log k_{\text{rel}}$
1	[Au(CH <sub>2</sub> CN)(IPr)] ( <b>8</b> )	1	1	0
2	[Au(CH(CN) <sub>2</sub> )(IPr)] ( <b>9</b> )	1.65	1.7	0.22
3	[Au(CH <sub>2</sub> NO <sub>2</sub> )(IPr)] ( <b>11</b> )	4.31	7.1	0.85
4	[Au(CH <sub>3</sub> )(IPr)] ( <b>3</b> )	1.34	9.5	0.98
5	[Au(CH(Ph)CN)(IPr)] ( <b>10</b> )	4.99	48	1.68
6	[Au(CH(C(O)CH <sub>3</sub> ) <sub>2</sub> )] ( <b>5</b> )	3.1	150	2.17
7	[Au(CH <sub>2</sub> C(O)Ph)(IPr)] ( <b>7</b> )	1.19	180	2.24
8	[Au(CH <sub>2</sub> C(O)CH <sub>3</sub> )(IPr)] ( <b>4</b> )	2.05	360	2.56
9	[Au(CH(CH <sub>3</sub> )NO <sub>2</sub> )(IPr)] ( <b>12</b> )	2.68	960	2.98
10	[Au(OH)(IPr)] ( <b>2</b> )	1.85	1800	3.25

## 9. Computational modelling

The experimental (solid-state) structures (Section 4) were used as starting point for geometry optimization through well-resolved DFT calculations with the PBE functional,<sup>42</sup> the Def2SVP basis set<sup>43</sup> for non-metals and the Stuttgart RSC 1997 ECP basis set for Au.<sup>44</sup> Implicit solvent effect was included (CHCl<sub>3</sub>) through the PCM method, incorporating solute-solvent dispersion, solute-solvent repulsion and solute cavitation energy contributions. The EDIIS/CDIIS procedure<sup>45</sup> was applied for the SCF and an ultrafine grid for integration was used. Explicit dispersion corrections were included with the D3 method.<sup>46</sup> Vibrational frequency calculations were carried out to confirm that optimized structures correspond with true energy minima (no imaginary frequencies). Whenever possible, symmetry was enforced and the C<sub>1</sub> point-group of symmetry was set. NMR chemical shifts <sup>1</sup>H and <sup>13</sup>C were obtained from single point calculations in the gas phase, calculated with ADF,<sup>47</sup> using the BP86 functional,<sup>48</sup> TZ2P basis set,<sup>49</sup> relativistic spin-orbit ZORA<sup>50</sup> and without symmetry considerations over the optimized structures from Gaussian09<sup>51</sup> at the aforementioned computational level.

## 10. Sets of parameters

Unique numbering and simple naming of all parameters simplified subsequent analysis (Table S12).

**Table S12.** Listing of all parameters, unique identifiers, symbols and units.<sup>a</sup>

ID	Name	Symbol	Unit
<i>Component</i>			
1	s0.0	$C_{s \geq 0.0}^{\alpha}$	%
2	s0.5	$C_{s \geq 0.5}^{\alpha}$	%
3	s1.0	$C_{s \geq 1.0}^{\alpha}$	%
<i>EDA<sup>b</sup></i>			
4	E-elstat	$E_{elstat}$	kcal·mol <sup>-1</sup>
5	E-Pauli	$E_{pauli}$	kcal·mol <sup>-1</sup>
6	E-steric	$E_{steric}$	kcal·mol <sup>-1</sup>
7	E-int	$E_{oi}$	kcal·mol <sup>-1</sup>
8	E-sigma	$E_{\sigma}$	kcal·mol <sup>-1</sup>
9	E-pi	$E_{\pi}$	kcal·mol <sup>-1</sup>
10	E-bind	$E_{bind}$	kcal·mol <sup>-1</sup>
11	sigma-DON	$E_{\sigma}^{L \rightarrow M}$	kcal·mol <sup>-1</sup>
12	sigma-RET	$E_{\sigma}^{L \leftarrow M}$	kcal·mol <sup>-1</sup>
13	pi-DON	$E_{\pi}^{L \rightarrow M}$	kcal·mol <sup>-1</sup>
14	pi-RET	$E_{\pi}^{L \leftarrow M}$	kcal·mol <sup>-1</sup>
15	percent-sigma	$\%E_{\sigma}$	%
16	percent-pi	$\%E_{\pi}$	%
17	sum-sigma	$E_{\sigma}^{L \leftrightarrow M}$	kcal·mol <sup>-1</sup>
18	sum-pi	$E_{\pi}^{L \leftrightarrow M}$	kcal·mol <sup>-1</sup>
<i>Hammett</i>			
34	meta-sum	$\Sigma\sigma_m$	
35	meta-product	$\Pi\sigma_m$	
36	para-sum	$\Sigma\sigma_p$	
37	para-product	$\Pi\sigma_p$	
<i>IR</i>			
38	substrate-exp	$\tilde{\nu}_a$	cm <sup>-1</sup>
39	complex-exp	$\tilde{\nu}_b$	cm <sup>-1</sup>
40	substrate-dft	$\tilde{\nu}_a'$	cm <sup>-1</sup>
41	complex-dft	$\tilde{\nu}_b'$	cm <sup>-1</sup>
42	delta-exp	$\Delta\tilde{\nu}$	cm <sup>-1</sup>
43	delta-dft	$\Delta\tilde{\nu}'$	cm <sup>-1</sup>
<i>NMR<sup>c,d</sup></i>			
44	Ca	$C^{\alpha}\text{-}\delta(^{13}\text{C})$	ppm
46	C45	$C^{45}\text{-}\delta(^{13}\text{C})$	ppm
48	C2	$C^2\text{-}\delta(^{13}\text{C})$	ppm
50	Ha	$H^{\alpha}\text{-}\delta(^1\text{H})$	ppm
52	H45	$H^{45}\text{-}\delta(^1\text{H})$	ppm
<i>Order</i>			
54	C2-Au	B(C-Au)	
55	Ca-Au	B(C <sup>α</sup> -Au)	
56	Ca-Cb	B(C <sup>α</sup> -C <sup>β</sup> )	
57	Ca-Ha	B(C <sup>α</sup> -H <sup>α</sup> )	
<i>pK<sub>a</sub></i>			
58	pka	pK <sub>a</sub>	
<i>Population</i>			
59	gold	M(Au)	
60	ligand	M(C <sup>α</sup> )	
61	carbene	M(C <sup>2</sup> )	
62	to-gold	M(→Au←)	
63	from-ligand	M(C <sup>α</sup> →)	
64	percent-ligand	M(%C <sup>α</sup> )	
65	percent-carbene	M(%C <sup>2</sup> )	
<i>Rate</i>			
66	relative	$k_{rel}$	
67	log	log $k_{rel}$	
<i>Structure<sup>c,e</sup></i>			
68	angle-C2-Au-Ca	$\angle C^2\text{-Au-C}^{\alpha}$	°
70	angle-Ca-D	$\theta$	°
72	angle-Ca-T	$\phi$	°
74	angle-Ca-valence	$\psi$	°
76	angle-N-C2-Ca-R	$\angle N^1\text{-C}^2\text{-C}^{\alpha}\text{-R}$	°
78	angle-N-C2-N	$\angle N^1\text{-C}^2\text{-N}^3$	°
80	angle-N-C45-N	$\angle N^1\text{-C}^5\text{-C}^4\text{-N}^3$	°
82	coulson-lambda-Au	$\lambda(C^{\alpha}\text{-Au})$	
84	coulson-sigma-Au	$\sigma(C^{\alpha}\text{-Au})$	%
86	distance-Au-C2	d(Au-C <sup>2</sup> )	Å
88	distance-Au-Ca	d(Au-C <sup>α</sup> )	Å
90	distance-C2-N	d(C <sup>2</sup> -N <sup>1/3</sup> )	Å
92	distance-C4-C5	d(C <sup>4</sup> -C <sup>5</sup> )	Å
94	distance-C45-N	d(C <sup>4/5</sup> -N <sup>1/3</sup> )	Å
96	distance-Ca-Ha	d(C <sup>α</sup> -H <sup>α</sup> )	Å
98	distance-Ca-T	h(C <sup>α</sup> )	Å

<sup>a</sup>In the data and regressions, percentages are given as fractions: 80% > 0.80. <sup>b</sup>Names are suffixed with “-C2”, “-Ca” to indicate the carbon to which the value refers. For IDs 4-18, Cx = Ca. For the analogous series with IDs 19-34, Cx = C2 (not shown). <sup>c</sup>Names are suffixed with “-exp” or “-dft” to distinguish between experimental and modelled (DFT) values. <sup>d</sup>For even IDs 44-52, suffix “-exp” is implied. For the analogous series with odd IDs 45-53, suffix “-dft” is implied. <sup>e</sup>For even IDs 68-98, suffix “-dft” is implied. For the analogous series with odd IDs 69-99, suffix “-dft” is implied.

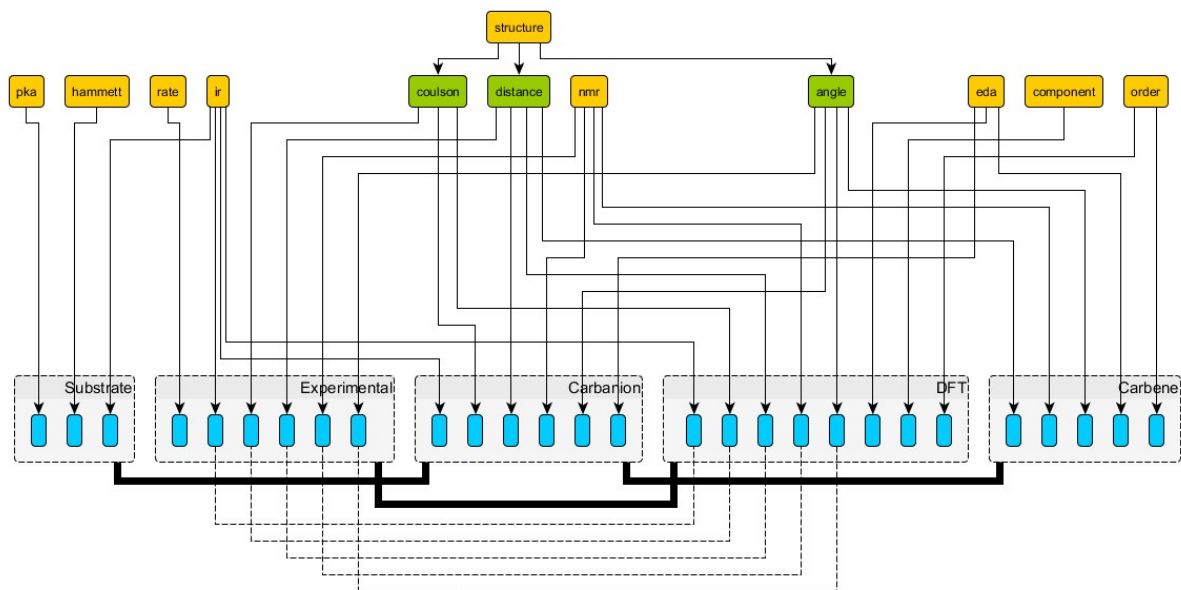
Each set was assigned a color for visualization purposes (Figure S29).

**Figure S29.** Set colors.

<span style="color:yellow">■</span>	component
<span style="color:purple">■</span>	eda
<span style="color:orange">■</span>	hammett
<span style="color:lightblue">■</span>	ir
<span style="color:darkred">■</span>	nmr
<span style="color:lightgrey">■</span>	order
<span style="color:darkgrey">■</span>	pka
<span style="color:green">■</span>	population
<span style="color:blue">■</span>	rate
<span style="color:darkred">■</span>	structure

The connectivity between groups of parameters associated with different parts of the complexes and those derived from different methods presented a high-level guide for the systematic evaluation of potential relations (Figure S30).

**Figure S30.** Complete grouping of parameters from different sets.<sup>a</sup>



<sup>a</sup>Color code: yellow = set, green = subset, blue = parameters.

Values for the  $pK_a$  parameter are given in the main text and values for parameters in the rate set are given in Section 8.3, Table S11. Sections 10.1-10.8 define and discuss all parameters included in the other sets.

## Component

As part of the computational modelling studies, all carbanion fragments ( $CR_2H^-$ ) from complexes  $[Au(CR_2H)(IPr)]$  (**3-12**) were subjected to further analysis. The proportions of s-character of the atomic orbital on  $C^\alpha$  occupied by the lone pair,  $C^\alpha_s$ , were recorded (Table S13). The value for  $[Au(CH(COCH_3)_2)(IPr)]$  (**5**) was missing from the output of the corresponding calculation because the software only outputs values greater than 1%. To account for this, three copies of  $C^\alpha_s$  were used in further analysis:  $C^\alpha_{s \geq 0.0}$ ,  $C^\alpha_{s \geq 0.5}$  and  $C^\alpha_{s \geq 1.0}$  with the value for **5** set to 0.0, 0.5 and 1.0, respectively. The values were lower than 0.25 expected for  $sp^3$ -hybridised orbitals and thus indicated that the  $CR_2H^-$  fragments had flattened and that the lone pair resides in an orbital of mostly p-character.

**Table S13.** Component values in  $[Au(CR_2H)(IPr)]$  (**3-12**).

Complex	$C^\alpha_s$ [%]
$[Au(CH_3)(IPr)]$ ( <b>3</b> )	6.73
$[Au(CH_2C(O)CH_3)(IPr)]$ ( <b>4</b> )	2.39
$[Au(CH(C(O)CH_3)_2)(IPr)]$ ( <b>5</b> )	< 1.00
$[Au(CH(C(O)OCH_3)_2)(IPr)]$ ( <b>6</b> )	2.72
$[Au(CH_2C(O)Ph)(IPr)]$ ( <b>7</b> )	2.19
$[Au(CH_2CN)(IPr)]$ ( <b>8</b> )	6.31
$[Au(CH(CN)_2)(IPr)]$ ( <b>9</b> )	4.7
$[Au(CH(Ph)CN)(IPr)]$ ( <b>10</b> )	3.59
$[Au(CH_2NO_2)(IPr)]$ ( <b>11</b> )	6.68
$[Au(CH(CH_3)NO_2)(IPr)]$ ( <b>12</b> )	5.69

## EDA

Binding energies,  $E_{bind}$ , between rigidly fragmented Au, IPr: and  $CR_2H^-$  parts in selected  $[Au(CR_2H)(IPr)]$  (**3, 5-6, 9** and **11**) were decomposed in steric energies,  $E_{steric}$  and orbital interaction (oi) energies,  $E_{oi}$ , for the Au- $C^\alpha$  and

Au-C<sup>2</sup> bonds through a computational energy decomposition analysis (EDA) (Eq. S7 and Table S14).<sup>52</sup> The steric term was further decomposed to a term accounting for electrostatic interactions ( $E_{elstat}$ ) and the Pauli repulsion energy ( $E_{pauli}$ ) (Eq. S8 and Table S14).

$$E_{bind} = E_{steric} + E_{oi} \quad (\text{Eq. S7})$$

$$E_{steric} = E_{elstat} + E_{pauli} \quad (\text{Eq. S8})$$

**Table S14.** EDA parameters in [Au(CR<sub>2</sub>H)(IPr)] (**3**, **5-6**, **9** and **11**).

Entry	Complex	$E_{elstat}$ [kcal·mol <sup>-1</sup> ]	$E_{pauli}$ [kcal·mol <sup>-1</sup> ]	$E_{steric}$ [kcal·mol <sup>-1</sup> ]	$E_{oi}$ [kcal·mol <sup>-1</sup> ]	$E_{bind}$ [kcal·mol <sup>-1</sup> ]
Au-C <sup>α</sup>						
1	[Au(CH <sub>3</sub> )(IPr)] ( <b>3</b> )	-364.19	259.18	-105.01	-94.42	-199.43
2	[Au(CH(C(O)CH <sub>3</sub> ) <sub>2</sub> )(IPr)] ( <b>5</b> )	-196.79	136.87	-59.93	-79.70	-139.63
3	[Au(CH(C(O)OCH <sub>3</sub> ) <sub>2</sub> )(IPr)] ( <b>6</b> )	-200.07	138.07	-62.00	-79.89	-141.88
4	[Au(CH(CN) <sub>2</sub> )(IPr)] ( <b>9</b> )	-199.61	139.37	-60.24	-73.00	-133.23
5	[Au(CH <sub>2</sub> NO <sub>2</sub> )(IPr)] ( <b>11</b> )	-235.16	-165.04	-70.12	-83.64	-153.76
Au-C <sup>2</sup>						
6	[Au(CH <sub>3</sub> )(IPr)] ( <b>3</b> )	-172.96	181.44	8.48	-59.8	-51.32
7	[Au(CH(C(O)OCH <sub>3</sub> ) <sub>2</sub> )(IPr)] ( <b>5</b> )	-189.72	196.32	6.60	-70.43	-63.82
8	[Au(CH(C(O)OCH <sub>3</sub> ) <sub>2</sub> )(IPr)] ( <b>6</b> )	-188.53	194.1	5.57	-69.27	-63.70
9	[Au(CH(CN) <sub>2</sub> )(IPr)] ( <b>9</b> )	-193.85	194.84	0.99	-71.69	-70.69
10	[Au(CH <sub>2</sub> NO <sub>2</sub> )(IPr)] ( <b>11</b> )	-184.51	185.63	1.12	-66.17	-65.05

The orbital interaction energies,  $E_{oi}$ , were further decomposed based on symmetry, giving separate energy values,  $E_{\sigma}$  and  $E_{\pi}$  for  $\sigma$ - and  $\pi$ -components (Eq. S9 and Table S15). The proportional interaction energies, % $E_{\sigma}$  and % $E_{\pi}$  were calculated from these values.

$$E_{oi} = E_{\sigma} + E_{\pi} \quad (\text{Eq. S9})$$

**Table S15.** EDA parameters ( $\sigma$  and  $\pi$ ) in [Au(CR<sub>2</sub>H)(IPr)] (**3**, **5-6**, **9** and **11**).

Entry	Complex	$E_{\sigma}$ [kcal·mol <sup>-1</sup> ]	$E_{\pi}$ [kcal·mol <sup>-1</sup> ]	% $E_{\sigma}$ [%]	% $E_{\pi}$ [%]
Au-C <sup>α</sup>					
1	[Au(CH <sub>3</sub> )(IPr)] ( <b>3</b> )	-81.73	-12.69	87	13
2	[Au(CH(C(O)CH <sub>3</sub> ) <sub>2</sub> )(IPr)] ( <b>5</b> )	-69.77	-9.93	88	12
3	[Au(CH(C(O)OCH <sub>3</sub> ) <sub>2</sub> )(IPr)] ( <b>6</b> )	-70.07	-9.82	88	12
4	[Au(CH(CN) <sub>2</sub> )(IPr)] ( <b>9</b> )	-64.77	-8.23	89	11
5	[Au(CH <sub>2</sub> NO <sub>2</sub> )(IPr)] ( <b>11</b> )	-74.59	-9.05	89	11
Au-C <sup>2</sup>					
6	[Au(CH <sub>3</sub> )(IPr)] ( <b>3</b> )	-49.08	-10.72	82	18
7	[Au(CH(C(O)OCH <sub>3</sub> ) <sub>2</sub> )(IPr)] ( <b>5</b> )	-58.53	-11.9	83	17
8	[Au(CH(C(O)OCH <sub>3</sub> ) <sub>2</sub> )(IPr)] ( <b>6</b> )	-57.53	-11.73	83	17
9	[Au(CH(CN) <sub>2</sub> )(IPr)] ( <b>9</b> )	-60.06	-11.63	84	16
10	[Au(CH <sub>2</sub> NO <sub>2</sub> )(IPr)] ( <b>11</b> )	-54.77	-11.4	83	17

A fragment analysis was performed to add directionality in terms of bonding and back-bonding interactions to the symmetry-separated energy values (Table S16).

**Table S16.** EDA parameters ( $\sigma$  and  $\pi$ ) in  $[\text{Au}(\text{CR}_2\text{H})(\text{IPr})]$  (**3**, **5-6**, **9** and **11**).

Entry	Complex	$E_{\sigma}^{\text{L}\rightarrow\text{M}}$	$E_{\sigma}^{\text{L}\leftarrow\text{M}}$	$E_{\pi}^{\text{L}\rightarrow\text{M}}$	$E_{\pi}^{\text{L}\leftarrow\text{M}}$	$E_{\sigma}^{\text{L}\leftrightarrow\text{M}}$	$E_{\pi}^{\text{L}\leftrightarrow\text{M}}$
		[kcal·mol <sup>-1</sup> ]	[kcal·mol <sup>-1</sup> ]	[kcal·mol <sup>-1</sup> ]	[kcal·mol <sup>-1</sup> ]	[kcal·mol <sup>-1</sup> ]	[kcal·mol <sup>-1</sup> ]
Au-C <sup>α</sup>							
1	$[\text{Au}(\text{CH}_3)(\text{IPr})]$ ( <b>3</b> )	-63.1	-31.97	-9.40	-3.58	-95.07	-12.98
2	$[\text{Au}(\text{CH}(\text{C}(\text{O})\text{CH}_3)_2)(\text{IPr})]$ ( <b>5</b> )	-49.08	-39.46	-5.77	-4.39	-88.54	-10.16
3	$[\text{Au}(\text{CH}(\text{C}(\text{O})\text{OCH}_3)_2)(\text{IPr})]$ ( <b>6</b> )	-49.37	-38.94	-5.61	-4.34	-88.31	-9.95
4	$[\text{Au}(\text{CH}(\text{CN})_2)(\text{IPr})]$ ( <b>9</b> )	-46.13	-37.09	-4.67	-3.85	-83.22	-8.52
5	$[\text{Au}(\text{CH}_2\text{NO}_2)(\text{IPr})]$ ( <b>11</b> )	-53.28	-37.93	-5.8	-3.44	-91.21	-9.24
Au-C <sup>2</sup>							
6	$[\text{Au}(\text{CH}_3)(\text{IPr})]$ ( <b>3</b> )	-36.75	-32.16	-1.71	-9.78	-68.91	-11.49
7	$[\text{Au}(\text{CH}(\text{C}(\text{O})\text{OCH}_3)_2)(\text{IPr})]$ ( <b>5</b> )	-44.45	-38.59	-1.99	-10.6	-83.04	-12.59
8	$[\text{Au}(\text{CH}(\text{C}(\text{O})\text{OCH}_3)_2)(\text{IPr})]$ ( <b>6</b> )	-43.48	-37.85	-1.90	-10.45	-81.33	-12.35
9	$[\text{Au}(\text{CH}(\text{CN})_2)(\text{IPr})]$ ( <b>9</b> )	-50.38	-39.97	-1.85	-10.55	-90.35	-12.40
10	$[\text{Au}(\text{CH}_2\text{NO}_2)(\text{IPr})]$ ( <b>11</b> )	-41.11	-36.17	-1.82	-10.37	-77.28	-12.19

This set contained too many parameters to be clearly visualized in a correlation graph or plot.

**Table S17.** Linear models for values for C<sup>α</sup> versus values for C<sup>2</sup>.<sup>a</sup>

Entry	$z$	Linear model		R <sup>2</sup>
		$i$	$a$	
1	E-elstat	-1842.61	-8.62	0.920
2	E-Pauli	-310.83	2.17	0.008
3	E-steric	-57.02	-3.17	0.308
4	E-int	-191.17	-1.62	0.953
5	E-sigma	-153.57	-1.45	0.972
6	E-pi	-41.30	-2.73	0.559
7	E-bind	-376.35	-3.54	0.884
8	sigma-DON	-104.88	-1.22	0.844
9	sigma-RET	-7.03	0.81	0.665
10	pi-DON	-29.22	-12.39	0.492
11	pi-RET	3.87	0.75	0.332
12	percent-sigma	0.03	1.02	0.372
13	percent-pi	-0.05	1.02	0.370
14	sum-sigma	-133.09	-0.55	0.983
15	sum-pi	-50.12	-3.27	0.668

<sup>a</sup>Using formula  $z_{\text{C}\alpha} = i + a \times z_{\text{C}2}$ .

## Hammett

Hammett parameters capture substituent effects in a single number (Table S18).<sup>53</sup>

**Table S18.** Hammett parameters for selected R groups.

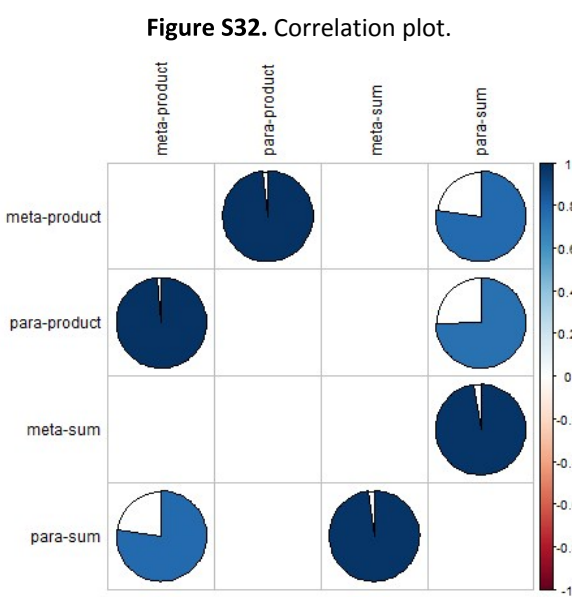
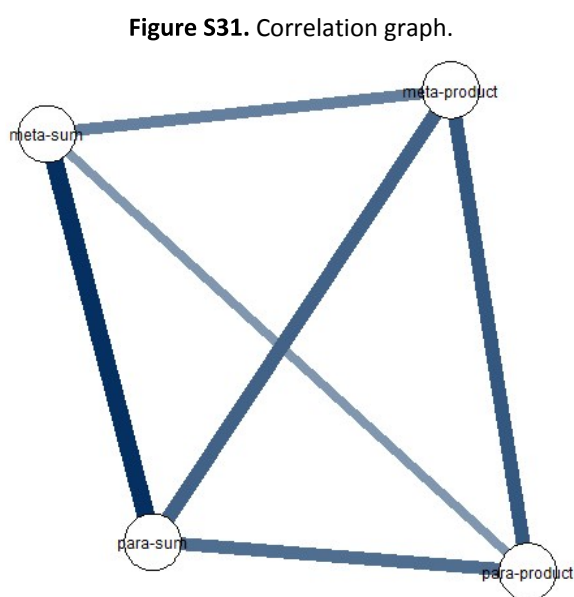
Entry	R	$\sigma_m$	$\sigma_p$
1	H	0.000	0.000
2	C(O)Me	0.376	0.502
3	CN	0.560	0.660
4	Ph	0.0600	-0.010
5	CH <sub>3</sub>	-0.069	-0.170
6	NO <sub>2</sub>	0.710	0.778

Sums and products of Hammett constants for individual substituents in the carbanion ligand (CR<sub>2</sub>H<sup>-</sup>) were computed to generate new parameters that quantified the overall properties (0). Absence of Hammett parameters for CH<sub>3</sub>O<sub>2</sub>C<sup>-</sup> and PhOC<sup>-</sup> substituents ruled out the computation of these parameters for complexes [Au(CH(C(O)OCH<sub>3</sub>)<sub>2</sub>)(IPr)] (**6**) and [Au(CH<sub>2</sub>C(O)Ph)(IPr)] (**7**).

**Table S19.** Derived Hammett parameters for complexes [Au(CR<sub>2</sub>H)(IPr)] (**3-5** and **8-12**).

Entry	Complex	$\Sigma\sigma_m$	$\Pi\sigma_m$	$\Sigma\sigma_p$	$\Pi\sigma_p$
1	[Au(CH <sub>3</sub> )(IPr)] ( <b>3</b> )	0.00	0.00	0.00	0.00
2	[Au(CH <sub>2</sub> C(O)CH <sub>3</sub> )(IPr)] ( <b>4</b> )	0.38	0.00	0.50	0.00
3	[Au(CH(C(O)CH <sub>3</sub> ) <sub>2</sub> )(IPr)] ( <b>5</b> )	0.75	0.14	1.00	0.25
4	[Au(CH <sub>2</sub> CN)(IPr)] ( <b>8</b> )	0.56	0.00	0.66	0.00
5	[Au(CH(CN) <sub>2</sub> )(IPr)] ( <b>9</b> )	1.12	0.31	1.32	0.44
6	[Au(CH(Ph)CN)(IPr)] ( <b>10</b> )	0.62	0.03	0.65	-0.01
7	[Au(CH <sub>2</sub> NO <sub>2</sub> )(IPr)] ( <b>11</b> )	0.71	0.00	0.78	0.00
8	[Au(CH(CH <sub>3</sub> )NO <sub>2</sub> )(IPr)] ( <b>12</b> )	0.64	-0.05	0.61	-0.13

The different sum parameters and product parameters based on  $\sigma_m$  and  $\sigma_p$  values displayed appreciable correlations (Table S20).

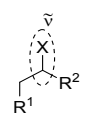
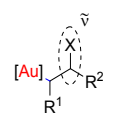
**Table S20.** Correlation of parameters in Hammett set.<sup>a</sup>

<sup>a</sup>Node positions in all correlation graphs are determined by the Fruchterman-Reingold algorithm.<sup>54</sup>

## IR

Lower IR stretching frequencies were measured in the various functional groups in  $[\text{Au}(\text{CR}_2\text{H})(\text{IPr})]$  (**4-5** and **7-12**) compared to the corresponding substrates  $\text{CR}_2\text{H}_2$  (Table S21). This seemed indicative of net transfer of electron density from  $\text{CR}_2^-$  to  $[\text{Au}]^+$ , consistent with the trend observed in  $\text{C}^\alpha\text{H}-\delta(^1\text{H})$  chemical shifts (Section 10.5).

**Table S21.** Prominent infrared bands of substrates ( $\text{CR}_2\text{H}_2$ ) and  $[\text{Au}(\text{CR}_2\text{H})(\text{IPr})]$  (**4-5** and **7-12**).<sup>a</sup>

Entry	Compound	Bond					
			Experimental $\tilde{\nu}$ [ $\text{cm}^{-1}$ ]	Modelled $\tilde{\nu}$ [ $\text{cm}^{-1}$ ]	Complex	Experimental $\tilde{\nu}$ [ $\text{cm}^{-1}$ ]	Modelled $\tilde{\nu}$ [ $\text{cm}^{-1}$ ]
1	acetone	C=O	1714 <sup>55</sup>	1675.38	$[\text{Au}(\text{CH}_2\text{C}(\text{O})\text{CH}_3)(\text{IPr})]$ ( <b>4</b> )	1643 <sup>56</sup>	1763.27
2	acetylacetone	C=O	1621 <sup>57</sup>	1715.28	$[\text{Au}(\text{CH}(\text{C}(\text{O})\text{CH}_3)_2)(\text{IPr})]$ ( <b>5</b> )	1635	1772.44
3	acetophenone	C=O	1684 <sup>58</sup>	1650.12	$[\text{Au}(\text{CH}_2\text{C}(\text{O})\text{Ph})(\text{IPr})]$ ( <b>7</b> )	1620	1721.95
4	acetonitrile	C≡N	2267 <sup>59</sup>	2235.53	$[\text{Au}(\text{CH}_2\text{CN})(\text{IPr})]$ ( <b>8</b> )	2197	2304.16
5	malononitrile	C≡N	2278 <sup>60</sup>	2257.8	$[\text{Au}(\text{CH}(\text{CN})_2)(\text{IPr})]$ ( <b>9</b> )	2214	2319.21
6	phenylacetonitrile	C≡N	2251 <sup>61</sup>	2248.65	$[\text{Au}(\text{CH}(\text{Ph})\text{CN})(\text{IPr})]$ ( <b>10</b> )	2193	2314.55
7	nitromethane	N=O	1379 <sup>62</sup>	1376.49	$[\text{Au}(\text{CH}_2\text{NO}_2)(\text{IPr})]$ ( <b>11</b> )	1358	1412.94
8	nitroethane	N=O	1374 <sup>63</sup>	1544.78	$[\text{Au}(\text{CH}(\text{CH}_3)\text{NO}_2)(\text{IPr})]$ ( <b>12</b> )	1334	1631.93

<sup>a</sup> $[\text{Au}] = \text{Au}(\text{IPr})$ . Values of neat compounds and complexes are given.

Experimental and modelled values of the stretching bands in the substrates and the complexes correlated well (Pane S7), but discrepancies were present in the differences,  $\Delta\tilde{\nu}$ , between the values of substrates and complexes (Table S22).

**Pane S7.** Correlation of parameters in IR set.<sup>a</sup>

**Figure S33.** Correlation graph.

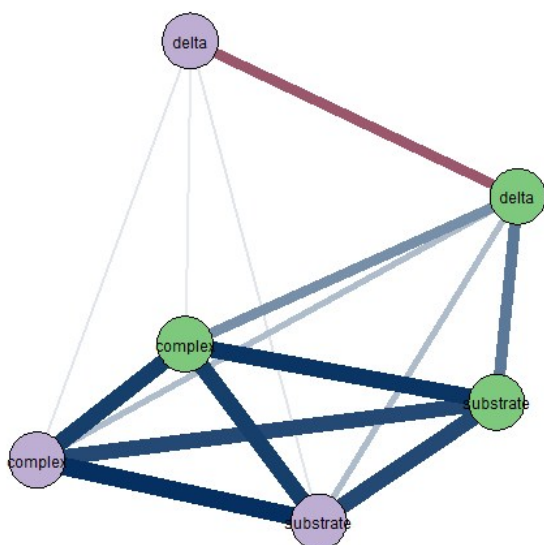
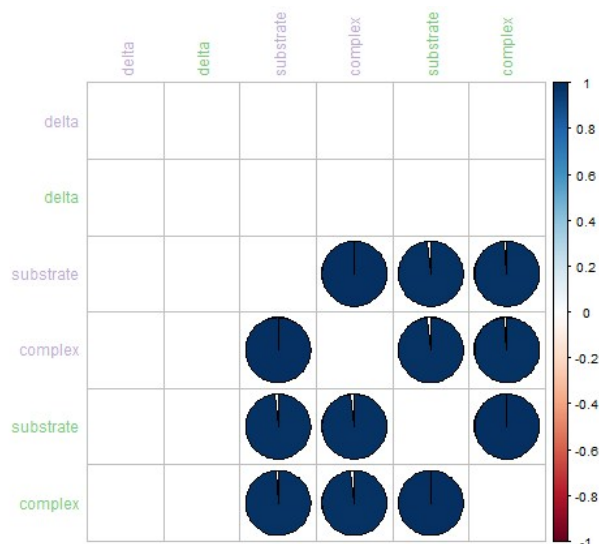


**Figure S34.** Correlation plot.



<sup>a</sup>Parameters representing experimental and modelled values are represented in green and purple, respectively.

**Table S22.** Linear models for experimental *versus* modelled values.<sup>a</sup>

Entry	z	Linear model		R <sup>2</sup>
		i	a	
1	substrate	-163.01	1.08	0.962
2	complex	-187.20	1.03	0.958
3	delta	-14.62	-0.92	0.135

<sup>a</sup>Using formula  $Z_{\text{exp}} = i + a X - Z_{\text{dft}}$ .

## NMR

Except for in **5**, all chemical shifts  $C^{\alpha}H-\delta(^1H)$  in  $[Au(CR_2H)(IPr)]$  (Table S24) were lower than  $C^{\alpha}-\delta(^1H)$  in the corresponding  $CR_2H_2$  (Table S23), but no such trend was found for chemical shift  $C^{\alpha}-\delta(^{13}C)$ . Next to the experimental chemical shift values. Variations of these chemical shifts did not seem to relate to the degree of substitution on  $C^{\alpha}$  but rather on the type of the substituents.<sup>64</sup> Development of density functional theory has enabled accurate computations of NMR parameters of transition metal complexes,<sup>65</sup> and modelled values for various positions were included in further analysis (Table S24 and Table S25).

**Table S23.** Chemical shifts of substrates ( $CR_2H_2$ ) and  $[Au(CR_2H)(IPr)]$  (**3-12**).<sup>a</sup>

Entry	Compound	Structure	$C^{\alpha}H-\delta(^1H)$ [ppm]	$C^{\alpha}-\delta(^{13}C)$ [ppm]	Complex <sup>b</sup>
1	methane		0.22 <sup>66</sup>	-4.6 <sup>66</sup>	$[Au(CH_3)(IPr)]$ ( <b>3</b> )
2	acetone		2.17 <sup>66</sup>	30.9 <sup>66</sup>	$[Au(CH_2COCH_3)(IPr)]$ ( <b>4</b> )
3	acetylacetone		3.61 <sup>67</sup>	100.1 <sup>68</sup>	$[Au(CH(C(O)CH_3)_2)(IPr)]$ ( <b>5</b> )
4	dimethyl malonate		3.40 <sup>66</sup>	41.1 <sup>66</sup>	$[Au(CH(C(O)OCH_3)_2)(IPr)]$ ( <b>6</b> )
5	acetophenone		2.62 <sup>69</sup>	26.5 <sup>69</sup>	$[Au(CH_2C(O)Ph)(IPr)]$ ( <b>7</b> )
6	acetonitrile		2.10 <sup>66</sup>	1.9 <sup>66</sup>	$[Au(CH_2CN)(IPr)]$ ( <b>8</b> )
7	malononitrile		3.59	8.8	$[Au(CH(CN)_2)(IPr)]$ ( <b>9</b> )
8	phenylacetonitrile		3.70 <sup>70</sup>	23.4 <sup>70</sup>	$[Au(CH(Ph)CN)(IPr)]$ ( <b>10</b> )
9	nitromethane		4.33 <sup>66</sup>	62.5 <sup>66</sup>	$[Au(CH_2NO_2)(IPr)]$ ( <b>11</b> )
10	nitroethane		4.42 <sup>71</sup>	12.3 <sup>71</sup>	$[Au(CH(CH_3)NO_2)(IPr)]$ ( <b>12</b> )

<sup>a</sup>All values are from measurements in  $CDCl_3$ . <sup>b</sup>Corresponding product of the deprotonated substrate.

**Table S24.** Chemical shifts  $\delta$  of  $CR_2H^-$  ligands in  $[Au(CR_2H)(IPr)]$  (**3-12**).<sup>a</sup>

Entry	Complex	$H^{\alpha}-\delta(^1H)$		$C^{\alpha}-\delta(^{13}C)$	
		Experimental [ppm]	Modelled [ppm]	Experimental [ppm]	Modelled [ppm]
1	$[Au(CH_3)(IPr)]$ ( <b>3</b> )	-0.21	-0.06767	-2.3	-4.714
2	$[Au(CH_2C(O)CH_3)(IPr)]$ ( <b>4</b> )	2.06 <sup>56</sup>	2.3495	40.7 <sup>56</sup>	42.078
3	$[Au(CH(C(O)CH_3)_2)(IPr)]$ ( <b>5</b> )	3.90	4.815	71.7	70.063
4	$[Au(CH(C(O)OCH_3)_2)(IPr)]$ ( <b>6</b> )	3.18	3.685	43.0	45.051
5	$[Au(CH_2C(O)Ph)(IPr)]$ ( <b>7</b> )	2.46	2.827	36.2	38.125
6	$[Au(CH_2CN)(IPr)]$ ( <b>8</b> )	1.20	1.007	-2.5	-1.772
7	$[Au(CH(CN)_2)(IPr)]$ ( <b>9</b> )	2.38	2.119	-0.50	2.348
8	$[Au(CH(Ph)CN)(IPr)]$ ( <b>10</b> )	2.95	2.863	23.2	28.282
9	$[Au(CH_2NO_2)(IPr)]$ ( <b>11</b> )	4.32	4.295	74.9	73.984
10	$[Au(CH(CH_3)NO_2)(IPr)]$ ( <b>12</b> )	4.40	4.362	83.6	85.38

<sup>a</sup>All values are from measurements in  $CDCl_3$ .

**Table S25.** Chemical shifts  $\delta$  of imidazole constituents of  $[\text{Au}(\text{CR}_2\text{H})(\text{IPr})]$  (**3-12**).<sup>a</sup>

Entry	Complex	C <sup>4</sup> /H		C <sup>4</sup> /C <sup>5</sup>		C <sup>2</sup>	
		Experimental <sup>1</sup> H [ppm]	Modelled <sup>1</sup> H [ppm]	Experimental <sup>13</sup> C [ppm]	Modelled <sup>13</sup> C [ppm]	Experimental <sup>13</sup> C [ppm]	Modelled <sup>13</sup> C [ppm]
1	$[\text{Au}(\text{CH}_3)(\text{IPr})]$ ( <b>3</b> )	7.05	7.0495	122.5	124.2635	202.0	199.99
2	$[\text{Au}(\text{CH}_2\text{C}(\text{O})\text{CH}_3)(\text{IPr})]$ ( <b>4</b> )	7.13	7.0735	122.8 <sup>56</sup>	124.607	193.1 <sup>56</sup>	192.471
3	$[\text{Au}(\text{CH}(\text{C}(\text{O})\text{CH}_3)_2)(\text{IPr})]$ ( <b>5</b> )	7.19 <sup>56</sup>	7.1765	123.2 <sup>56</sup>	124.8615	186.5 <sup>56</sup>	187.459
4	$[\text{Au}(\text{CH}(\text{C}(\text{O})\text{OCH}_3)_2)(\text{IPr})]$ ( <b>6</b> )	7.15 <sup>40</sup>	7.112	122.9 <sup>40</sup>	124.773	187.0 <sup>40</sup>	187.768
5	$[\text{Au}(\text{CH}_2\text{C}(\text{O})\text{Ph})(\text{IPr})]$ ( <b>7</b> )	7.09	7.0465	122.8	124.8425	192.6	193.871
7	$[\text{Au}(\text{CH}_2\text{CN})(\text{IPr})]$ ( <b>8</b> )	7.13	7.114	123.0	124.9495	192.7	192.736
6	$[\text{Au}(\text{CH}(\text{CN})_2)(\text{IPr})]$ ( <b>9</b> )	7.21	7.165	123.5	125.7155	184.7	186.37
8	$[\text{Au}(\text{CH}(\text{Ph})\text{CN})(\text{IPr})]$ ( <b>10</b> )	7.12	7.08	122.9	124.5035	189.3	188.813
9	$[\text{Au}(\text{CH}_2\text{NO}_2)(\text{IPr})]$ ( <b>11</b> )	7.15	7.097	123.2	125.195	189.8	191.481
10	$[\text{Au}(\text{CH}(\text{CH}_3)\text{NO}_2)(\text{IPr})]$ ( <b>12</b> )	7.14	7.127	123.1	125.017	189.1	191.157

<sup>a</sup>All values are from measurements in  $\text{CDCl}_3$ .

Parameters associated with the NHC ligand (C2, C45 and H45) and those associated with the carbanion ligand ( $\text{CR}_2\text{H}^-$ , Ca and Ch) formed two groups (Pane S8Table S20).

**Pane S8.** Correlation of parameters in NMR set.<sup>a</sup>

**Figure S35.** Correlation graph.

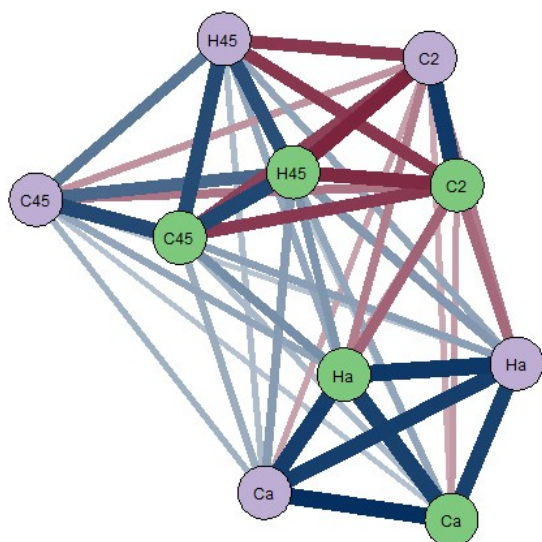
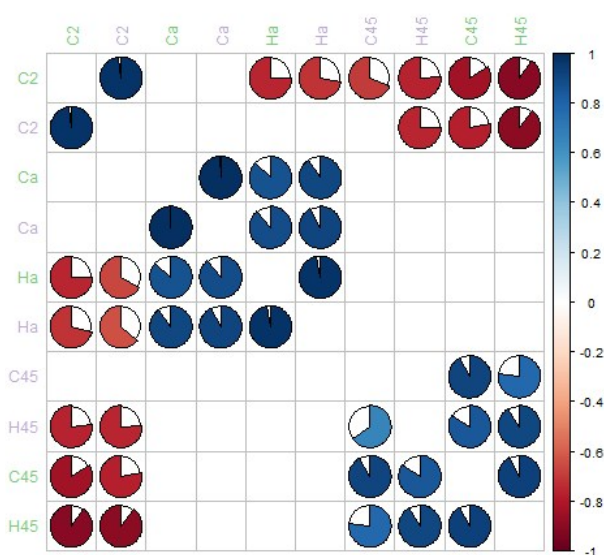


**Figure S36.** Correlation plot.



<sup>a</sup>Parameters representing experimental and modelled values are represented in green and purple, respectively.

Correlations between experimental and modelled (DFT) values were confirmed by linear models (Table S26).

**Table S26.** Linear models for experimental *versus* modelled values.<sup>a</sup>

Entry	z	Linear model		R <sup>2</sup>
		i	a	
1	Ca	-1.31	1.01	0.995
2	C45	43.63	0.64	0.838
3	C2	-37.67	1.19	0.956
4	Ha	0.12	0.90	0.947
5	H45	0.49	0.94	0.822

<sup>a</sup>Using formula  $z_{\text{exp}} = i + a \times z_{\text{dft}}$ .

## Order

Wiberg bond orders were calculated for the bonds Au-C<sup>2</sup>, Au-C<sup>α</sup> and C<sup>α</sup>-H<sup>α</sup> in [Au(CR<sub>2</sub>H)(IPr)] (**3-12**) (Table S27).

**Table S27.** Wiberg indices of selected bonds in [Au(CR<sub>2</sub>H)(IPr)] (**3-12**).

Complex	B(C <sup>2</sup> -Au)	B(C <sup>α</sup> -Au)	B(C <sup>α</sup> -C <sup>β</sup> )	B(C <sup>α</sup> -H <sup>α</sup> )
[Au(CH <sub>3</sub> )(IPr)] ( <b>3</b> )	0.4731	0.6176		
[Au(CH <sub>2</sub> C(O)CH <sub>3</sub> )(IPr)] ( <b>4</b> )	0.5312	0.481	1.1552	0.9491
[Au(CH(C(O)CH <sub>3</sub> ) <sub>2</sub> )(IPr)] ( <b>5</b> )	0.5907	0.3724	1.10575	0.8798
[Au(CH(C(O)OCH <sub>3</sub> ) <sub>2</sub> )(IPr)] ( <b>6</b> )	0.5876	0.3849	1.0824	0.8721
[Au(CH <sub>2</sub> C(O)Ph)(IPr)] ( <b>7</b> )	0.5361	0.4757	1.1597	0.9063
[Au(CH <sub>2</sub> CN)(IPr)] ( <b>8</b> )	0.5353	0.4886	1.1836	0.8783
[Au(CH(CN) <sub>2</sub> )(IPr)] ( <b>9</b> )	0.5974	0.3782	1.11855	0.826
[Au(CH(Ph)CN)(IPr)] ( <b>10</b> )	0.5686	0.412	1.0954	0.8564
[Au(CH <sub>2</sub> NO <sub>2</sub> )(IPr)] ( <b>11</b> )	0.5368	0.492	0.9781	0.9096
[Au(CH(CH <sub>3</sub> )NO <sub>2</sub> )(IPr)] ( <b>12</b> )	0.5465	0.4645	0.99965	0.8881

Statistically significant correlations were found (in descending order of correlation strength) between parameters Ca-Au and C2-Au (positive), C2-Au and Ca-Ha (positive) and Ca-Au and Ca-Ha (negative) (Pane S9). Weaker bonds between C<sup>α</sup> and H<sup>α</sup> thus appeared to lead to stronger bonds between Au and the ligands.

**Pane S9.** Correlation of parameters in order set.

**Figure S37.** Correlation graph.

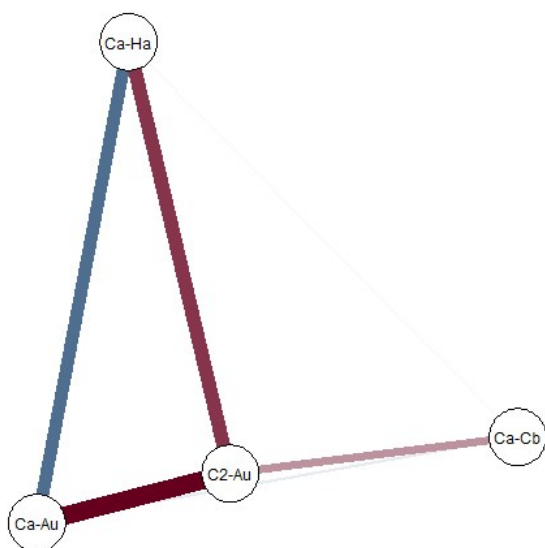
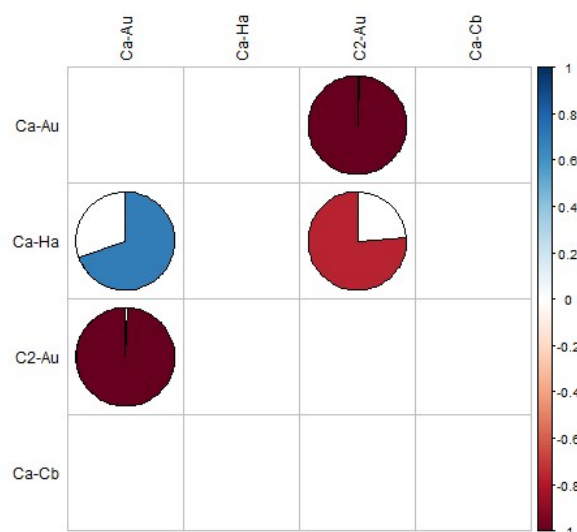


**Figure S38.** Correlation plot.



## Population

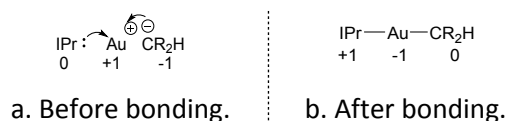
Mulliken populations were calculated for different parts of the complexes for [AuCl(IPr)] (1), [Au(OH)(IPr)] (2) and [Au(CR<sub>2</sub>H)(IPr)] (3-12): C<sup>2</sup>, Au and C<sup>α</sup> (Table S28).<sup>72</sup>

**Table S28.** Mulliken population analysis for [AuCl(IPr)] (1), [Au(OH)(IPr)] (2) and [Au(CR<sub>2</sub>H)(IPr)] (3-12).

Complex	M(C <sup>2</sup> )	M(Au)	M(C <sup>α</sup> )
[AuCl(IPr)] (1)	1.02	-0.86	-0.16
[Au(OH)(IPr)] (2)	0.90	-0.74	-0.15
[Au(CH <sub>3</sub> )(IPr)] (3)	1.00	-1.1	0.10
[Au(CH <sub>2</sub> C(O)CH <sub>3</sub> )(IPr)] (4)	1.12	-1.22	0.10
[Au(CH(C(O)CH <sub>3</sub> ) <sub>2</sub> )(IPr)] (5)	1.20	-1.28	0.08
[Au(CH(C(O)OCH <sub>3</sub> ) <sub>2</sub> )(IPr)] (6)	1.16	-1.17	0.01
[Au(CH <sub>2</sub> C(O)Ph)(IPr)] (7)	0.97	-1.02	0.05
[Au(CH <sub>2</sub> CN)(IPr)] (8)	1.24	-1.05	-0.19
[Au(CH(CN) <sub>2</sub> )(IPr)] (9)	1.02	-0.82	-0.20
[Au(CH(Ph)CN)(IPr)] (10)	1.15	-1.02	-0.13
[Au(CH <sub>2</sub> NO <sub>2</sub> )(IPr)] (11)	1.09	-1.13	0.04
[Au(CH(CH <sub>3</sub> )NO <sub>2</sub> )(IPr)] (12)	1.03	-1.05	0.02

When neutral, cationic and anionic fragments IPr-, Au<sup>+</sup> and CR<sub>2</sub>H<sup>-</sup> would engage in σ-bonding interactions to form [Au(CR<sub>2</sub>H)(IPr)], charges of +1, -1 and 0 would be expected (Figure S39). Deviations from these values might be indicative of additional back-bonding interactions or interactions of π-symmetry.

**Figure S39.** Extreme expected populations values.



As a measure of “population transfer” from C<sup>α</sup> to Au,  $1 + M(\text{Au})$  was added to the dataset as  $M(\text{C}^\alpha \rightarrow)$ . As a measure of combined “population transfer” from both C<sup>2</sup> and C<sup>α</sup> to Au,  $M(\rightarrow \text{Au} \leftarrow)$  was added to the dataset as  $1 - M(\text{Au})$ . It follows from (the figure) that extreme values of these parameters approach 1 and 2, respectively. Relative “population transfers” from C<sup>2</sup> and C<sup>α</sup> were added as  $M(\% \text{C}^\alpha)$  and  $M(\% \text{C}^2)$ . Other “population distribution” and all other possible “population transfers” were not included in the dataset. Note that care should be taken to ascribe chemical meaning to all population numbers and use of relative values between different values should be preferred.

The three initial parameters (carbene, gold and ligand) were found to be only modestly correlated, with the strongest correlation between ligand (CR<sub>2</sub>H<sup>-</sup> fragment) and gold (Pane S10). Addition of derived parameters (from-ligand, to-gold, percent-ligand and percent-from) resulted in high collinearity in the population set.

**Pane S10.** Correlation of parameters in population set.  
**Figure S40.** Correlation graph.

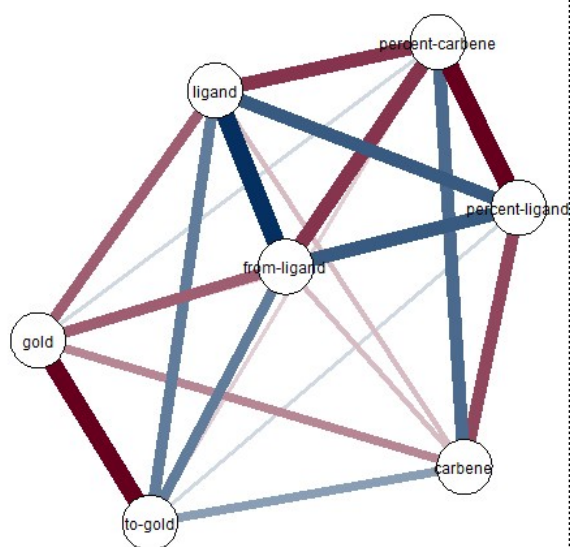
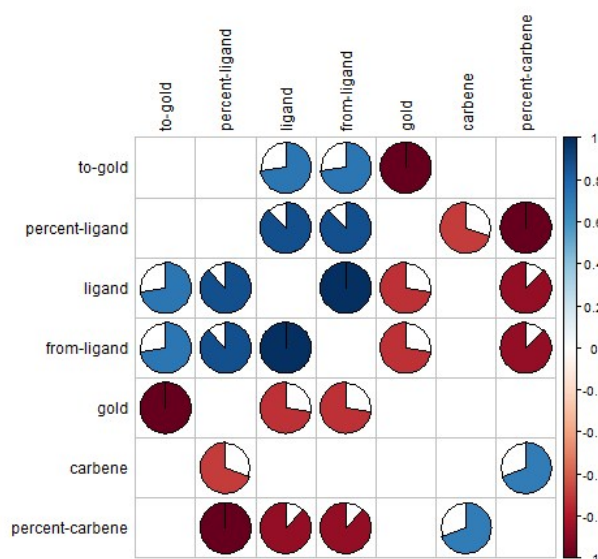


**Figure S41.** Correlation plot.



## Structure

Experimental and modelled bond lengths  $d(\text{Au}-\text{C}^2)$ ,  $d(\text{Au}-\text{C}^\alpha)$  and angle  $\angle \text{C}^2-\text{Au}-\text{C}^\alpha$  of  $[\text{Au}(\text{CR}_2\text{H})(\text{IPr})]$  (**3-12**) were measured (Table S29). Experimental measurements for known complexes were taken from data in the CCDC: **3** (775773), **4** (1039066), **5** (1039066), **6** (759013).

**Table S29.** Selected bond lengths and angles in  $[\text{Au}(\text{CR}_2\text{H})(\text{IPr})]$  (**3-12**).

Entry	Complex	$d(\text{Au}-\text{C}^2)$		$d(\text{Au}-\text{C}^\alpha)$		$\angle \text{C}^2-\text{Au}-\text{C}^\alpha$	
		Experimental [Å]	Modelled [Å]	Experimental [Å]	Modelled [Å]	Experimental [°]	Modelled [°]
1	$[\text{Au}(\text{CH}_3)(\text{IPr})]$ ( <b>3</b> )	2.038(5)	2.076	2.039(5)	2.039	180.000(2)	180.000
2	$[\text{Au}(\text{CH}_2\text{C}(\text{O})\text{CH}_3)(\text{IPr})]$ ( <b>4</b> )	2.024(7)	2.050	2.091(9)	2.091	175.7(3)	175.680
3	$[\text{Au}(\text{CH}(\text{C}(\text{O})\text{CH}_3)_2)(\text{IPr})]$ ( <b>5</b> )	1.997(3)	2.026	2.120(3)	2.120	178.40(11)	177.460
4	$[\text{Au}(\text{CH}(\text{C}(\text{O})\text{OCH}_3)_2)(\text{IPr})]$ ( <b>6</b> )	2.014(7)	2.026	2.140(7)	2.140	174.6(3)	174.559
5	$[\text{Au}(\text{CH}_2\text{C}(\text{O})\text{Ph})(\text{IPr})]$ ( <b>7</b> )	2.019(3)	2.050	2.094(3)	2.093	179.64(13)	179.636
6 <sup>a</sup>	$[\text{Au}(\text{CH}_2\text{CN})(\text{IPr})]$ ( <b>8</b> )	2.004(3) - 2.017(3)	2.048	2.060(4) - 2.093(3)	2.093	176.33(12) - 177.97(17)	176.342
7	$[\text{Au}(\text{CH}(\text{CN})_2)(\text{IPr})]$ ( <b>9</b> )	2.018(11)	2.030	2.113(12)	2.113	178.3(4)	178.269
8	$[\text{Au}(\text{CH}(\text{Ph})\text{CN})(\text{IPr})]$ ( <b>10</b> )	2.021(5)	2.036	2.087(5)	2.087	175.4(2)	175.387
9	$[\text{Au}(\text{CH}_2\text{NO}_2)(\text{IPr})]$ ( <b>11</b> )	2.020(4)	2.046	2.077(4)	2.077	177.23(16)	177.222
10	$[\text{Au}(\text{CH}(\text{CH}_3)\text{NO}_2)(\text{IPr})]$ ( <b>12</b> )	1.995(6)	2.043	2.085(7)	2.085	174.9(3)	174.922

<sup>a</sup>Two molecules were found in the crystal lattice: the range of distances and angles obtained is shown, average values were used in further analysis.

Various bond were measured in the IPr and carbanion ( $\text{CR}_2\text{H}^-$ ) ligands of  $[\text{Au}(\text{CR}_2\text{H})(\text{IPr})]$  (**3-12**) (Pane S11). Of the bond lengths associated with the IPr ligand and Table S30),  $d(\text{C}^4-\text{C}^5)$ ,  $d(\text{C}^{4/5}-\text{N}^{1/3})$  and  $d(\text{C}^2-\text{N}^{1/3})$ , the last one has previously been related to electron donation of the ligand.<sup>73</sup> The pyramid height,  $h(\text{C}^\alpha)$ , measured the distance from  $\text{C}^\alpha$  to a plane defined by its substituents (Figure S43) and was used in addition to bond length  $d(\text{C}^\alpha-\text{H}^\alpha)$  (Table S31).

**Pane S11.** Definition of structural parameters.

**Figure S42.** Distances in IPr ligand. **Figure S43.** Tetrahedron height.<sup>32</sup>

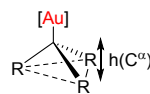
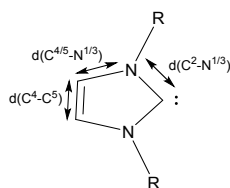


**Table S30.** Selected bond lengths and angles in  $[Au(CR_2H)(IPr)]$  (**3-12**).

Entry	Complex	$d(C^4-C^5)$		$d(C^{4/5}-N^{1/3})$		$d(C^2-N^{1/3})$	
		Experimental [Å]	Modelled [Å]	Experimental [Å]	Modelled [Å]	Experimental [°]	Modelled [°]
1	$[Au(CH_3)(IPr)]$ ( <b>3</b> )	1.250	1.370	1.381	1.392	1.350	1.368
2	$[Au(CH_2C(O)CH_3)(IPr)]$ ( <b>4</b> )	1.343	1.371	1.394	1.391	1.344	1.365
3	$[Au(CH(C(O)CH_3)_2)(IPr)]$ ( <b>5</b> )	1.350	1.373	1.377	1.391	1.351	1.362
4	$[Au(CH(C(O)OCH_3)_2)(IPr)]$ ( <b>6</b> )	1.337	1.372	1.392	1.391	1.351	1.363
5	$[Au(CH_2C(O)Ph)(IPr)]$ ( <b>7</b> )	1.340	1.371	1.387	1.392	1.358	1.365
6	$[Au(CH_2CN)(IPr)]$ ( <b>8</b> )	1.348	1.371	1.379	1.391	1.353	1.365
7	$[Au(CH(CN)_2)(IPr)]$ ( <b>9</b> )	1.336	1.371	1.387	1.391	1.357	1.363
8	$[Au(CH(Ph)CN)(IPr)]$ ( <b>10</b> )	1.330	1.372	1.384	1.391	1.350	1.363
9	$[Au(CH_2NO_2)(IPr)]$ ( <b>11</b> )	1.342	1.371	1.380	1.391	1.352	1.365
10	$[Au(CH(CH_3)NO_2)(IPr)]$ ( <b>12</b> )	1.334	1.372	1.374	1.390	1.349	1.364

**Table S31.** Selected bond lengths and pyramid heights  $[Au(CR_2H)(IPr)]$  (**3-12**).

Entry	Complex	$d(C^\alpha-H^\alpha)$		$h(C^\alpha)$	
		Experimental [Å]	Modelled [Å]	Experimental [Å]	Modelled [Å]
1	$[Au(CH_3)(IPr)]$ ( <b>3</b> )	0.980	1.111	0.327	0.405
2	$[Au(CH_2C(O)CH_3)(IPr)]$ ( <b>4</b> )	0.990	1.107	0.352	0.340
3	$[Au(CH(C(O)CH_3)_2)(IPr)]$ ( <b>5</b> )	1.001	1.108	0.329	0.252
4	$[Au(CH(C(O)OCH_3)_2)(IPr)]$ ( <b>6</b> )	0.980	1.103	0.365	0.297
5	$[Au(CH_2C(O)Ph)(IPr)]$ ( <b>7</b> )	0.990	1.106	0.355	0.341
6	$[Au(CH_2CN)(IPr)]$ ( <b>8</b> )	0.990	1.108	0.374	0.396
7	$[Au(CH(CN)_2)(IPr)]$ ( <b>9</b> )	1.001	1.108	0.401	0.365
8	$[Au(CH(Ph)CN)(IPr)]$ ( <b>10</b> )	0.999	1.107	0.417	0.360
9	$[Au(CH_2NO_2)(IPr)]$ ( <b>11</b> )	0.990	1.104	0.377	0.399
10	$[Au(CH(CH_3)NO_2)(IPr)]$ ( <b>12</b> )	0.998	1.106	0.405	0.425

Structural variation in  $[Au(CR_2H)(IPr)]$  (**3-12**) was also measured by dihedral angles  $\angle N^1-C^5-C^4-N^3$ , angles  $\angle N^1-C^2-N^3$  associated with the IPr ligand and dihedral angle  $\angle N^1-C^2-C^\alpha-R$  associated with the relative orientations of the IPr and carbanion ( $CR_2H^-$ ) ligands (Table S32).

**Table S32.** Selected angles in  $[Au(CR_2H)(IPr)]$  (**3-12**).

Entry	Complex	$\angle N^1-C^5-C^4-N^3$		$\angle N^1-C^2-N^3$		$\angle N^1-C^2-C^\alpha-R$	
		Experimental [°]	Modelled [°]	Experimental [°]	Modelled [°]	Experimental [°]	Modelled [°]
1	$[Au(CH_3)(IPr)]$ ( <b>3</b> )	0.935	0.147	104.408	103.972		
2	$[Au(CH_2C(O)CH_3)(IPr)]$ ( <b>4</b> )	0.617	0.086	105.759	104.422	11.510	27.989
3	$[Au(CH(C(O)CH_3)_2)(IPr)]$ ( <b>5</b> )	0.040	0.027	104.587	105.212	20.346	13.290
4	$[Au(CH(C(O)OCH_3)_2)(IPr)]$ ( <b>6</b> )	0.427	0.059	104.511	105.040	5.906	8.222
5	$[Au(CH_2C(O)Ph)(IPr)]$ ( <b>7</b> )	0.478	0.094	104.583	104.710	84.620	83.956
6	$[Au(CH_2CN)(IPr)]$ ( <b>8</b> )	0.388	0.125	104.408	104.517	59.957	86.595
7	$[Au(CH(CN)_2)(IPr)]$ ( <b>9</b> )	0.125	0.320	105.299	104.982	7.130	46.216
8	$[Au(CH(Ph)CN)(IPr)]$ ( <b>10</b> )	0.181	0.228	105.171	104.825	48.242	54.966
9	$[Au(CH_2NO_2)(IPr)]$ ( <b>11</b> )	0.000	0.001	104.471	104.630		
10	$[Au(CH(CH_3)NO_2)(IPr)]$ ( <b>12</b> )	0.271	0.260	104.870	104.737	23.845	21.862

In the coordinating carbon atom of the carbanion ligand ( $CR_2H^-$ ),  $C^\alpha$ , the nature of the hybridised atomic orbital,  $sp^\lambda$ , could be derived from the position of its substituents. The orbitals involved in bonds  $Au-C^\alpha$ ,  $C^\alpha-$

R<sup>1</sup>, C<sup>α</sup>-R<sup>2</sup> and C<sup>α</sup>-R<sup>3</sup> were labelled as λ<sub>1</sub>, λ<sub>2a</sub>, λ<sub>2b</sub> and λ<sub>2c</sub> with corresponding bond angles ∠ Au-C<sup>α</sup>-R<sup>1</sup>, ∠ Au-C<sup>α</sup>-R<sup>2</sup> and ∠ Au-C<sup>α</sup>-R<sup>3</sup> labelled as Θ<sub>12a</sub>, Θ<sub>12b</sub> and Θ<sub>12c</sub>. Using Eq. S7 (or in rearranged form, Eq. S8), products λ<sub>1</sub>×λ<sub>2a</sub>, λ<sub>1</sub>×λ<sub>2b</sub> and λ<sub>1</sub>×λ<sub>2c</sub> could be derived.<sup>74</sup> Because of the equivalence of λ and %s (Eq. S8), values %s<sub>1</sub>, %s<sub>2a</sub>, %s<sub>2b</sub> and %s<sub>2c</sub> could be expressed as a function of these products. Given that the sum of these four quantities adds up to 100%, all equations could be solved numerically.

$$1 + \sqrt{\lambda_i \times \lambda_j} \times \cos(\Theta_{ij}) = 0 \quad (\text{S7})$$

$$\lambda_i \times \lambda_j = \frac{1}{\cos(\Theta_{ij})^2} \quad (\text{S8})$$

$$\%s_i = \frac{100}{\lambda_i + 1} \quad (\text{S9})$$

Values for the hybridisation parameters of the Au-C<sup>α</sup> bond (λ<sub>1</sub>) and average for the bonds C<sup>α</sup>-R<sup>1</sup>, C<sup>α</sup>-R<sup>2</sup> and C<sup>α</sup>-R<sup>3</sup> (⟨λ<sub>2a</sub>, λ<sub>2b</sub>, λ<sub>2c</sub>⟩) as well as the corresponding s-character values (%s<sub>1</sub> and ⟨%s<sub>2a</sub>, %s<sub>2b</sub>, %s<sub>2c</sub>⟩) were calculated from the experimental (Table S33) and the modelled (DFT) structures (Table S34).

**Table S33.** Coulson parameters for experimental data of [Au(CR<sub>2</sub>H)(IPr)] (**3-12**).

Entry	Complex	hybridisation parameter		s character	
		λ <sub>1</sub> [-]	⟨λ <sub>2a</sub> , λ <sub>2b</sub> , λ <sub>2c</sub> ⟩ [-]	%s <sub>1</sub> [%]	⟨%s <sub>2a</sub> , %s <sub>2b</sub> , %s <sub>2c</sub> ⟩ [%]
1	[Au(CH <sub>3</sub> )(IPr)] ( <b>3</b> )	3.0	3.0	25	25
2	[Au(CH <sub>2</sub> C(O)CH <sub>3</sub> )(IPr)] ( <b>4</b> )	3.5	3.3	22	26
3	[Au(CH(C(O)CH <sub>3</sub> ) <sub>2</sub> )(IPr)] ( <b>5</b> )	6.0	2.8	14	29
4	[Au(CH(C(O)OCH <sub>3</sub> ) <sub>2</sub> )(IPr)] ( <b>6</b> )	4.5	4.0	18	27
5	[Au(CH <sub>2</sub> C(O)Ph)(IPr)] ( <b>7</b> )	3.4	3.2	23	26
6	[Au(CH <sub>2</sub> CN)(IPr)] ( <b>8</b> )	2.8	3.1	26	25
7	[Au(CH(CN) <sub>2</sub> )(IPr)] ( <b>9</b> )	3.5	2.9	22	26
8	[Au(CH(Ph)CN)(IPr)] ( <b>10</b> )	3.2	3.0	24	25
9	[Au(CH <sub>2</sub> NO <sub>2</sub> )(IPr)] ( <b>11</b> )	2.7	3.1	27	24
10	[Au(CH(CH <sub>3</sub> )NO <sub>2</sub> )(IPr)] ( <b>12</b> )	3.4	3.0	23	26

**Table S34.** Coulson parameters for modelled data of complexes [Au(CR<sub>2</sub>H)(IPr)] (**3-12**).

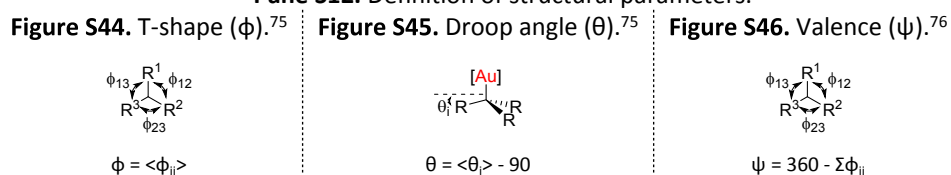
Entry	Complex	hybridisation parameter		s-character	
		λ <sub>1</sub> [-]	⟨λ <sub>2a</sub> , λ <sub>2b</sub> , λ <sub>2c</sub> ⟩ [-]	%s <sub>1</sub> [%]	⟨%s <sub>2a</sub> , %s <sub>2b</sub> , %s <sub>2c</sub> ⟩ [%]
1	[Au(CH <sub>3</sub> )(IPr)] ( <b>3</b> )	2.3	3.2	31	23
2	[Au(CH <sub>2</sub> C(O)CH <sub>3</sub> )(IPr)] ( <b>4</b> )	4.9	3.2	17	28
3	[Au(CH(C(O)CH <sub>3</sub> ) <sub>2</sub> )(IPr)] ( <b>5</b> )	12.8	2.0	7	31
4	[Au(CH(C(O)OCH <sub>3</sub> ) <sub>2</sub> )(IPr)] ( <b>6</b> )	8.6	2.9	10	30
5	[Au(CH <sub>2</sub> C(O)Ph)(IPr)] ( <b>7</b> )	4.8	3.0	17	28
6	[Au(CH <sub>2</sub> CN)(IPr)] ( <b>8</b> )	3.1	3.1	24	25
7	[Au(CH(CN) <sub>2</sub> )(IPr)] ( <b>9</b> )	5.0	2.9	17	28
8	[Au(CH(Ph)CN)(IPr)] ( <b>10</b> )	5.3	3.1	16	28
9	[Au(CH <sub>2</sub> NO <sub>2</sub> )(IPr)] ( <b>11</b> )	3.0	3.3	25	25
10	[Au(CH(CH <sub>3</sub> )NO <sub>2</sub> )(IPr)] ( <b>12</b> )	3.6	3.1	22	26

Hybridisation parameters λ<sub>1</sub> and s-character parameters %s<sub>1</sub> associated with the Au-C<sup>α</sup> bond were subsequently referred to as Coulson parameters λ(C<sup>α</sup>-Au) and σ(C<sup>α</sup>-Au) (Table S35).

**Table S35.** Coulson parameters in  $[\text{Au}(\text{CR}_2\text{H})(\text{IPr})]$  (**3-12**).

Entry	Complex	$\lambda(\text{C}^\alpha\text{-Au})$		$\sigma(\text{C}^\alpha\text{-Au})$	
		Experimental [-]	Modelled [-]	Experimental [%]	Modelled [%]
1	$[\text{Au}(\text{CH}_3)(\text{IPr})]$ ( <b>3</b> )	2.997	2.267	25	31
2	$[\text{Au}(\text{CH}_2\text{C}(\text{O})\text{CH}_3)(\text{IPr})]$ ( <b>4</b> )	3.470	4.870	22	17
3	$[\text{Au}(\text{CH}(\text{C}(\text{O})\text{CH}_3)_2)(\text{IPr})]$ ( <b>5</b> )	6.034	12.775	14	7
4	$[\text{Au}(\text{CH}(\text{C}(\text{O})\text{OCH}_3)_2)(\text{IPr})]$ ( <b>6</b> )	4.494	8.584	18	10
5	$[\text{Au}(\text{CH}_2\text{C}(\text{O})\text{Ph})(\text{IPr})]$ ( <b>7</b> )	3.390	4.759	23	17
6	$[\text{Au}(\text{CH}_2\text{CN})(\text{IPr})]$ ( <b>8</b> )	2.829	3.089	26	24
7	$[\text{Au}(\text{CH}(\text{CN})_2)(\text{IPr})]$ ( <b>9</b> )	3.486	4.968	22	17
8	$[\text{Au}(\text{CH}(\text{Ph})\text{CN})(\text{IPr})]$ ( <b>10</b> )	3.234	5.304	24	16
9	$[\text{Au}(\text{CH}_2\text{NO}_2)(\text{IPr})]$ ( <b>11</b> )	2.744	3.028	27	25
10	$[\text{Au}(\text{CH}(\text{CH}_3)\text{NO}_2)(\text{IPr})]$ ( <b>12</b> )	3.410	3.583	23	22

The geometry of the carbanion ligands ( $\text{CR}_2\text{H}^-$ ) was measured by various derived angles around  $\text{C}^\alpha$  (Pane S12 and Table S36). The T-shape angle,  $\phi$ , was defined as the average of the angles between different substituents of  $\text{C}^\alpha$  (Figure S44). Figure S45. The Droop angle,  $\theta$ , and the valence angle,  $\psi$ , measured the flatness of the ligand from the average values of the angles  $\angle \text{Au}-\text{C}^\alpha-\text{R}$  (Figure S45) and the average of the angles between different substituents of  $\text{C}^\alpha$  (Figure S46), respectively.

**Pane S12.** Definition of structural parameters.**Table S36.** Derived angles in  $[\text{Au}(\text{CR}_2\text{H})(\text{IPr})]$  (**3-12**).

Entry	Complex	$\phi$		$\theta$		$\psi$		Averages <i>p</i> -values
		Experimental [°]	Modelled [°]	Experimental [°]	Modelled [°]	Experimental [°]	Modelled [°]	
1	$[\text{Au}(\text{CH}_3)(\text{IPr})]$ ( <b>3</b> )	109.465	107.513	19.477	21.365	31.604	37.460	
2	$[\text{Au}(\text{CH}_2\text{C}(\text{O})\text{CH}_3)(\text{IPr})]$ ( <b>4</b> )	110.410	112.418	18.513	16.322	28.770	22.746	
3	$[\text{Au}(\text{CH}(\text{C}(\text{O})\text{CH}_3)_2)(\text{IPr})]$ ( <b>5</b> )	113.628	116.556	14.995	10.792	19.117	10.331	
4	$[\text{Au}(\text{CH}(\text{C}(\text{O})\text{OCH}_3)_2)(\text{IPr})]$ ( <b>6</b> )	111.969	115.176	16.815	12.926	24.092	14.473	
5	$[\text{Au}(\text{CH}_2\text{C}(\text{O})\text{Ph})(\text{IPr})]$ ( <b>7</b> )	110.266	112.320	18.666	16.446	29.201	23.040	
6	$[\text{Au}(\text{CH}_2\text{CN})(\text{IPr})]$ ( <b>8</b> )	109.065	109.670	19.868	19.277	32.804	30.989	
7	$[\text{Au}(\text{CH}(\text{CN})_2)(\text{IPr})]$ ( <b>9</b> )	110.453	112.584	18.463	16.164	28.640	22.247	
8	$[\text{Au}(\text{CH}(\text{Ph})\text{CN})(\text{IPr})]$ ( <b>10</b> )	109.919	112.942	18.975	15.759	30.243	21.173	
9	$[\text{Au}(\text{CH}_2\text{NO}_2)(\text{IPr})]$ ( <b>11</b> )	108.847	109.457	20.076	19.415	33.460	31.629	
10	$[\text{Au}(\text{CH}(\text{CH}_3)\text{NO}_2)(\text{IPr})]$ ( <b>12</b> )	110.288	110.383	18.626	18.326	29.136	28.851	
		110.4±1.4	111.9±2.7	18.4±1.5	16.7±3.1	28.7±4.3	24.3±8.2	
		0.07	0.02	0.06	0.02	0.07	0.02	

Values derived from experimental and modelled (DFT) structures agreed well for parameters angle-C2-Au-Ca, angle-Ca-D, angle-Ca-T, angle-Ca-valence, angle-N-C2-Ca-R, coulson-lambda-Au, coulson-sigma-Au and distance-Au-Ca, but not for other angles and bond distances (Table S37).

**Table S37.** Linear models for experimental *versus* modelled values.<sup>a</sup>

Entry	z	Linear model		R <sup>2</sup>
		i	a	
1	angle-C2-Au-Ca	33.73	0.81	0.684
2	angle-Ca-D	11.11	0.44	0.833
3	angle-Ca-T	59.09	0.46	0.774
4	angle-Ca-valence	17.56	0.46	0.774
5	angle-N-C2-Ca-R	-1.79	0.80	0.733
6	angle-N-C2-N	96.16	0.08	0.004
7	angle-N-C45-N	0.35	-0.05	0.000
8	coulson-lambda-Au	1.99	0.30	0.951
9	coulson-sigma-Au	0.14	0.47	0.760
10	distance-Au-C2	0.87	0.56	0.443
11	distance-Au-Ca	-0.33	1.14	0.782
12	distance-C2-N	1.60	-0.18	0.006
13	distance-C4-C5	-21.09	16.35	0.277
14	distance-C45-N	-1.57	2.13	0.037
15	distance-Ca-Ha	0.66	0.30	0.008
16	distance-Ca-T	0.28	0.25	0.181

<sup>a</sup>Using formula  $Z_{\text{exp}} = i + a \times Z_{\text{dft}}$ .

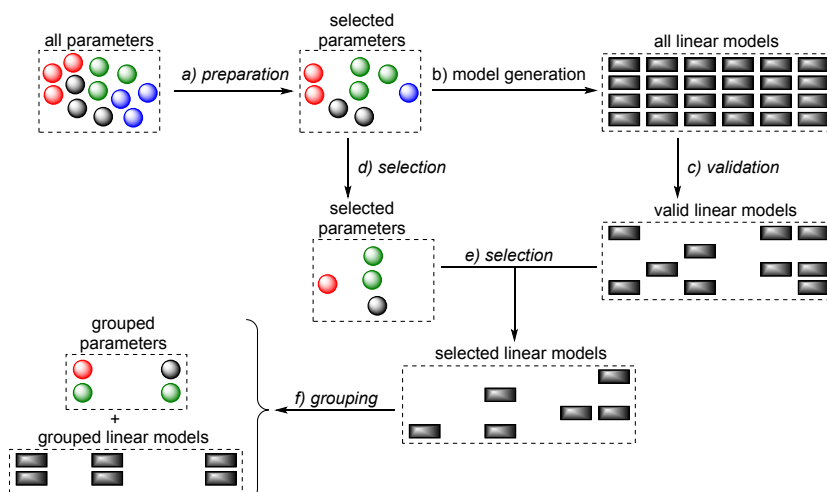
This set contained too many parameters to be clearly visualized in a correlation graph or plot.

## 11. Regression analysis

With all data available (Section 10), A stepwise regression analysis was performed to obtain groups of parameters and linear models for combination of parameters within groups (Figure S47):

- Collinearity between variables was addressed (Section 11.1).
- Linear models were generated from different combinations of parameters (Section 11.2).
- Statistical tests rejected most of the linear models (Section 11.3).
- The most important parameters were identified (Section 11.4).
- Linear models containing important parameters were selected (Section 11.5).
- Parameters and corresponding models were grouped to facilitate explanations (Section 11.6).

**Figure S47.** Overview of regression analysis.<sup>a</sup>



<sup>a</sup>Parameters and linear models are depicted as spheres (colored by set) and cubes, respectively.

### Data preparation

Correlation of variables (Section 12) jointly included in linear models (collinearity) degrades the quality of the model or could lead to incorrect predictions.<sup>77</sup> Since data for some parameters was found not to be normally distributed (Table S38), Spearman correlations<sup>78</sup> were used rather than Pearson correlations to assess collinearity.<sup>79</sup> For this purpose, correlations were considered statistically significant if their false-discovery rate adjusted (FDR) *p*-values fell below 0.05.<sup>80</sup>

**Table S38.** Non-normally distributed parameters.<sup>a</sup>

Set	Parameters
EDA	E-elstat-Ca, E-steric-Ca, pi-DON-Ca
Hammett	meta-product and para-product
IR	delta-exp
$pK_a$	pka-pka
Population	ligand and from-ligand
Rate	relative
Structure	angle-N-C2-N-exp, coulson-lambda-Au-dft, coulson-lambda-Au-exp, distance-C4-C5-exp

<sup>a</sup>Based on the Shapiro test *p*-value lower than 0.05.<sup>81</sup>

For further correlation-based analysis (Section 11.4), a number of parameters was excluded (Table S39),<sup>82</sup> but these were still considered when the final linear models were selected (Section 11.5).

**Table S39.** Excluded collinear parameters.<sup>a</sup>

Set	Parameters
Component	s0.5, s1.0
NMR	Ha-dft, Ca-dft, C2-dft
Order	C2-Au, Ca-Au
Population	to-gold, from-ligand, percent-carbene
Structure	angle-Ca-T-exp, angle-Ca-D-exp, angle-Ca-D-dft, coulson-sigma-Au-dft, coulson-lambda-Au-exp, coulson-lambda-Au-dft, distance-Au-C2-dft, angle-N-C2-N-dft, angle-Ca-valence

<sup>a</sup>Based on the Spearman correlations higher than 0.999.<sup>81</sup>

## Model generation

All possible combinations of (up to three) parameters were initially evaluated to generate a pool of one-parameter (point-to-point) and multi-parameter (point-to-plane or higher dimension) linear models. In this process, models containing collinear parameters were rejected. Usability of the models was initially assessed by the goodness of fit ( $R^2 > 0.6$ ), or the adjusted variant for multi-parameter models.<sup>83</sup> From the approximately 7.000, 70.000 and 600.000 possible combinations of parameters for linear models with 1, 2 and 3 explanatory variables, about 250.000 remained.

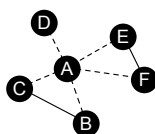
None of these linear models included parameters from the rate set and another 50.000 four-parameter models with this variable were evaluated to give 20 models for further analysis.

## Model validation

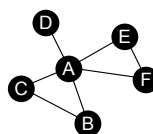
Statistical significance was tested for the overall models and for the contributions of the intercept and the variables included. About 3.000 model were found to be significant based on  $p$ -values lower than 0.05 (same cut-off was used for other tests). The same number of models remained when those with non-normal residuals (Shapiro test), those with outliers (Bonferonni test) or those heteroscedastic ones (Studentized Breusch-Pagan) were removed from the initial pool. About 2.000 models were free of multicollinear artefacts (based on the variance inflation factor test)<sup>84</sup> and about 400 contained no influential points (based on Cook distance).<sup>85</sup> When all selection criteria were applied together, about 300 linear models remained.

## Parameter selection

Possible relations between different parameters within each group were investigated by using these as edges in a graph with vertex weights defined by the significant correlation of pairs of parameters. The importance of different parameters could then be ranked based on their connectivity to other parameters by means of a network analysis.<sup>86</sup> For this purpose, network parameters degree and betweenness were used (Table S40).

**Table S40.** Illustration of selected network properties.<sup>87</sup>**Figure S48.** Degree of node-connectivity.

The degree of a node is the number of edges linking it to other nodes of the network. For A, these edges are drawn as dotted line: degree = 5.

**Figure S49.** Node betweenness centrality.

The edge betweenness centrality of a node is the proportion of geodesic distances between any two nodes that contain the node. For A: betweenness = 8.

		passing through node				
		a	b	c	d	e
geodesic distance	a					
	b			x	✓	✓
	c	x			✓	✓
	d		✓	✓		✓
	e	✓	✓	✓		x
	f	✓	✓	✓	x	

For each set, the three parameters with highest values for the degree and betweenness properties were prioritized for further analysis (Table S41).

**Table S41.** Network properties for parameters of complexes [Au(CR<sub>2</sub>H)(IPr)] (**3-12**).

Entry	Parameter	Degree	Betweenness
Component			
1	s0.0	3	0.11
EDA			
2	E-int-Ca	11	275.73
3	E-Pauli-Ca	6	28.28
4	E-Pauli-C2	3	26.00
Hammett			
5	meta-sum	7	147.86
6	para-sum	4	14.86
IR			
7	delta-dft	5	41.62
8	substrate-exp	5	34.62
9	substrate-dft	4	13.12
NMR			
10	C2-exp	7	198.00
11	C2-dft	6	18.00
12	C45-exp	3	16.00
Order			
13	C2-Au	9	225.00
14	Ca-Ha	3	52.00
15	Ca-Cb	2	3.92
Population			
16	percent-ligand	2	1.00
17	carbene	1	0.00
Structure			
18	angle-Ca-D-dft	2	0.11
19	angle-Ca-T-dft	2	0
20	angle-Ca-D-exp	1	0

### Model selection

With a pool of statistically significant linear models (Section 11.3) and a list of highly correlated parameters (Section 11.4), a finer selection of models could be made. First, all models were selected that contained at least one of the parameters from Table S41, their collinear ones (Section 11.1), or parameters from the  $pK_a$  or rate sets. Linear models that contained parameters derived from both experimental and modelled (DFT) data were rejected. For single-parameter linear models, “duplicated” ones with dependent and explanatory variables reversed were rejected. For multi-parameter models, the number of other linear models with the same explanatory variables was then used to prioritize combinations of parameters. For these models, those with explanatory variables with conflicting units (*e.g.* angles and distances) were rejected in favour of those with matching units (*e.g.* different chemical shifts). About 150 linear models remained after this selection procedure.

### Parameter and model grouping

The remaining models were next ordered by chemical intuition; *e.g.* constant parameters such as Hammett and  $pK_a$  appeared best to be used as independent variables whereas high level properties (electronic character, EDA) appeared to be best used as explanatory variables.<sup>88</sup> The counts of explanatory variables in both single-parameter and multi-parameter linear models were also used to guide this manual process. In some instances, dependent and independent variables are swapped to maximize the number of entries to be included.<sup>89</sup>

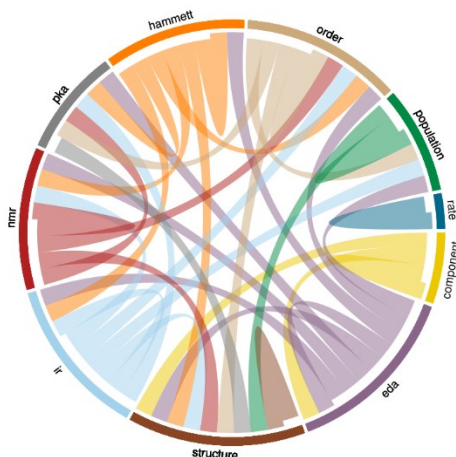
Based on their mutual correlations, the parameters present in the remaining linear models were assigned to different groups. At this stage, correlation plots of the different groups were generated (Section 13) and plots of the linear models were generated (Section 14). In-depth analysis of correlations within these groups, the coefficients of the selected linear models and iterative refinement of the assignment of parameters to groups resulted in the final analysis as presented in the main text.

## 12. Correlation analysis

Correlation of parameters within the different sets might give information if descriptors quantify different properties. Collinear parameters should not be used in linear models if their values provide alternative representations of the same property. This situation arises when parameters are transformed or obtained by different techniques that measure the same underlying quantity.

Representation of statistically significant Spearman correlations (FDR corrected  $p$ -value less than 0.05) between parameters within and between sets in a chord diagram (Figure S50) allows for easier interpretation than tabulated values would (Table S42). The limited connectivity of parameters from the component and population sets to parameters in other sets, for example, might be used as a starting point for exploratory analysis.

**Figure S50.** Pairwise correlations between sets.<sup>a</sup>



<sup>a</sup>Different sets are color coded (Figure S29).

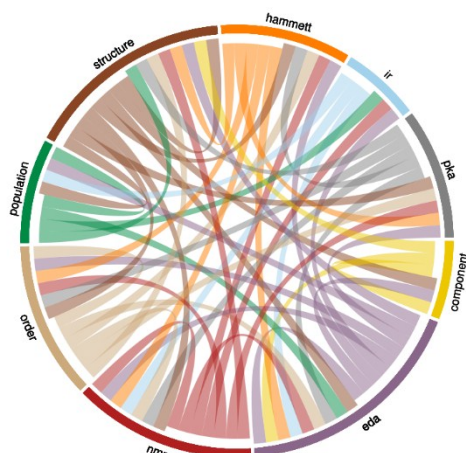
**Table S42.** Numbers of correlations within and between sets.<sup>a</sup>

	component	eda	hammett	ir	nmr	order	pka	population	rate	structure
component	3	27	0	0	0	0	0	0	0	39
eda		189	28	80	79	53	3	43	0	195
hammett			2	1	12	2	1	0	0	13
ir				6	15	3	1	6	0	8
nmr					18	11	8	0	0	32
order						2	1	4	0	27
pka							0	0	0	1
population								9	0	4
rate									1	0
structure										123

<sup>a</sup>Only the upper triangle is given. Spearman, correlation at least 0.7, FDR corrected  $p$ -value less than 0.05.

An analogous representation of the connectivity of sets was generated based on numbers of statistically significant linear models ( $R^2 > 0.6$  and  $p$ -value  $< 0.05$ ) containing variables of different sets (Figure S51 and Table S43).

**Figure S51.** Connectivity between sets based on single variable linear models.<sup>a</sup>



<sup>a</sup>Approximately 1000 models (Section 11.2). Different sets are color coded (Figure S29).

**Table S43.** Numbers of single variable linear models split on sets.<sup>a</sup>

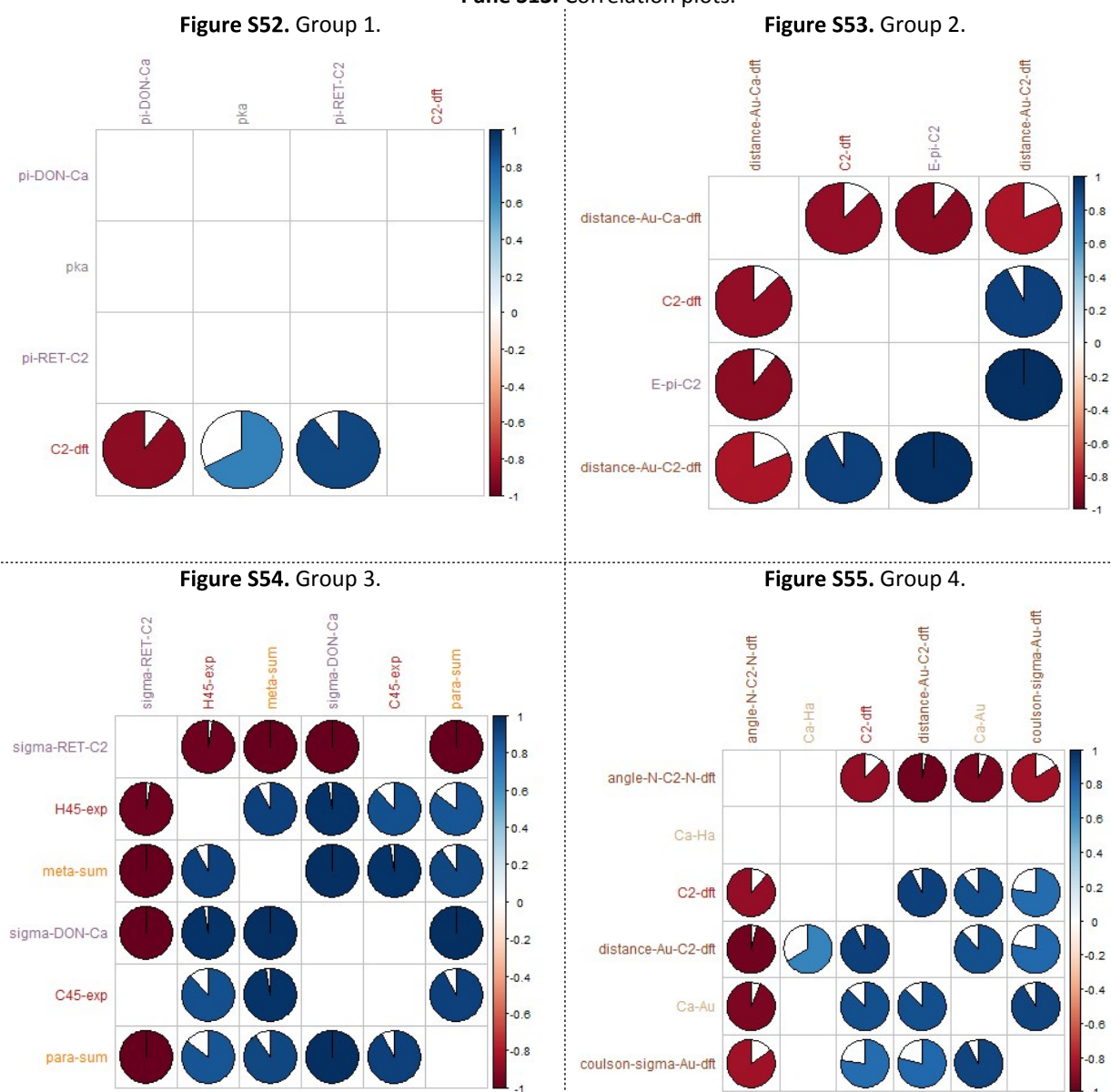
	component	eda	hammett	ir	nmr	order	pka	population	structure
component	1	6	0	0	0	0	0	0	26
eda	6	63	28	20	87	38	15	33	132
hammett	0	32	0	0	12	4	1	0	10
ir	0	21	0	0	9	0	0	16	0
nmr	0	76	12	9	6	7	6	0	13
order	0	43	4	0	7	1	1	0	16
pka	0	16	1	0	6	1	0	0	3
population	0	27	0	12	0	0	0	6	2
structure	20	123	10	0	13	17	3	2	29

<sup>a</sup>Matrix is not symmetric because of missing values and differences in significance of intercepts and contribution when regression models are inverted.

### 13. Correlation plots

Correlation plots of the groups of parameters obtained in the regression analysis (Section 11) highlighted correlations (Pane S13) in addition to the network graphs (main text, Figure 6). Parameter C2-dft (NMR) was the only parameter that correlated significantly to other parameters in group 1 (Figure S52). Parameter distance-Au-C-Ca-dft (structure) was negatively correlated with parameters distance-Au-C-C2-dft (structure), C2-dft (NMR) and E-pi-C2 (EDA) in group 2 (Figure S53). Parameter distance-Au-C-C2-dft (structure) was positively correlated to C2-dft (NMR) and E-pi-C2 (EDA). The negative correlation between parameter sigma-RET-C2 (EDA) and most other parameters in group 3 was most noteworthy (Figure S54). No large difference in correlations appeared between those other parameters. Parameter C45-exp (NMR) was only positively correlated to H45-exp (NMR), meta-sum (Hammett) and para-sum (Hammett). Parameter Ca-Ha (order) displayed lower (significant) correlations to the other parameters in group 4 than related parameter Ca-Au (order) did (Figure S55).

Pane S13. Correlation plots.<sup>a</sup>



<sup>a</sup>Spearman correlations, clustered using the Ward.D2 method.<sup>90</sup> Labels of parameters from different sets are color coded (Figure S29). Only pairs with p-values < 0.05 (FDR corrected) are shown.

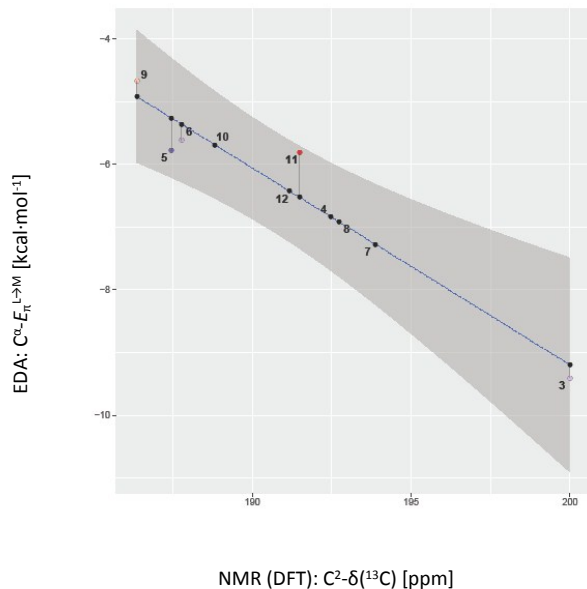
## 14. Linear models

Linear models listed in Tables 4 and 5 of the main text are presented in Section 14.1 and illustrative other ones are presented in Section 14.2. All plots depict single linear models, for clarity.<sup>91</sup>

### Main linear models

Pane S14. Linear models of EDA parameters *versus* modelled (DFT) NMR parameters.

Figure S56.  $C^{\alpha}-E_{\pi}^{L \rightarrow M}$  versus  $C^2-\delta(^{13}\text{C})$ .

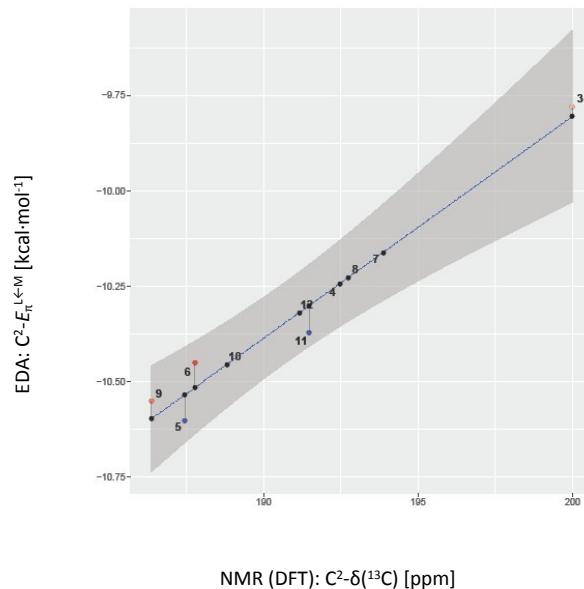


$$R^2 = 0.93$$

$$\text{EDA: } C^{\alpha}-E_{\pi}^{L \rightarrow M} = 53.6 - 0.314 \times \text{NMR (DFT): } C^2-\delta(^{13}\text{C})$$

Main text, Table 5, entry 1.

Figure S57.  $C^2-E_{\pi}^{L \leftarrow M}$  versus  $C^2-\delta(^{13}\text{C})$ .



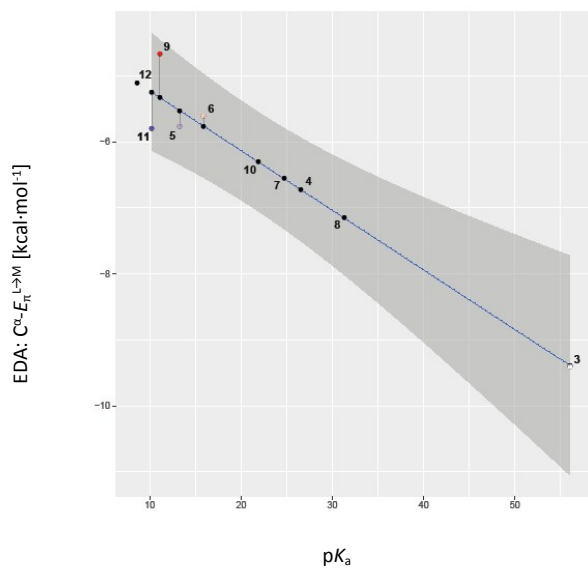
$$R^2 = 0.96$$

$$\text{EDA: } C^2-E_{\pi}^{L \leftarrow M} = -21.4 + 0.058 \times \text{NMR (DFT): } C^2-\delta(^{13}\text{C})$$

Main text, Table 5, entry 2.

**Pane S15.** Linear models of EDA parameters *versus*  $pK_a$ .

**Figure S58.**  $C^\alpha-E_{\pi}^{L \rightarrow M}$  *versus*  $pK_a$ .

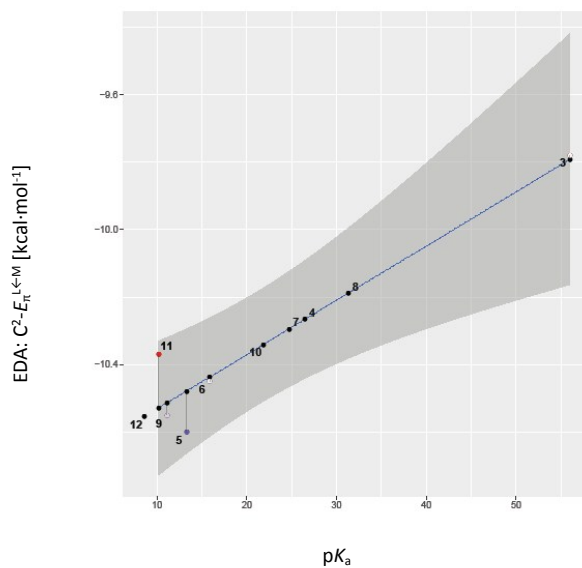


$$R^2 = 0.938$$

$$\text{EDA: } C^\alpha-E_{\pi}^{L \rightarrow M} = -4.33 - 0.090 \times pK_a$$

Main text, Table 5, entry 3.

**Figure S59.**  $C^2-E_{\pi}^{L \leftarrow M}$  *versus*  $pK_a$ .



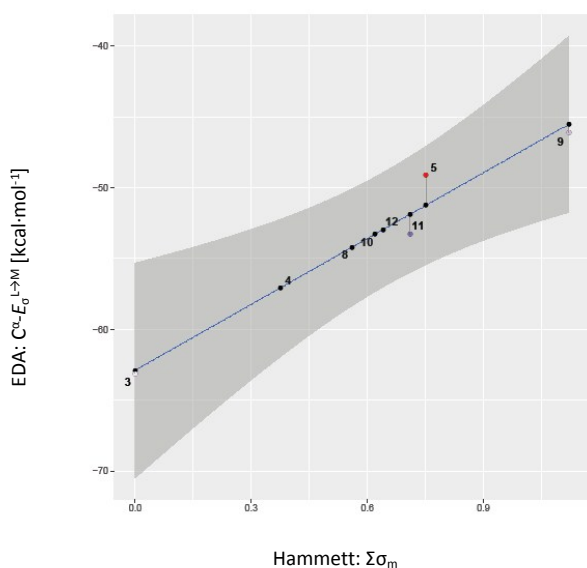
$$R^2 = 0.905$$

$$\text{EDA: } C^2-E_{\pi}^{L \leftarrow M} = -10.7 + 0.016 \times pK_a$$

Main text, Table 5, entry 4.

**Pane S16.** Linear models of EDA parameters *versus* sums of Hammett constants.

**Figure S60.**  $C^\alpha-E_{\sigma}^{L \rightarrow M}$  *versus*  $\Sigma\sigma_m$ .

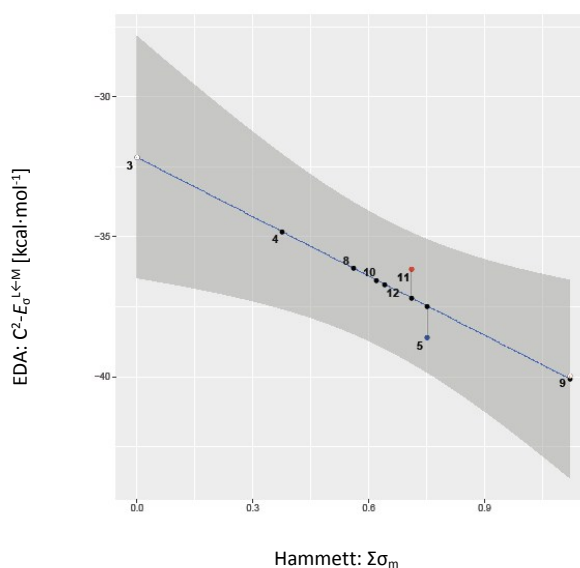


$$R^2 = 0.958$$

$$\text{EDA: } C^\alpha-E_{\sigma}^{L \rightarrow M} = -62.9 + 15.5 \times \text{Hammett: } \Sigma\sigma_m$$

Main text, Table 5, entry 5.

**Figure S61.**  $C^2-E_{\sigma}^{L \leftarrow M}$  *versus*  $\Sigma\sigma_m$ .

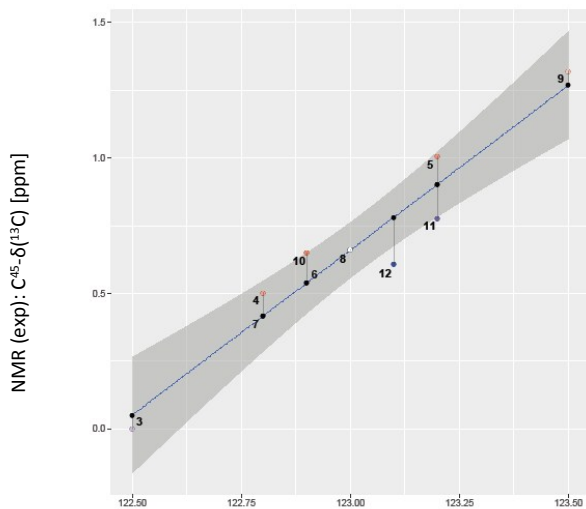


$$R^2 = 0.905$$

$$\text{EDA: } C^2-E_{\sigma}^{L \leftarrow M} = -32.2 - 7.07 \times \text{Hammett: } \Sigma\sigma_m$$

Main text, Table 5, entry 6.

**Pane S17.** Linear models of experimental NMR parameters *versus* sums of Hammett constants.  
**Figure S62.**  $C^{45}\text{-}\delta(^{13}\text{C})$  *versus*  $\Sigma\sigma_p$ .



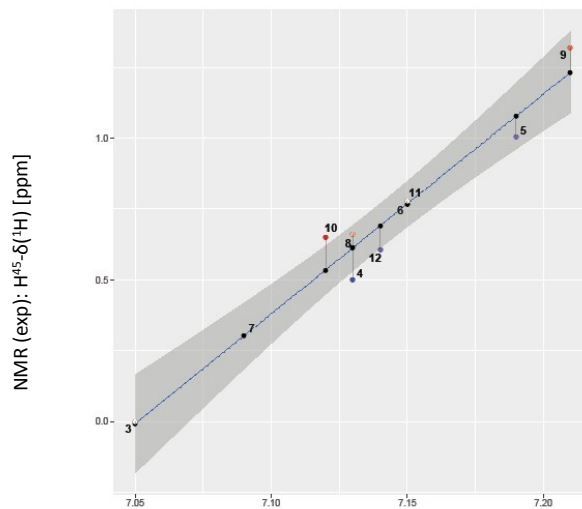
Hammett:  $\Sigma\sigma_p$

$$R^2 = 0.921$$

$$\text{NMR (exp): } C^{45}\text{-}\delta(^{13}\text{C}) = 122.5 + 0.756 \times \text{Hammett: } \Sigma\sigma_p$$

Main text, Table 5, entry 7.

**Figure S63.**  $H^{45}\text{-}\delta(^1\text{H})$  *versus*  $\Sigma\sigma_p$ .



Hammett:  $\Sigma\sigma_p$

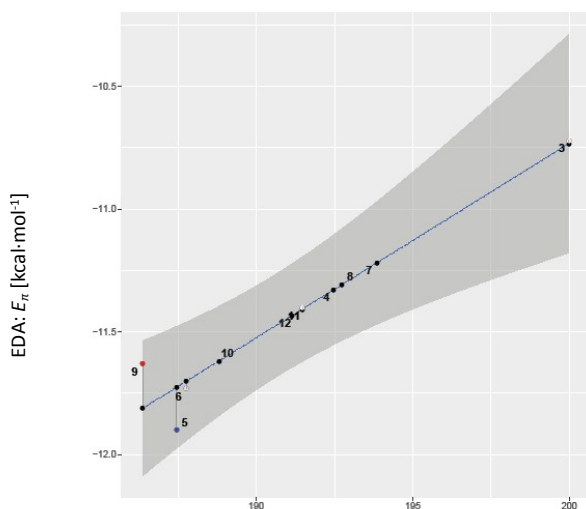
$$R^2 = 0.954$$

$$\text{NMR (exp): } H^{45}\text{-}\delta(^1\text{H}) = 7.06 + 0.123 \times \text{Hammett: } \Sigma\sigma_p$$

Main text, Table 5, entry 8.

**Pane S18.** Linear models of EDA parameter  $E_\pi$  *versus* modelled (DFT) and experimental NMR parameter  $C^2\text{-}\delta(^{13}\text{C})$ .

**Figure S64.**  $C^2\text{-}E_\pi$  *versus*  $C^2\text{-}\delta(^{13}\text{C})$  (DFT).



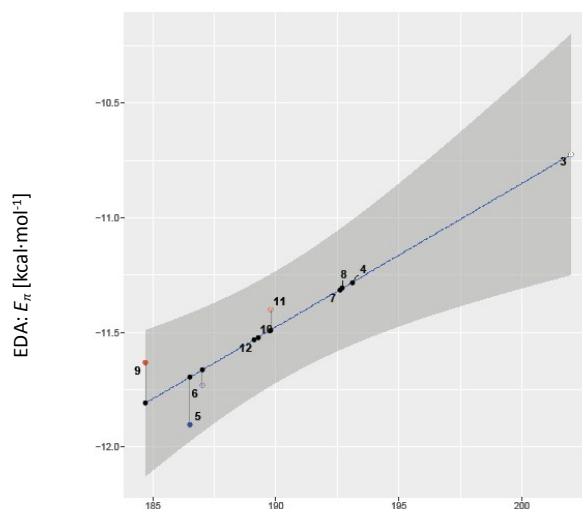
NMR (DFT):  $C^2\text{-}\delta(^{13}\text{C})$  [ppm]

$$R^2 = 0.924$$

$$\text{EDA: } C^2\text{-}E_\pi = -26.6 + 0.0791 \times \text{NMR (DFT): } C^2\text{-}\delta(^{13}\text{C})$$

Main text, Table 5, entry 9.

**Figure S65.**  $C^2\text{-}E_\pi$  *versus*  $C^2\text{-}\delta(^{13}\text{C})$  (exp).



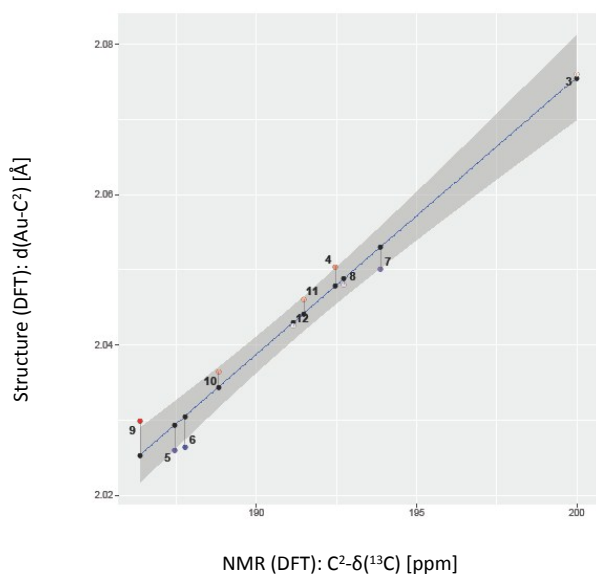
NMR (exp):  $C^2\text{-}\delta(^{13}\text{C})$  [ppm]

$$R^2 = 0.899$$

$$\text{EDA: } C^2\text{-}E_\pi = -23.4 + 0.0627 \times \text{NMR (exp): } C^2\text{-}\delta(^{13}\text{C})$$

**Pane S19.** Linear models of structural parameters *versus* NMR parameter  $C^2-\delta(^{13}C)$ .

**Figure S66.** Modelled (DFT)  $d(Au-C^2)$  *versus*  $C^2-\delta(^{13}C)$ .



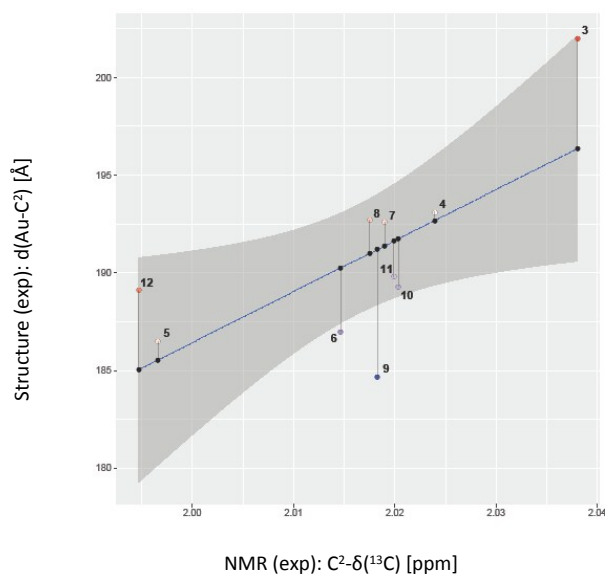
NMR (DFT):  $C^2-\delta(^{13}C)$  [ppm]

$$R^2 = 0.964$$

$$\text{Structure (DFT): } d(Au-C^2) = 1.339 + 0.0037 \times \text{NMR (DFT): } C^2-\delta(^{13}C)$$

Main text, Table 5, entry 10.

**Figure S67.** Experimental  $d(Au-C^2)$  *versus*  $C^2-\delta(^{13}C)$ .

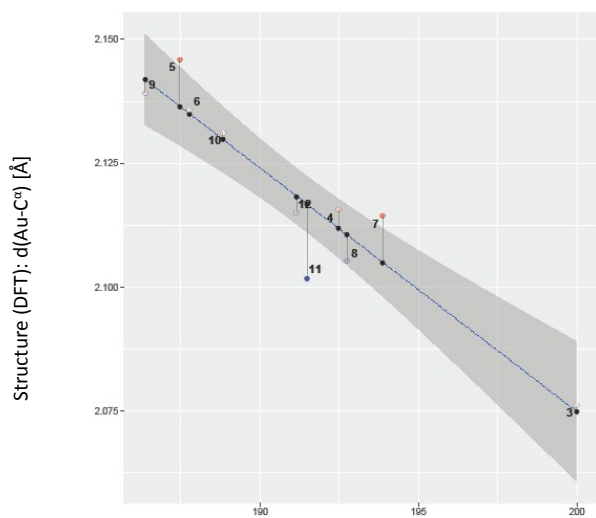


NMR (exp):  $C^2-\delta(^{13}C)$  [ppm]

$$R^2 = 0.457$$

$$\text{Structure (exp): } d(Au-C^2) = 1.683 + 0.0017 \times \text{NMR (exp): } C^2-\delta(^{13}C)$$

**Figure S68.** Modelled  $d(Au-C^\alpha)$  *versus*  $C^2-\delta(^{13}C)$ .



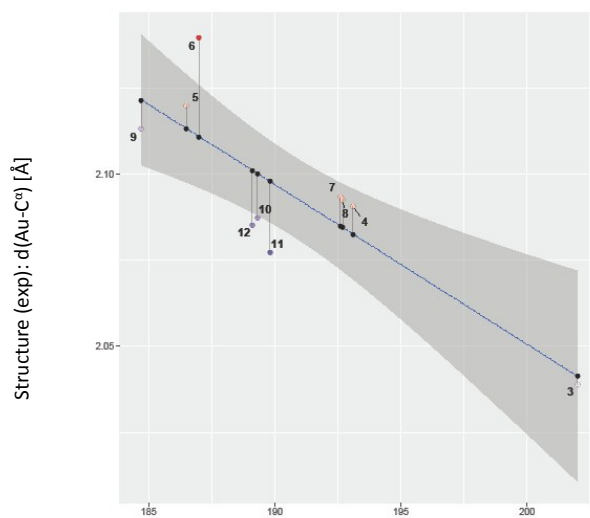
NMR (DFT):  $C^2-\delta(^{13}C)$  [ppm]

$$R^2 = 0.881$$

$$\text{Structure (DFT): } d(Au-C^\alpha) = 3.058 - 0.0049 \times \text{NMR (DFT): } C^2-\delta(^{13}C)$$

Main text, Table 5, entry 11.

**Figure S69.** Experimental  $d(Au-C^\alpha)$  *versus*  $C^2-\delta(^{13}C)$ .



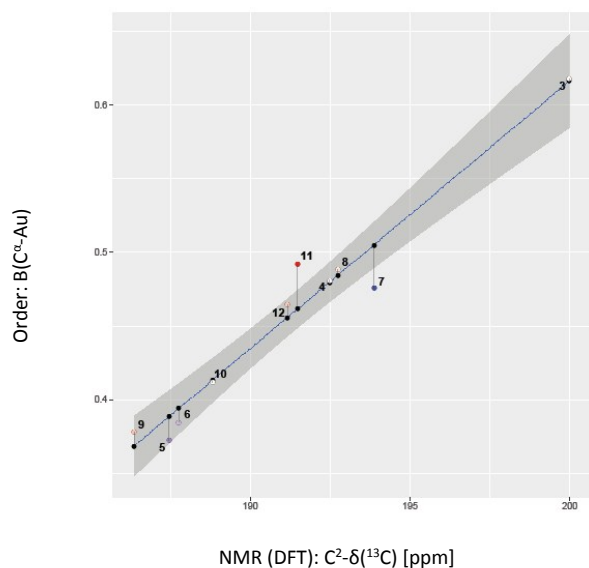
NMR (exp):  $C^2-\delta(^{13}C)$  [ppm]

$$R^2 = 0.697$$

$$\text{Structure (exp): } d(Au-C^\alpha) = 2.977 - 0.0046 \times \text{NMR (exp): } C^2-\delta(^{13}C)$$

**Pane S20.** Linear models of order parameters *versus* NMR and structural parameters.

**Figure S70.**  $B(C^\alpha-Au)$  *versus*  $C^2-\delta(^{13}C)$  (NMR, DFT).



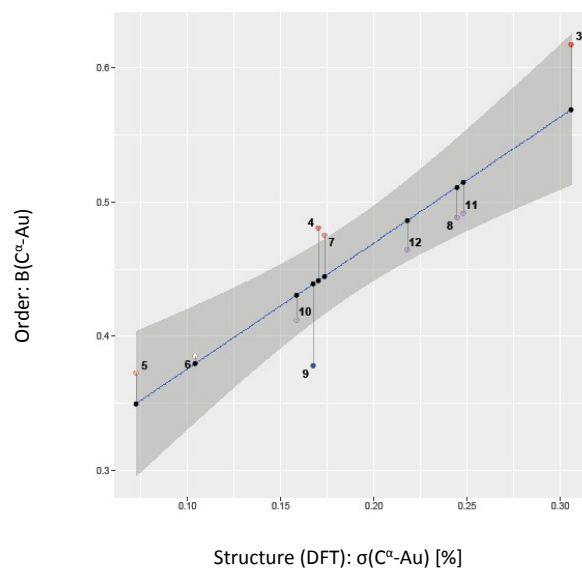
NMR (DFT):  $C^2-\delta(^{13}C)$  [ppm]

$$R^2 = 0.953$$

$$\text{Order: } B(C^\alpha-Au) = -3.02 + 0.0182 \times \text{NMR: } C^2-\delta(^{13}C)$$

Main text, Table 5, entry 12.

**Figure S71.**  $B(C^\alpha-Au)$  (order) *versus*  $\sigma(C^\alpha-Au)$  (structure, DFT).



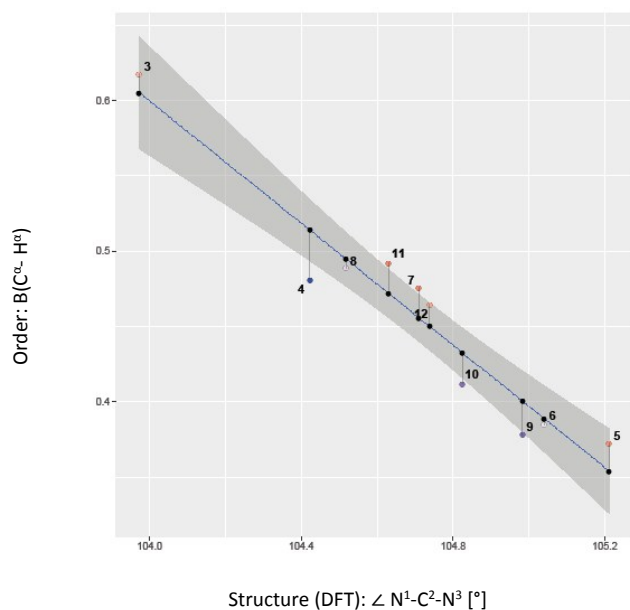
Structure (DFT):  $\sigma(C^\alpha-Au)$  [%]

$$R^2 = 0.779$$

$$\text{Order: } B(C^\alpha-Au) = 0.282 + 0.939 \times \text{Structure (DFT): } \sigma(C^\alpha-Au)$$

Main text, Table 5, entry 13.

**Figure S72.**  $B(C^\alpha-H^\alpha)$  *versus*  $\angle N^1-C^2-N^3$  (structure, DFT).



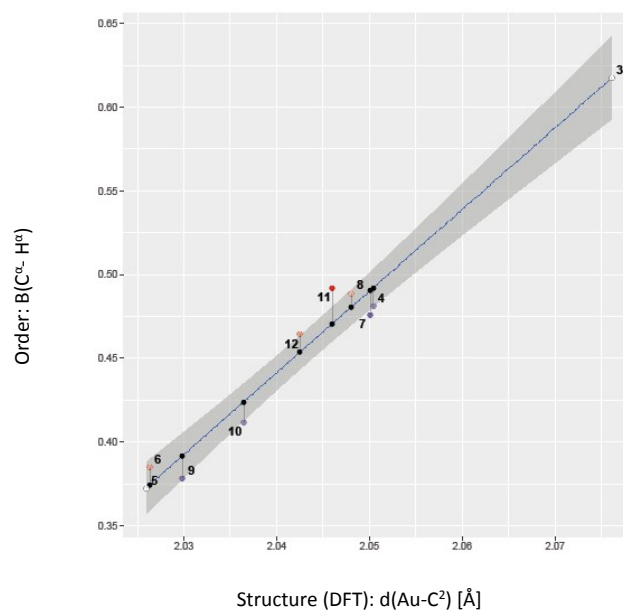
Structure (DFT):  $\angle N^1-C^2-N^3$  [°]

$$R^2 = 0.971$$

$$\text{Order: } B(C^\alpha-H^\alpha) = 21.7 - 0.203 \times \text{Structure (DFT): } \angle N^1-C^2-N^3$$

Main text, Table 5, entry 14.

**Figure S73.**  $B(C^\alpha-H^\alpha)$  *versus*  $d(Au-C^2)$  (structure, DFT).



Structure (DFT):  $d(Au-C^2)$  [Å]

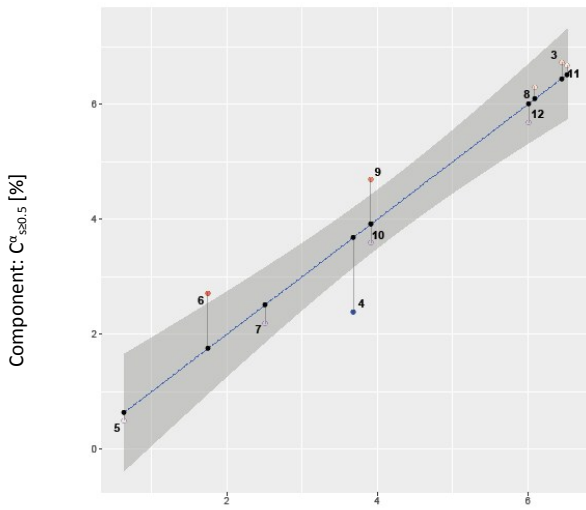
$$R^2 = 0.971$$

$$\text{Order: } B(C^\alpha-H^\alpha) = -9.52 + 4.89 \times \text{Structure (DFT): } d(Au-C^2)$$

Main text, Table 5, entry 15.

**Pane S21.** Linear models based on composite structural parameters.

**Figure S74.** Model of  $C^{\alpha}_{s \geq 0.5}$  (order).

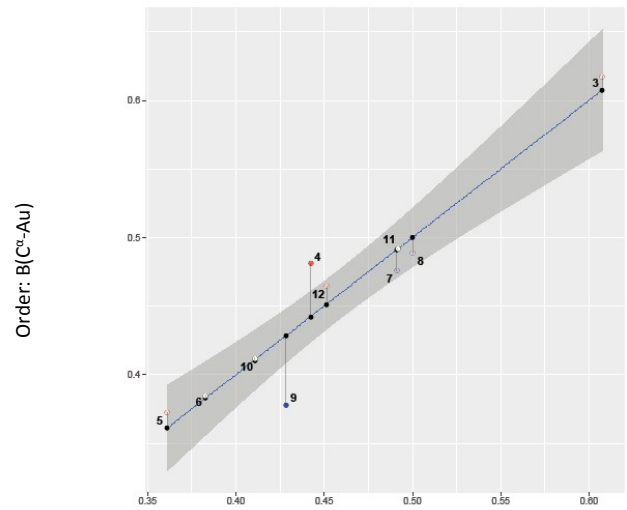


Fitted Component:  $C^{\alpha}_{s \geq 0.5}$  [%]

$$R^2 = 0.914$$

$$\begin{aligned} & \{ \text{Component: } C^{\alpha}_{s \geq 0.5} \} = 1740 \\ & + 30.6 \times \{ \text{Structure (DFT): } \sigma(C^{\alpha}\text{-Au}) \} \\ & - 1250 \times \{ \text{Structure (DFT): } d(C^{4/5}\text{-N}^{1/3}) \} \\ & \text{Main text, Table 6, entry 1.} \end{aligned}$$

**Figure S75.** Model of  $B(C^{\alpha}\text{-Au})$  (order).



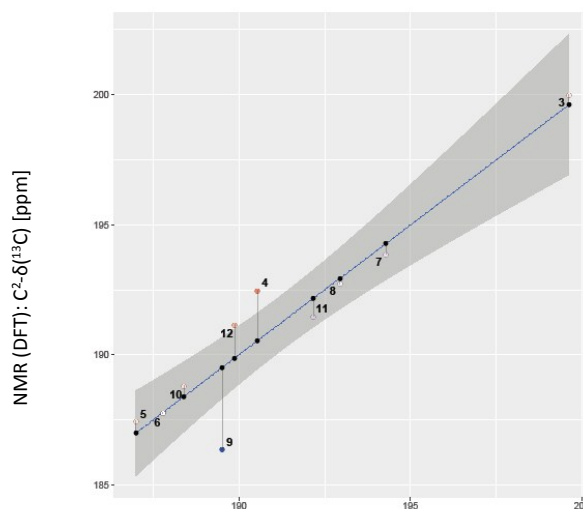
Fitted Order:  $B(C^{\alpha}\text{-Au})$

$$R^2 = 0.904$$

$$\begin{aligned} & \{ \text{Order: } B(C^{\alpha}\text{-Au}) \} = -63.0 \\ & + 0.849 \times \{ \text{Structure (DFT): } \sigma(C^{\alpha}\text{-Au}) \} \\ & + 45.50 \times \{ \text{Structure (DFT): } d(C^{4/5}\text{-N}^{1/3}) \} \\ & \text{Main text, Table 6, entry 2} \end{aligned}$$

**Table S44.** Linear models of experimental or modelled (DFT) NMR parameter  $C^2-\delta(^{13}C)$  versus two structural properties.

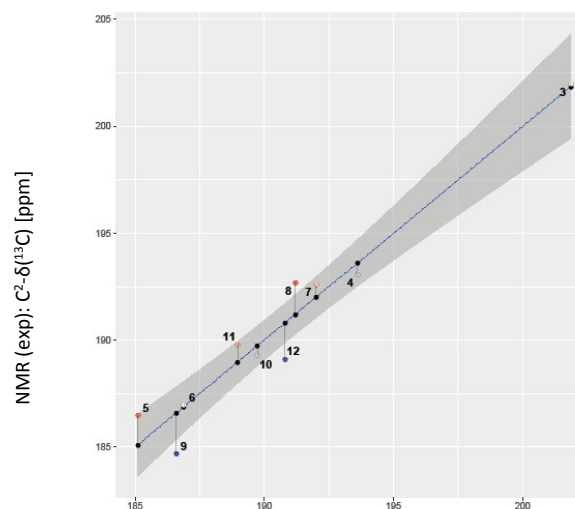
**Figure S76.** Model of  $C^2-\delta(^{13}C)$  (DFT).



Fitted NMR (DFT):  $C^2-\delta(^{13}C)$  [ppm]

$$\begin{aligned}
 R^2 &= 0.885 \\
 \text{NMR (DFT): } \angle C^2-\delta(^{13}C) &= -4790 \\
 &+ 37.8 \times \text{Structure (DFT): } \sigma(C^2-Au) \\
 &+ 3580 \times \text{Structure (DFT): } d(C^{4/5}-N^{1/3}) \\
 &\text{Main text, Table 6, entry 4}
 \end{aligned}$$

**Figure S77.** Model of  $C^2-\delta(^{13}C)$  (exp).

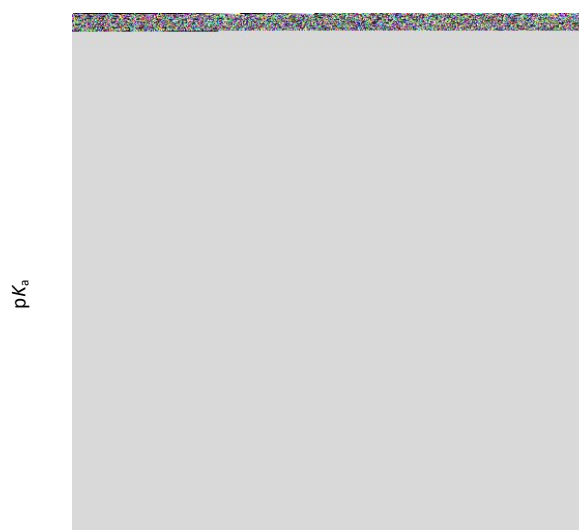


Fitted NMR (exp):  $C^2-\delta(^{13}C)$  [ppm]

$$\begin{aligned}
 R^2 &= 0.943 \\
 \text{NMR (exp): } \angle C^2-\delta(^{13}C) &= 396.1 \\
 &+ 9.96 \times \text{Structure (exp): } \angle N^1-C^5-C^4-N^3 \\
 &- 99.7 \times \text{Structure (exp): } d(Au-C^6)
 \end{aligned}$$

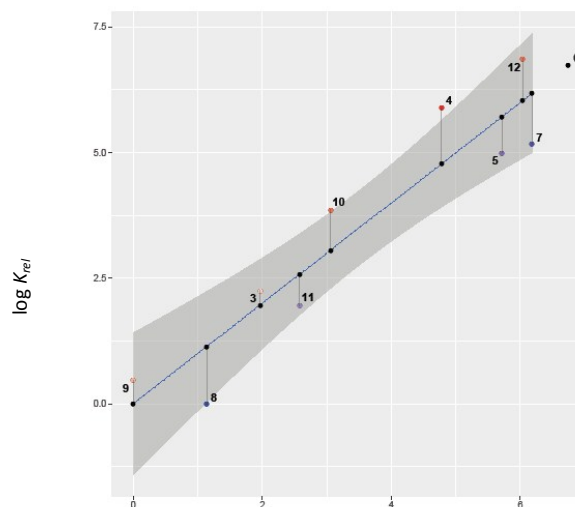
**Pane S22.** Linear models based on composite NMR parameters.

**Figure S78.**  $pK_a$  versus three NMR parameters.



$$\begin{aligned}
 & pK_a \\
 & R^2 = 0.978 \\
 & pK_a = 1332 \\
 & - 0.213 \times \text{NMR (DFT): } C^\alpha\text{-}\delta(^{13}\text{C}) \\
 & - 13.01 \times \text{NMR (DFT): } C^{45}\text{-}\delta(^{13}\text{C}) \\
 & + 1.68 \times \text{NMR (DFT): } C^2\text{-}\delta(^{13}\text{C}) \\
 & \text{Main text, Table 6, entry 4.}
 \end{aligned}$$

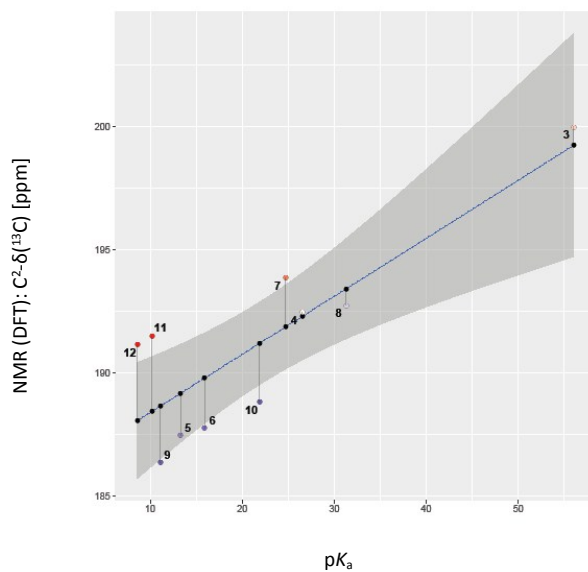
**Figure S79.**  $\log K_{rel}$  versus four NMR parameters.



$$\begin{aligned}
 & \text{Fitted } \log K_{rel} \\
 & R^2 = 0.872 \\
 & \log K_{rel} = 998 \\
 & + 0.212 \times \text{NMR (exp): } C^\alpha\text{-}\delta(^{13}\text{C}) \\
 & - 1.596 \times \text{NMR (exp): } C^2\text{-}\delta(^{13}\text{C}) \\
 & - 5.66 \times \text{NMR (exp): } H^\alpha\text{-}\delta(^1\text{H}) \\
 & - 95.69 \times \text{NMR (exp): } H^{45}\text{-}\delta(^1\text{H}) \\
 & \text{Main text, Table 6, entry 5.}
 \end{aligned}$$

## Additional linear models

Figure S80. Linear model of modelled (DFT) NMR parameter  $C^2-\delta(^{13}C)$  versus  $pK_a$ .

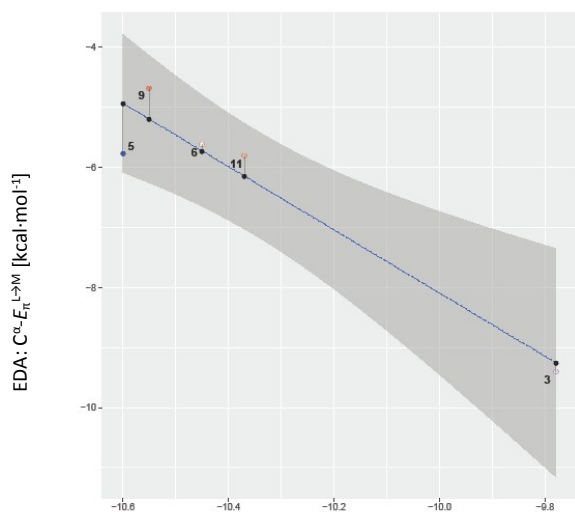


$$R^2 = 0.708$$

$$\text{NMR (DFT): } C^2-\delta(^{13}C) = 186.0 + 0.236 \times pK_a$$

Pane S23. Linear models of EDA parameters.

Figure S81.  $C^\alpha-E_\pi^{L \rightarrow M}$  versus  $C^2-E_\pi^{L \leftarrow M}$ .

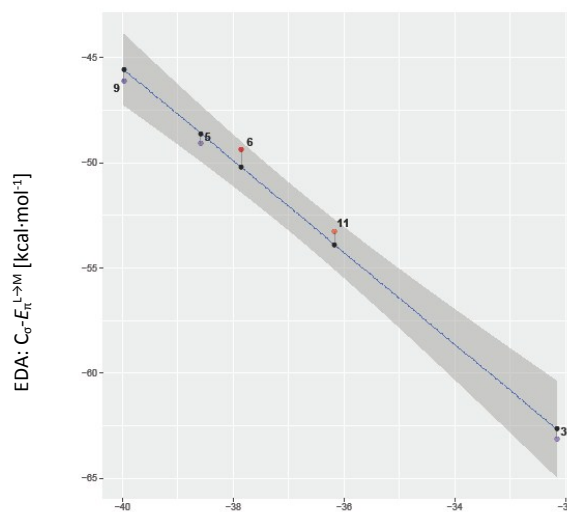


$$\text{EDA: } C^2-E_\pi^{L \leftarrow M} \text{ [kcal} \cdot \text{mol}^{-1}]$$

$$R^2 = 0.915$$

$$\text{EDA: } C^\alpha-E_\pi^{L \rightarrow M} = -60.73 - 5.264 \times \text{EDA: } C^2-E_\pi^{L \leftarrow M}$$

Figure S82.  $C^\alpha-E_\sigma^{L \rightarrow M}$  versus  $C^2-E_\sigma^{L \leftarrow M}$ .



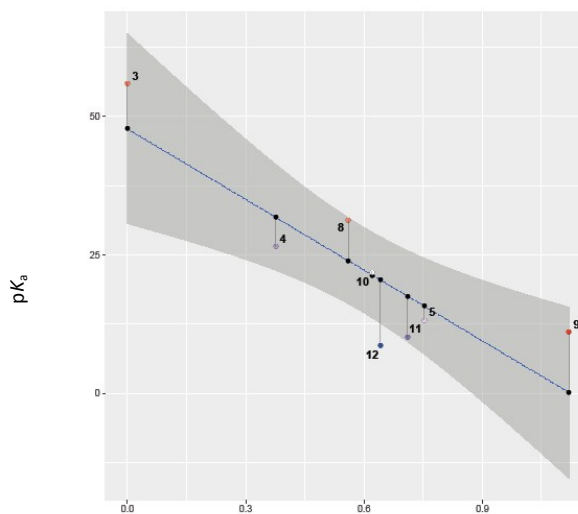
$$\text{EDA: } C^2-E_\sigma^{L \leftarrow M} \text{ [kcal} \cdot \text{mol}^{-1}]$$

$$R^2 = 0.990$$

$$\text{EDA: } C^\alpha-E_\sigma^{L \rightarrow M} = -60.73 - 5.264 \times \text{EDA: } C^2-E_\sigma^{L \leftarrow M}$$

Pane S24. Linear models of  $pK_a$  versus sums of Hammett constants.

Figure S83.  $pK_a$  versus  $\Sigma\sigma_m$ .

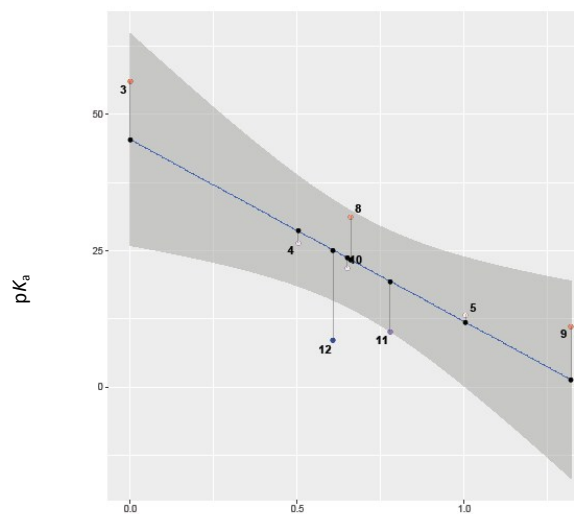


Hammett:  $\Sigma\sigma_m$

$$R^2 = 0.734$$

$$pK_a = 47.8 - 42.6 \times \text{Hammett: } \Sigma\sigma_m$$

Figure S84.  $pK_a$  versus  $\Sigma\sigma_p$ .

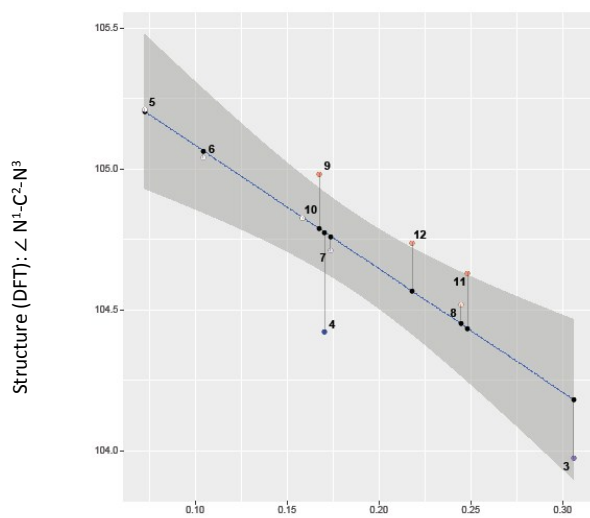


Hammett:  $\Sigma\sigma_p$

$$R^2 = 0.641$$

$$pK_a = 45.4 - 33.3 \times \text{Hammett: } \Sigma\sigma_p$$

Figure S85. Linear model of modelled (DFT) structural parameters:  $\angle N^1-C^2-N^3$  versus  $\sigma(C^\alpha-Au)$ .



Structure (DFT):  $\sigma(C^\alpha-Au)$  [%]

$$R^2 = 0.748$$

$$\text{Structure (DFT): } \angle N^1-C^2-N^3 = 105.5 - 4.376 \times \text{Structure (DFT): } \sigma(C^\alpha-Au)$$

**Figure S86.** Linear model of order parameter  $B(C^\alpha\text{-Au})$  versus modelled (DFT) NMR parameter  $C^2\text{-}\delta(^{13}\text{C})$ .

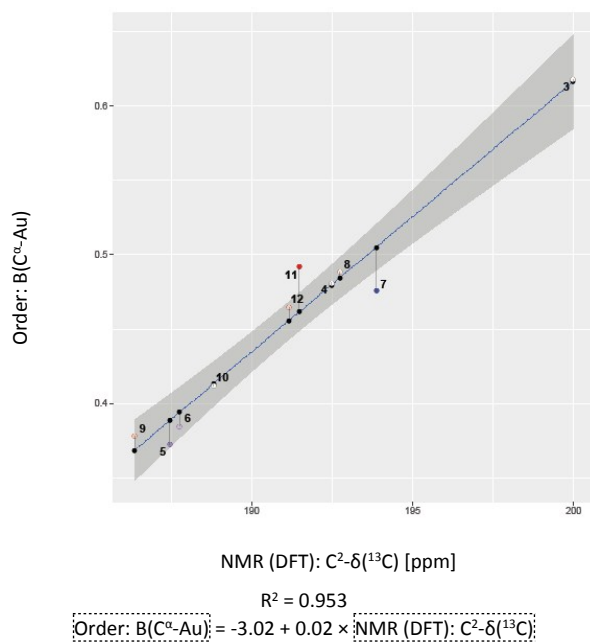


**Figure S87.** Linear model of  $\log K_{rel}$  versus  $pK_a$ .

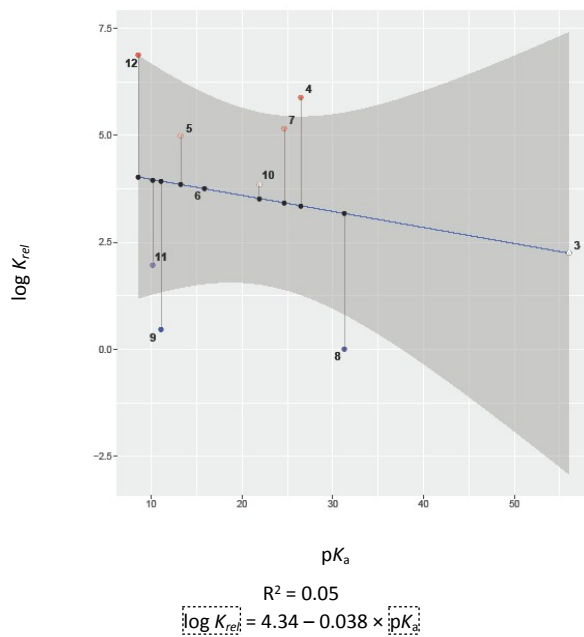
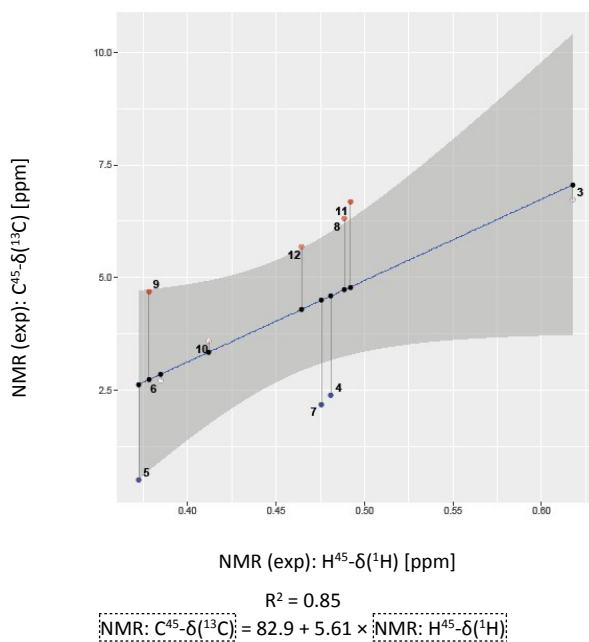


**Figure S88.** Linear model of experimental NMR parameters:  $C^{45}\text{-}\delta(^{13}\text{C})$  versus  $H^{45}\text{-}\delta(^1\text{H})$ .



**Pane S25.** Linear models of structural parameter  $\angle N^1\text{-}C^5\text{-}C^4\text{-}N^3$  and NMR parameter  $C^2\text{-}\delta(^{13}\text{C})$ .

**Figure S89.**  $\angle N^1\text{-}C^5\text{-}C^4\text{-}N^3$  (DFT) versus  $C^2\text{-}\delta(^{13}\text{C})$  (DFT).

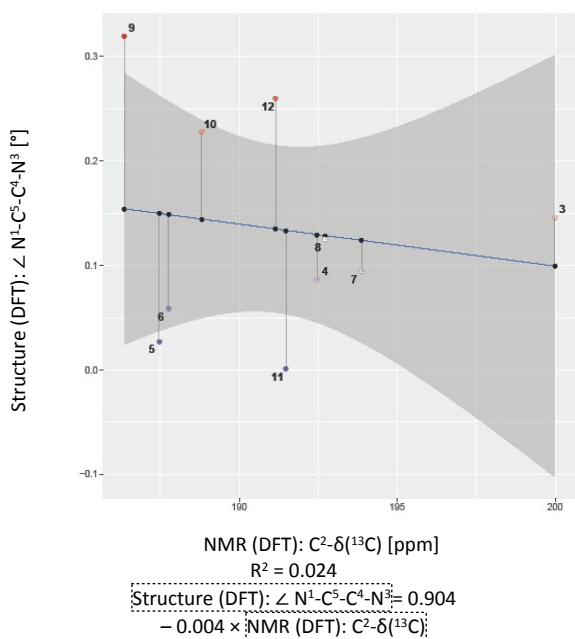
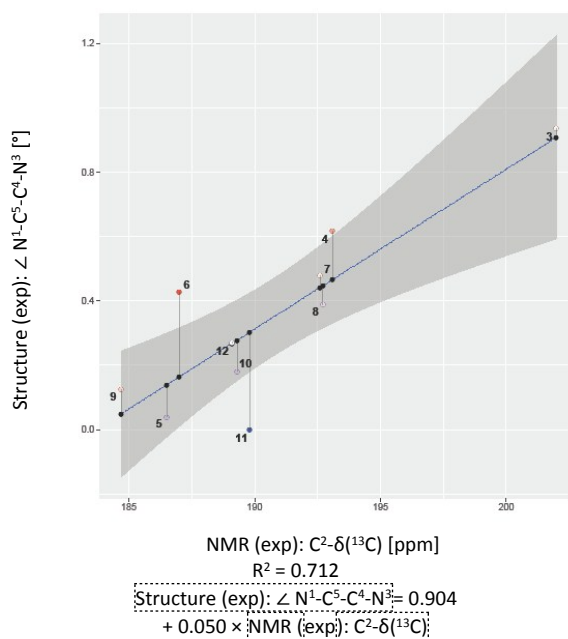


**Figure S90.**  $\angle N^1\text{-}C^5\text{-}C^4\text{-}N^3$  (exp) versus  $C^2\text{-}\delta(^{13}\text{C})$  (exp).



## 15. Surface plots

The coefficients of the multi-parameter linear models of “Component:  $C^{\alpha}_{s \geq 0.5}$ ” (Figure S74), “Order:  $B(C^{\alpha}-Au)$ ” (Figure S75) and “NMR (DFT):  $\angle C^2-\delta(^{13}C)$ ” (Figure S76) were scaled and translated along their intercepts to span values between 0 and 1 for the range of values for  $d(C^{4/5}-N^{1/3})$  and  $\sigma(C^{\alpha}-Au)$  (Table S45).

**Table S45.** Coefficients of linear models and scaled coefficients.<sup>a</sup>

Entry	z	Linear model			Scaled coefficients		
		i	a	b	i	a	b
1	Component: $C^{\alpha}_{s \geq 0.5}$	1740	31	-1250	185	3	-133
2	Order: $B(C^{\alpha}-Au)$	-63	1	45	-226	3	163
3	NMR (DFT): $\angle C^2-\delta(^{13}C)$	-4790	38	3580	-326	2	235

<sup>a</sup>Using formula  $z = i + a \times x + b \times y$ , with  $x = \text{Structure (DFT): } \sigma(C^{\alpha}-Au)$ ; and  $y = \text{Structure (DFT): } d(C^{4/5}-N^{1/3})$ .

## 16. References

1. CrystalClear: Data collection and Processing Software, Rigaku Corporation (1998-2014). Tokyo 196-8666, Japan.
2. PATTY: Beurskens, P. T.; Admiraal, G.; Behm, H.; Beurskens, G.; Smits, J. M. M.
3. Beurskens, P. T.; Admiraal, G.; Behm, H.; Beurskens, G.; Smits, J. M. M.; Smykalla, C., *Z. Kristallogr. Suppl.* **1991**, *4*, 99.
4. CrystalStructure 4.1: Crystal Structure Analysis Package, Rigaku Corporation (2000-2014). Tokyo 196-8666, Japan.
5. Sheldrick, G. M., *Acta Crystallographica Section A Foundations of Crystallography* **2008**, *64*, 112-122.
6. R 3.4.1: R Core Team, R, A Language and Environment for Statistical Computing, Vienna, Austria: R Foundation for Statistical Computing. Available at <http://www.r-project.org>.
7. Scott, V. J.; Labinger, J. A.; Bercaw, J. E., *Organometallics* **2010**, *29*, 4090-4096.
8. Yousef, R. I.; Walfort, B.; Rüffer, T.; Wagner, C.; Schmidt, H.; Herzog, R.; Steinborn, D., *J. Organomet. Chem.* **2005**, *690*, 1178-1191.
9. Baker, M. V.; Barnard, P. J.; Brayshaw, S. K.; Hickey, J. L.; Skelton, B. W.; White, A. H., *Dalton Trans.* **2005**, 37-43.
10. CrystalClear-SM Expert v2.1. Rigaku Americas, The Woodlands, Texas, USA, and Rigaku Corporation, Tokyo, Japan, 2015.
11. DIRDIF-99. Beurskens, P. T.; Beurskens, G.; de Gelder, R.; Garcia-Granda, S.; Gould, R. O.; Israel, R.; Smits, J. M. M. Crystallography Laboratory, University of Nijmegen, The Netherlands, 1999.
12. Sheldrick, G. M. *Acta Crystallogr., Sect. A.* 2015, *71*, 3-8.
13. Burla, M. C.; Caliandro, R.; Camalli, M.; Carrozzini, B.; Cascarano, G. L.; Giacovazzo, C.; Mallamo, M.; Mazzone, A.; Polidori, G.; Spagna, R. *J. Appl. Cryst.* 2012, *45*, 357-361.
14. Sheldrick, G. M. *Acta Crystallogr., Sect. C.* 2015, *71*, 3-8.
15. CrystalStructure v4.2. Rigaku Americas, The Woodlands, Texas, USA, and Rigaku Corporation, Tokyo, Japan, 2015.
16. Tanimoto, Y.; Kobayashi, H.; Nagakura, S.; Saito, Y., *Acta Crystallographica Section B* **1973**, *29*, 1822-1826.
17. de Frémont, P.; Stevens, E. D.; Fructos, M. R.; Mar Díaz-Requejo, M.; Pérez, P. J.; Nolan, S. P., *Chem. Commun.* **2006**, 2045-2047.
18. Obatake, K.; Tanisaki, S., *Phys. Lett. A* **1973**, *44*, 341-342.
19. Nayak, S. K.; Sathishkumar, R.; Row, T. N. G., *CrystEngComm* **2010**, *12*, 3112.
20. Wright, A. M.; Wu, G.; Hayton, T. W., *J. Am. Chem. Soc.* **2010**, *132*, 14336-14337.
21. Bencini, A.; Benelli, C.; Caneschi, A.; Dei, A.; Gatteschi, D., *Inorg. Chem.* **1986**, *25*, 572-575.
22. Bayat, M.; Sedghi, A.; Ebrahimkhani, L.; Sabounchei, S. J., *Dalton Trans.* **2017**, 46.
23. Hashmi, A. S. K.; Schäfer, S.; Wölflle, M.; Diez Gil, C.; Fischer, P.; Laguna, A.; Blanco, M. C.; Gimeno, M. C., *Angew. Chem. Int. Ed.* **2007**, *46*, 6184-6187.
24. Murakami, M.; Inouye, M.; Sugimoto, M.; Ito, Y., *Bull. Chem. Soc. Jpn.* **1988**, *61*, 3649-3652.
25. Kuzmina, L. G., *Koord. Khim.* **1994**, *20*, 540.
26. Emeljanenko, D.; Peters, A.; Vitske, V.; Kaifer, E.; Himmel, H.-J., *Eur. J. Inorg. Chem.* **2010**, *2010*, 4783-4789.
27. Johnson, M. W.; Shevick, S. L.; Toste, F. D.; Bergman, R. G., *Chem. Sci.* **2013**, *4*, 1023-1027.
28. Martinez, C. R.; Iverson, B. L., *Chem. Sci.* **2012**, *3*, 2191.
29. Anslyn, E. V.; Dougherty, D. A., *Modern Physical Organic Chemistry*. University Science: 2005.
30. Sanguramath, R. A.; Hooper, T. N.; Butts, C. P.; Green, M.; McGrady, J. E.; Russell, C. A., *Angew. Chem. Int. Ed.* **2011**, *50*, 7592-7595.
31. Zhu, Y.; Day, C. S.; Jones, A. C., *Organometallics* **2012**, *31*, 7332-7335.
32. Sriram, M.; Zhu, Y.; Camp, A. M.; Day, C. S.; Jones, A. C., *Organometallics* **2014**, *33*, 4157-4164.
33. York, J. T., *J. Phys. Chem. A* **2016**, *120*, 6064-6075.
34. Gaillard, S.; Slawin, A. M. Z.; Bonura, A. T.; Stevens, E. D.; Nolan, S. P., *Organometallics* **2010**, *29*, 394-402.
35. Marchione, D.; Belpassi, L.; Bistoni, G.; Macchioni, A.; Tarantelli, F.; Zuccaccia, D., *Organometallics* **2014**, *33*, 4200-4208.

36. Wang, H. M. J.; Vasam, C. S.; Tsai, T. Y. R.; Chen, S.-H.; Chang, A. H. H.; Lin, I. J. B., *Organometallics* **2005**, *24*, 486-493.
37. Veenboer, R. M. P.; Gasperini, D.; Nahra, F.; Cordes, D. B.; Slawin, A. M. Z.; Cazin, C. S. J.; Nolan, S. P., *Organometallics* **2017**, *36*, 3645-3653.
38. Mullins, R. J.; Vedernikov, A.; Viswanathan, R., *J. Chem. Educ.* **2004**, *81*, 1357.
39. Limpert, E.; Stahel, W. A.; Abbt, M., *Bioscience* **2001**, *51*, 341-352.
40. Gaillard, S.; Slawin, A. M. Z.; Nolan, S. P., *Chem. Commun.* **2010**, *46*, 2742-2744.
41. COPASI 4.20, a COmplex PATHway Simulator: S. Hoops, S. Sahle, R. Gauges, C. Lee, J. Pahle, N. Simus, M. Singhal, L. Xu, P. Mendes, U. Kummer, *Bioinformatics* **2006**, *22*, 3067-3074.
42. Perdew, J. P.; Burke, K.; Ernzerhof, M., *Phys. Rev. Lett.* **1996**, *77*, 3865-3868.
43. (a) Weigend, F.; Ahlrichs, R., *Phys. Chem. Chem. Phys.* **2005**, *7*, 3297; (b) Weigend, F., *Phys. Chem. Chem. Phys.* **2006**, *8*, 1057.
44. Kaupp, M.; Schleyer, P. v. R.; Stoll, H.; Preuss, H., *J. Chem. Phys.* **1991**, *94*, 1360-1366.
45. Kudin, K. N.; Scuseria, G. E.; Cancès, E., *J. Chem. Phys.* **2002**, *116*, 8255.
46. Grimme, S.; Antony, J.; Ehrlich, S.; Krieg, H., *J. Chem. Phys.* **2010**, *132*, 154104.
47. ADF 2016.104: G. te Velde, F. M. Bickelhaupt, E. J. Baerends, C. Fonseca Guerra, S. J. A. van Gisbergen, J. G. Snijders, T. Ziegler, *J. Comput. Chem.* **2001**, *22*, 931-967.
48. (a) Perdew, J. P., *Phys. Rev. B* **1986**, *33*, 8822-8824; (b) Perdew, J. P., *Phys. Rev. B* **1986**, *34*, 7406-7406; (c) Becke, A. D., *Phys. Rev. A* **1988**, *38*, 3098-3100.
49. (a) Schäfer, A.; Horn, H.; Ahlrichs, R., *J. Chem. Phys.* **1992**, *97*, 2571-2577; (b) Schäfer, A.; Huber, C.; Ahlrichs, R., *J. Chem. Phys.* **1994**, *100*, 5829-5835.
50. van Lenthe, E.; Snijders, J. G.; Baerends, E. J., *J. Chem. Phys.* **1996**, *105*, 6505-6516.
51. Gaussian09 Revision B.01: Frisch, M. J.; Trucks, G. W.; Schlegel, H. B.; Scuseria, G. E.; Robb, M. A.; Cheeseman, J. R.; Montgomery, J. J., Jr.; Vreven, T.; Kudin, K. N.; Burant, J. C.; Millam, J. M.; Iyengar, S. S.; Tomasi, J.; Barone, V.; Mennucci, B.; Cossi, M.; Scalmani, G.; Rega, N.; Petersson, G. A.; Nakatsuji, H.; Hada, M.; Ehara, M.; Toyota, K.; Fukuda, R.; Hasegawa, J.; Ishida, M.; Nakajima, T.; Honda, Y.; Kitao, O.; Nakai, H.; Klene, M.; Li, X.; Knox, J. E.; Hratchian, H. P.; Cross, J. B.; Adamo, C.; Jaramillo, J.; Gomperts, R.; Stratmann, R. E.; Yazyev, O.; Austin, A. J.; Cammi, R.; Pomelli, C.; Ochterski, J. W.; Ayala, P. Y.; Morokuma, K.; Voth, G. A.; Salvador, P.; Dannenberg, J. J.; Zakrzewski, V. G.; Dapprich, S.; Daniels, A. D.; Strain, M. C.; Farkas, O.; Malick, D. K.; Rabuck, A. D.; Raghavachari, K.; Foresman, J. B.; Ortiz, J. V.; Cui, Q.; Baboul, A. G.; Clifford, S.; Cioslowski, J.; Stefanov, B. B.; Liu, G.; Liashenko, A.; Piskorz, P.; Komaromi, I.; Martin, R. L.; Fox, D. J.; Keith, T.; Al-Laham, M. A.; Peng, C. Y.; Nanayakkara, A.; Challacombe, M.; Gill, P. M. W.; Johnson, B.; Chen, W.; Wong, M. W.; Gonzalez, C.; Pople, J. A.
52. Stasyuk, O. A.; Szatyłowicz, H.; Krygowski, T. M.; Fonseca Guerra, C., *Phys. Chem. Chem. Phys.* **2016**, *18*, 11624-11633.
53. Hansch, C.; Leo, A.; Taft, R. W., *Chem. Rev.* **1991**, *91*, 165-195.
54. Fruchterman, T. M. J.; Reingold, E. M., *Software: Practice and Experience* **1991**, *21*, 1129-1164.
55. Bisogno, F. R.; García-Urdiales, E.; Valdés, H.; Lavandera, I.; Kroutil, W.; Suárez, D.; Gotor, V., *Chem. Eur. J.* **2010**, *16*, 11012-11019.
56. Gasperini, D.; Collado, A.; Gómez-Suárez, A.; Cordes, D. B.; Slawin, A. M. Z.; Nolan, S. P., *Chem. Eur. J.* **2015**, *21*, 5403-5412.
57. He, C.; Zhang, G.; Ke, J.; Zhang, H.; Miller, J. T.; Kropf, A. J.; Lei, A., *J. Am. Chem. Soc.* **2013**, *135*, 488-493.
58. Tachinami, T.; Nishimura, T.; Ushimaru, R.; Noyori, R.; Naka, H., *J. Am. Chem. Soc.* **2013**, *135*, 50-53.
59. Šimečková, M.; Urban, Š.; Fuchs, U.; Lewen, F.; Winnewisser, G.; Morino, I.; Yamada, K. M. T., *J. Mol. Spectrosc.* **2004**, *226*, 123-136.
60. Le Calvé, N.; Pasquier, B.; Novak, A., *J. Chem. Phys.* **1980**, *72*, 6409.
61. Bhosale, A.; Yoshida, H.; Fujita, S.-i.; Arai, M., *Green Chem.* **2015**, *17*, 1299-1307.
62. Deák, J. C.; Iwaki, L. K.; Dlott, D. D., *J. Phys. Chem. A* **1999**, *103*, 971-979.
63. Kwok, W. M., *Mol. Phys.* **1996**, *88*, 517-531.
64. Dixon, D. A.; Charlier, P. A.; Gassman, P. G., *J. Am. Chem. Soc.* **1980**, *102*, 3957-3959.
65. (a) Autschbach, J., The Calculation of NMR Parameters in Transition Metal Complexes. In *Principles and Applications of Density Functional Theory in Inorganic Chemistry I*, Springer: 2004; Vol. 112; (b) Falivene, L.; Cavallo, L., *Coord. Chem. Rev.* **2017**, 101-114.

66. Fulmer, G. R.; Miller, A. J. M.; Sherden, N. H.; Gottlieb, H. E.; Nudelman, A.; Stoltz, B. M.; Bercaw, J. E.; Goldberg, K. I., *Organometallics* **2010**, *29*, 2176-2179.
67. SDBSWeb: <http://sdb.sdb.aist.go.jp> (National Institute of Advanced Industrial Science and Technology, September 5th, 2016)
68. Wilkie, C. A.; Harworth, D. T., *J. Inorg. Nucl. Chem.* **1978**, *40*, 195-197.
69. Zhang, G.; Xie, X.; Wang, Y.; Wen, X.; Zhao, Y.; Ding, C., *Org. Biomol. Chem.* **2013**, *11*, 2947.
70. Shen, T.; Wang, T.; Qin, C.; Jiao, N., *Angew. Chem. Int. Ed.* **2013**, *52*, 6677-6680.
71. Bailey, W. F.; Cioffi, E. A., *Magn. Reson. Chem.* **1987**, *25*, 181-183.
72. Saha, S.; Roy, R. K.; Ayers, P. W., *Int. J. Quantum Chem.* **2009**, *109*, 1790-1806.
73. Benitez, D.; Shapiro, N. D.; Tkatchouk, E.; Wang, Y.; Goddard, W. A.; Toste, F. D., *Nat. Chem.* **2009**, *1*, 482-486.
74. Alabugin, I. V.; Bresch, S.; Manoharan, M., *J. Phys. Chem. A* **2014**, *118*, 3663-3677.
75. Root, D. M.; Landis, C. R.; Cleveland, T., *J. Am. Chem. Soc.* **1993**, *115*, 4201-4209.
76. Radhakrishnan, T. P.; Agranat, I., *Structural Chemistry* **1991**, *2*, 107-115.
77. Zuur, A. F.; Ieno, E. N.; Elphick, C. S., *Methods Ecol. Evol.* **2010**, *1*, 3-14.
78. Spearman, C., *The American Journal of Psychology* **1904**, *15*, 72.
79. SOPER, H. E.; YOUNG, A. W.; B. M., C. A. V. E.; A., L. E. E.; PEARSON, K., *Biometrika* **1917**, *11*, 328-413.
80. Benjamini, Y.; Hochberg, Y., *Journal of the Royal Statistical Society. Series B (Methodological)* **1995**, *57*, 289-300.
81. SHAPIRO, S. S.; M. B., W. I. L. K., *Biometrika* **1965**, *52*, 591-611.
82. Tu, Y.-K.; Kellett, M.; Clerehugh, V.; Gilthorpe, M. S., *Br. Dent. J.* **2005**, *199*, 457-461.
83. Yin, P.; Fan, X., *The Journal of Experimental Education* **2001**, *69*, 203-224.
84. O'Brien, R. M., *Quality & Quantity* **2007**, *41*, 673-690.
85. Altman, N.; Krzywinski, M., *Nat. Methods* **2016**, *13*, 281-282.
86. (a) Croes, D.; Couche, F.; Wodak, S. J.; van Helden, J., *Journal of Molecular Biology* **2006**, *356*, 222-236;  
(b) Batushansky, A.; Toubiana, D.; Fait, A., *BioMed Research International* **2016**, *2016*, 1-9.
87. Toubiana, D.; Fernie, A. R.; Nikoloski, Z.; Fait, A., *Trends in Biotechnology* **2013**, *31*, 29-36.
88. In linear formulas such as  $y=i+ax$  or  $z=i+ax+by$ , the parameter on the left-hand side is referred to as the dependent variable (y and z, respectively) and the parameter(s) on the right hand side are referred to as explanatory variables (x, respectively, x and y).
89. A representative selection of models is discussed. Illustrative examples of analogous models with modelled values instead of experimental values (or vice versa) are presented in the Supporting Information.
90. Murtagh, F.; Legendre, P., *Journal of Classification* **2014**, *31*, 274-295.
91. Isenberg, P.; Bezerianos, A.; Dragicevic, P.; Fekete, J.-D., *IEEE Transactions on Visualization and Computer Graphics* **2011**, *17*, 2469-2478.